The role of miR-135b in normal and aberrant late lung development

Inaugural Dissertation

submitted to the
Faculty of Medicine
in partial fulfilment of the requirements
for the PhD Degree
of the Faculties of Veterinary Medicine and Medicine
of the Justus Liebig University Giessen

by
Claudio Nardiello
of
Potenza, Basilicata, Italy

Giessen (2020)

From the Institute of Max Planck Institute for Heart and Lung Research
Director / Chairman: Prof. Dr. Werner Seeger
of the Faculty of Medicine of the Justus Liebig University Giessen

First Supervisor and Committee Member: Prof. Dr. Werner Seeger

Second Supervisor and Committee Member: Prof. Dr. Reinhard Dammann

Committee Members: Prof. Dr. Ralph Schermuly
Prof. Dr. Werner Seeger
Prof. Dr. Reinhard Dammann
Prof. Dr. Susanne Krauss-Etschmann

Date of Doctoral Defense:
11 May 2021

I Index

II List of tables

III List of figures

IV Abbreviations

AEI	Alveolar epithelial type I
AEII	Alveolar epithelial type II
AGO	Argonaute
alv	Alveoli
alv air	Alveolar space
alv epi	Alveolar epithelium
BMP	Bone morphogenetic protein
BMPR	Bone morphogenetic protein receptor
bp	Base pair
BPD	Bronchopulmonary dysplasia
BrdU	5-Bromo-2′-deoxyuridine
BSA	Bovine serum albumin
CE	Coefficient of error
Cre	Cre recombinase
Ct	Threshold cycle
CV	Coefficient of variation
DAPI	4′,6 diamidino-2-phenylindole
ddH_2O	Double distilled water
DEPC	Diethyl pyrocarbonate
DNase	Deoxyribonuclease I
dNTP	Deoxynucleotide triphosphates
E	Embryonic day
FACS	Fluorescence-activated cell sorting
FCS	Fetal bovine serum
FISH	Fluorescent *in situ* hybridization
FITC	Fluorescein isothiocyanate
Flp	Recombinase flippase
FRT	Flippase recognition target
FSC-A	Forward scatter area
FSC-H	Forward scatter height
g	Gram

GFP	Green fluorescent protein
GiΔ	Global induced deletion
h	Hours
hAE	Human alveolar epithelial
HEPES	4-(2-hydroxyethyl)-1-piperazineethanesulfonic acid
Igf1	Insulin-like growth factor-1
IP	Intraperitoneal
kDa	Kilodalton
kg	Kilogram
LNA	Locked-nucleic acid
M	Molar
mG	N-terminal membrane-tagged enhanced green fluorescent protein
mg	Milligram
miR	microRNA
µg	Microgram
µl	Microliter
M-MLV	Moloney Murine Leukemia Virus
ml	Milliliter
MLI	Mean linear intercept
mT	N-terminal membrane-tagged tdTomato
MTT	3-(4,5-dimethylthiazol-2-yl)-2,5-diphenyltetrazolium bromide
n	Number
N	Number
ng	Nanogram
Nv	Numerical density
P	Postnatal day
P/S	Penicillin-streptomycin
pA	Polyadenylation
par	Parenchyma
PBS	Phosphate-buffered saline
pCA	CMV enhancer/chicken β-actin core promoter
PCR	Polymerase chain reaction

PDGFR	Platelet-derived growth factor receptor
PFA	Paraformaldehyde
POD	Horseradish-peroxidase
Polr2A	RNA polymerase II
qPCR	Quantitative polymerase chain reaction
RISC	RNA-induced silencing complex
rpm	Revolutions per minute
S	Surface area
s	Seconds
SD	Standard deviation
SDS	Sodium dodecyl sulphate
Smad	Small mothers against decapentaplegic
Sftpc	Surfactant protein C
SSC	Saline-sodium citrate
SSC-A	Side scatter area
S_v	Surface density
T1α	Podoplanin
TEMED	N,N,N′,N′-tetramethylethylenediamine
Tnc	Tenascin C
TGF	Transforming growth factors
TGFBR	Transforming growth factor-β receptor
TGF-β	Transforming growth factor-β
TN	Tris-sodium chloride
TNT	Tris-sodium chloride-tween
TSB	Target site blocker
U	Unit
UTR	Untranslated region
V	Volume
V_v	Volume density
Wt	Wild type
w	Weight
X-Gal	5-bromo-4-chloro-3-indolyl-β-D-galactopyranoside

τ (sep)	Arithmetic mean septal thickness
°C	Degree Celsius

V Abstract

Bronchopulmonary dysplasia (BPD) is a chronic lung disease that occurs in premature infants. BPD is a consequence of oxygen supplementation and/or mechanical ventilation and is characterized by fewer, larger alveoli and thus associated with decreased surface area for gas exchange and increased alveolar wall thickness. The pathogenesis of BPD is not fully understood but several reports indicate microRNAs as potential key players during normal and aberrant lung development. In the present study, the expression of microRNA (miR)-135b-5p was significantly increased in lungs of BPD patients and in an experimental mouse model of BPD. MiR-135b-5p was found expressed in alveolar epithelial type II (AEII) cells and targeted Smad5, a regulatory protein of transforming growth factor-β (TGF-β)/bone morphogenetic protein (BMP) signaling. The AEII cells exposed to hyperoxia *in vivo* and *in vitro* presented higher miR-135b-5p expression and consequently reduced levels of Smad5. The same pattern was observed when human alveolar epithelial cells were exposed to hyperoxic conditions. Overexpression of miR-135b-5p in A549 cells revealed Smad5 as a target, and that increased expression of miR-135b-5p reduced cell proliferation. The inhibition of miR-135b-5p *in vivo* using a locked-nucleic acid (LNA)-stabilized antimiR directed against miR-135b-5p revealed a significant improvement in lung architecture after hyperoxic exposure. The same grade of improvement in lung structure was observed when miR-135b was genetically ablated using a Cre-ER^{T2} driver line. Moreover, to assess if Smad5 played a crucial role in lung development, Smad5 was genetically ablated and revealed a worsening of lung structure. The use of a target site blocker, a compound which should block the binding of miR-135b-5p to Smad5, dramatically reduced Smad5 expression and completely disrupted the lung architecture. The present study revealed the importance of miR-135b-5p and the ability to target and to regulate Smad5 during normal and aberrant lung development. The inhibition of miR-135b-5p is suggested as a potential therapeutic drug to treat premature infants with BPD.

VI Zusammenfassung

Bronchopulmonale Dysplasie (BPD) ist eine chronische Lungenerkrankung, die bei frühgeborenen Kindern auftritt. BPD ist eine Konsequenz von erhöhter Sauerstoffkonzentration und/oder mechanischer Beatmung von Frühchen. Die Hauptmerkmale von BPD sind erweitere und weniger Alveolen, reduzierte Gasaustauschfläche und eine Septum Vergrößerung. BPD ist bis heute noch nicht vollständig verstanden, aber viele wissenschaftliche Berichte weisen darauf hin, dass die microRNAs eine wichtige Rolle spielen, sowohl in der normalen als auch in der abnormalen Lungenentwicklung. In der vorliegenden Studie war die Gen Expression von microRNA (miR)-135b-5p in BPD und im experimentellen Mausmodell von BPD signifikant erhöht. Die miR-135b-5p wurde hauptsächlich in alveolären Epithel-Typ-II- (AEII) Zellen gefunden und regulierte Smad5, ein regulatorisches Protein der TGF-β/BMP-Signalübertragung. Die AEII, die *in vivo* und *in vitro* unter Hyperoxie Konditionen ausgesetzt waren, zeigten eine erhöhte miR-135b-5p Expression und als Folge eine reduzierte Smad5 Expression. Das gleiche Muster konnte man observieren, wenn humane Alveolarepithelzellen unter Hyperoxie Konditionen ausgesetzt wurden. Eine Überexpression von miR-135b-5p in A549-Zellen zeigte eine konsequente Reduzierung von Smad5 und Zellproliferationen. Die miR-135b-5p Expression wurde *in vivo* mit locked-nucleic acid (LNA)-antimiR neutralisiert, mit erfolgreicher Verbesserung der Lungenstruktur. Derselbe Grad von Verbesserung in der Lungenentwicklung wurde observiert, wenn das miR-135b Gen abgeschaltet wird. Nachdem das Smad5 Gen ausgeschaltet wurde, konnte eine konsequente Verschlechterung der Lungenstruktur festgestellt werden; dieses Ergebnis wies darauf hin, dass Smad5 eine entscheidende Rolle in der Lungenentwicklung spielt. Die Verwendung von einem Target Site Blocker, die die Bindung zwischen miR-135b-5p und Smad5 mRNA verhindern sollte, reduzierte die Smad5 Expression und zerstörte dramatisch die Lungenarchitektur. Die vorliegende Studie wies darauf hin, dass die miR-135b-5p eine wichtige Rolle für die Regulierung von Smad5 in der normalen und abnormalen Lungenentwicklung spielt. Die Blockierung von miR-135b-5p könnte als potenzielles therapeutisches Medikament zur Behandlung von Frühgeborenen mit BPD vorgeschlagen werden.

1 Introduction

The main function of the lung is to capture oxygen from the atmosphere and to transfer oxygen to the bloodstream, to produce energy. Oxygen is metabolized into carbon dioxide, which is later expelled from the bloodstream into the atmosphere. Gas exchange takes place in the alveolus which is the unit of gas exchange in the lung. The alveolus is optimized to have the largest surface area of gas exchange possible to allow gas exchange across the alveolo-capillary barrier (55). Lung development is the process to create an optimized system of gas exchange that finds into the alveolus the main component.

1.1 Lung development

Mammalian lung development is a complex process regulated by genetic, epigenetic physical and mechanical factors. The balance and coordination between transcriptor factors, growth factors, and environmental influences play a key role in lung development (148, 149). Lung development begins in the fetus and is divided into two major periods: the prenatal period, also known as early lung development, and the postnatal period. Lung development in mice and humans shares the same phases, namely the embryonic, the pseudoglandular, the canalicular, the saccular, and the alveolar phase (**Figure 1**) (114). However, mice are born in the saccular phase and humans are born in the alveolar phase.

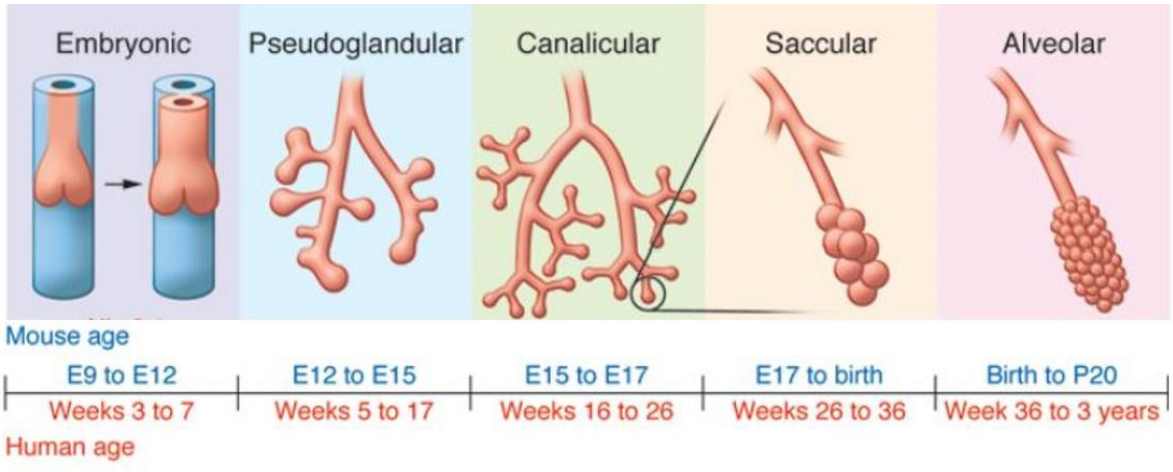

Figure 1. Mouse and human lung development.

Mouse and human lung development through five phases: embryonic, pseudoglandular, canalicular, saccular, and alveolar. E, embryonic day; P, postnatal day. Picture adapted from (114).

Early lung development initiates with the embryonic phase where the two lung buds elongate and begin a continuous process of branching and formation of mayor

airways and the pleura (92). This process takes place in mice at embryonic day (E)9-E12 and in humans at E26-E49. The embryonic phase is followed by the pseudoglandular phase, which is mainly characterized by the formation of the bronchial tree and large parts of the respiratory parenchyma. This process takes place at E12-E16 in mice and E35-E119 in humans and ends with the generation of the first alveolar ducts (18). The next phase is the canalicular phase, which takes place in mice at E16-E17 and in humans at E112-E182. During this phase, distal airways are formed together with the alveolar epithelium which forms with the mesenchymal capillary network the future air-blood barrier (21). After the canalicular phase, the saccular phase takes place in mice at E17-postnatal day (P)4 and in humans at E168-E266. During this phase, the terminal airways grow and form larger airspaces, or sacculi, which are the primitive region for future gas exchange. The sacculus is formed by mesenchymal cell condensation exactly where airspaces and septa encounter each other, to expand the gas exchange area. The septum surface contains a layer of capillaries separated by mesenchymal connective tissue and is covered by alveolar epithelial type I (AEI) cells. The remaining surface of the septum contains alveolar epithelial type II (AEII) cells that are progenitor cells of the AEI cells, and produce surfactant proteins (150).

At the end of the saccular stage, late lung development begins, with the alveolarization phase taking place in mice at P4-P21, and in humans at E252-2 years-adolescence. New septa, known as secondary septa, are created from the immature septa and divide the previously formed large alveolar space, to generate and expand as much as possible the surface area of gas exchange. The new septa or new alveoli are formed at any time until the maturation of the microvasculature (19, 20, 58, 113, 144). Normal lung development ends in fully functional lungs that are capable for optimal gas exchanges. Any perturbations during this process can lead to aberrant lung development resulting in lungs that are maladapted for gas exchange.

1.2 Bronchopulmonary dysplasia

Bronchopulmonary dysplasia (BPD) is a chronic lung disease that occurs in premature infants, described for the first time by Dr. Northway and his team (105). BPD is a consequence of oxygen supplementation and mechanical ventilation of preterm birth, defined as birth before 36 completed weeks of gestation (1, 61). BPD is associated with high mortality, complications during the early neonatal intensive care unit (139) and the most affected survivors could be symptomatic with airway obstruction even as

adults (10, 12, 48). The main consequences to the development of the lung structure after oxygen supplementation and/or prolonged mechanical ventilation of premature infants (49), as well as other disease-related variables such as infections and inflammation (10), are fewer and larger alveoli, a decreased surface area of gas exchange and a thickening of the septa (65, 122). Treatment with oxygen supplementation saves preterms life, the high oxygen prevents the lung structure. For this reason, there is a pressure need to study clinical BPD. However, the study of the pathophysiology and pathogenic mechanisms of BPD is challenging due to the rarity of human material. Therefore, to understand better the mechanisms that drive the pathology of BPD, experimental animal models need to be employed and refined (102). Experimental animal models of BPD are important to understand normal and aberrant lung development and to evaluate the beneficial or adverse effects of therapeutic interventions. To correctly model human BPD, the experimental animal model must phenocopy an increased septal thickness, fewer total alveoli, and decreased surface area of gas exchange. In the literature, different animal models are employed to model BPD and some of them yielded opposite results when the same therapeutic intervention have been employed (135). There is a clear need to find a standard animal model of BPD to define the correct oxygen concentration toxicity and the perfect window of oxygen exposure, to mimic the disease (103). The most commonly employed animal model to mimic human BPD is the exposure of newborn mice to hyperoxia.

To understand the severity of BPD, many studies have been conducted to investigate aberrant lung development and the application of drugs that could mitigate oxygen toxicity. In a recent review article, Lignelli and coworkers observed a general increase in the number of publications related to BPD, lung development, and alveolarization over the period between 2008 and 2018, with particular attention to cigarette smoke and nicotine, maternal factors, noncoding RNA, microbiome and BPD biomarkers (81). Taking all these research articles together, and the progress in the field of clinical and experimental BPD, there is still the “least common multiple” that combines all these studies: “today BPD is still not fully understood”. There is evidence that many factors play a role in the pathogenesis of BPD, however, the latest scientific reports emphasized that microRNA-(miR)s could be one of these key players. For example, miR-489 was found to play a crucial role in the alveolar septation by targeting insulin-like growth factor-1 (Igf1) and tenascin C (Tnc) (109). Moreover, the miR-17~92

cluster was found to play an important role in epigenetic regulation of the pathogenesis of BPD (119). Furthermore, the restoration of miR-29b gene expression in the developing lung improved lung alveolarization and extracellular matrix deposition (35). Two other scientific reports found that miR-34a plays an important role during alveolarization, regulating the anti-apoptotic Ang1/Tie2 signaling (142), and the platelet-derived growth factor receptor (PDGFR)α (124). MiR-30a was found as a proangiogenic regulator and as a candidate underlying sex-specific differences in BPD (163). MiR-154 was identified as an important physiological regulator for correct alveolarization, where lower expression of miR-154 leads to alveolar simplification (24). MiR-206 was found to modulate the Fibronectin-1 gene expression in mice exposed to hyperoxia and BPD patients. This interaction may contribute to the pathogenesis of BPD (161). MiR-155 regulates the effects of mechanical stretch on dynamic changes in bronchial epithelial cells (69). Taking these research articles together, amongst other reports, there is clear evidence of the potential role of miRs as causal players in normal and aberrant lung development (104, 156).

1.3 microRNA

The miRs discovered in 1993 by Drs. Lee, Feinbaum, and Ambros in *Caenorhabditis elegans* (76) are small non-coding RNAs that are about 22 nucleotides long and have been found in animals and plants (70, 71, 74, 75, 82, 95, 116). To date, more than 1000 miRs have been identified and most regulate gene expression at the transcription level, RNA processing, and/or translation repression (22). MiR precursors, or pri-miRNA, are synthesized by the RNA polymerase II and undergo a complex process of maturation that begins in the nucleus and ends in the cytoplasm (**Figure 2**) (51, 153). The pri-miRNA is 1 kb long and has a stem-loop of 33-35 bp in the structure. The RNase III Drosha and DGCR8 proteins cut and release the stem-loop as a small hairpin-shaped RNA of about 65 nucleotides called pre-microRNA (77). The pre-microRNA is exported into the cytoplasm by exportin 5 which binds processed pre-microRNAs directly in the presence of the Ran guanosine triphosphate (16, 83, 157). In the cytoplasm, the regulator protein TRBP binds the RNase III endonuclease Dicer to modulate higher efficiency to process pre-microRNAs (42). The pre-microRNA is cleaved by Dicer at the terminal stem-loop to release a 22-nucleotide RNA duplex (13, 66). The 22-nucleotide RNA duplex is recruited by argonaute (AGO) 2, which is fundamental for the RNA-induced silencing complex (RISC) (52). The two strands of the RNA duplex are fed into the RISC, where one strand inside the RISC is processed

into a mature miR and the other strand is degraded (131). This process of selection is due to the stability of the base pairs at the two ends of the 22-nucleotide RNA duplex (63). The mature functional miR can silence target gene expressions by cleavage the mRNA, posttranscriptional regulation, or deadenylation of the mRNA (51, 153).

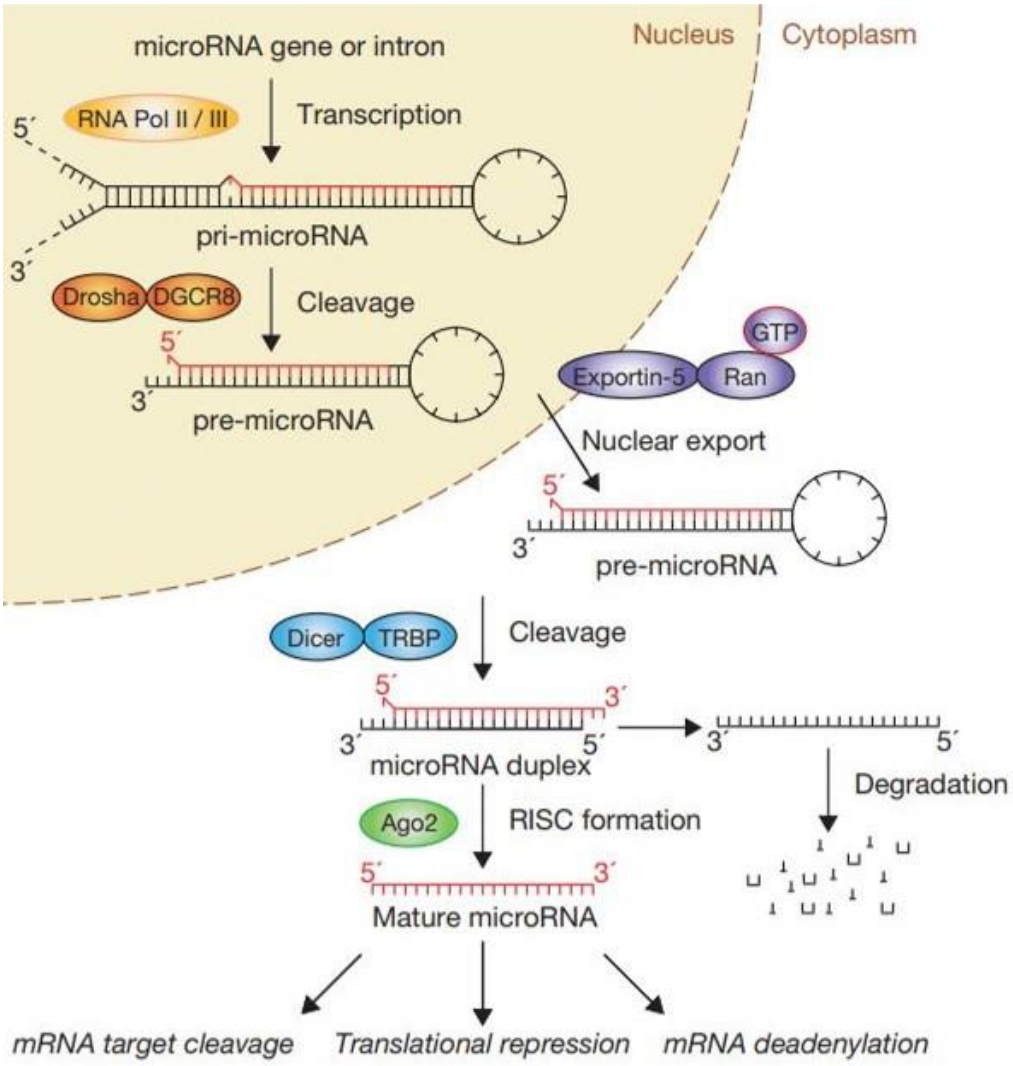

Figure 2. The biosynthesis of microRNA.

AGO, Argonaute; GTP, Guanosine triphosphate; Pol, Polymerase; RISC, RNA-induced silencing complex. Picture adapted from (153).

The miRs play a crucial function in gene regulation during lung development. Many different pathways could be impacted by dysregulated miRs, such as the transforming growth factor-β (TGF-β)/bone morphogenetic protein (BMP) pathway that is known to play a key role in lung development (7). Deregulated miRs might significantly impact TGF-β/BMP signaling, for example, the miR-154 suppresses lung alveolarization after modulating the phosphorylation of small mothers against decapentaplegic homolog (Smad) 3 and TGF-β signaling (24). MiR-431-5p regulates the pulmonary surfactant

protein expression *in vitro* through the TGF-β/Smad4 pathway (79). MiR-155 regulates BMP signal in lung epithelial cells inhibiting Smad1 and Smad5 expression (158). MiR-26a regulates the pulmonary surfactant synthesis by modulating Smad1 expression in alveolar epithelial type II cells (162). The overexpression of Let-7c inhibits TGF-β1 expression and leads to abnormal extracellular matrix deposition (26). miR-876-5p overexpression blocks the BMP-4 expression and suppresses the epithelial-mesenchymal transition (11). All these reports clearly show a pressure need to investigate the action of deregulated miRs on the TGF-β/BMP signaling during postnatal lung development.

1.4 TGF-β/BMP signaling

Alveolarization is driven by growth factors that communicate between different cell types during postnatal lung development (106, 123). This communication needs precise coordination of signals such as TGF-β/BMP signaling. Perturbations to TGF-β/BMP signaling might cause an aberrant outcome during lung development (132).

Transforming growth factors (TGF) were discovered in 1978 by Drs. Todaro and De Larco. Researchers observed changes in fibroblasts cultured *in vitro* after RNA virus infection (30). This observation was further investigated by two independent groups and in the year 1981, Drs. Harold Moses and Anita Roberts, isolated and purified the TGF from different cell types. These TGF turned out to be the TGF-β (94, 120). Different scientific groups began to investigate TGF-β signaling for the ability to modify phenotypically cells and cell function. Moreover, in 1988 new regulatory members of the TGF-β family, BMP-2A and BMP-3 were discovered (155). The members of the TGF-β/BMP “superfamily” regulate different biological responses such as cell differentiation (68), apoptosis (2), and cell growth (87) in different cell types (96, 140). TGF-β signaling begins with the binding of TGF-β ligands to the TGF-β receptor (TGFBR) type II. The ligand connects the TGFBR type II next to the TGFBR type I to form a heterotetramer that phosphorylates the TGFBR type I on the glycine and serine-rich region by the constitutive kinase activity of the TGFBR type II. The phosphorylation of TGFBR type I transduces the signals via Smad proteins (133). Similarly, the BMP signal starts with the binding of BMPs ligands to the BMP receptors (BMPR): BMPR type I and BMPR type II. Also, in this case, the cascade signal is mediated by kinases present over the surface of the receptors and leads to transduce the signal by Smad proteins (89) (**Figure 3**).

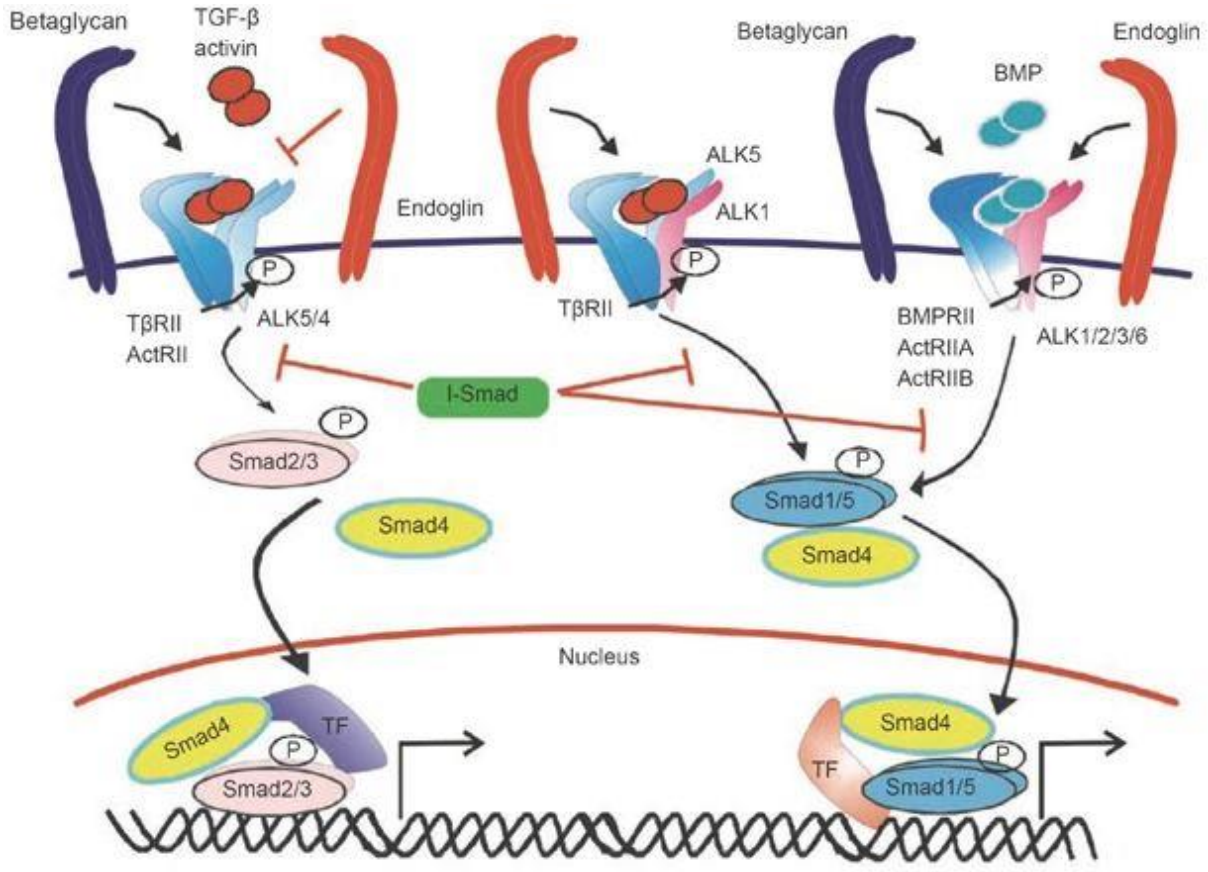

Figure 3. TGF-β/BMP signaling.

ActRII, Activin type 2 receptors; ALK1, Activin receptor-like kinase 1; ALK2, Activin A receptor, type I; ALK3, Bone morphogenetic protein receptor, type IA; ALK4, Activin receptor type-1B; ALK5, Activin A receptor type II-like kinase or Transforming growth factor-beta receptor I; ALK6, Bone morphogenetic protein receptor type-1B; BMP, Bone morphogenetic protein; I, Inhibitor; P, Phosphorylation; Smad, Small mothers against decapentaplegic TβRII, TGF-β receptor type II; TF, Transcriptor factor; TGF-β, Transforming growth factor-β. Picture adapted from (46).

The Smad proteins constitute a family of eight members with a molecular mass between 42 kDa and 60 kDa that can transduce the signals from the cellular membrane to the nucleus (54, 133). This transduction is accomplished by a complex mechanism of interaction and phosphorylation between the different Smads. The regulatory Smads or R-Smads, Smad2, and Smad3 are phosphorylated directly by TGF-β. The other members of the R-Smads, Smad1, Smad5, and Smad9, are indirectly phosphorylated by TGFBRs and directly by the BMP receptors (28, 160). The phosphorylated R-Smads form a heteromeric complex with the co-regulator Smad4. This complex enters the nucleus in which initiates and regulates the transcription of genes. The process of phosphorylation and transduction of signals can be controlled by the inhibitory Smads,

Smad6, and Smad7, which negatively regulate the TGF-β/BMP pathway by preventing the phosphorylation of the R-Smads. In detail, Smad6 binds Smad4 blocking the heteromeric complex and the signal transduction in the nucleus (45, 53). Smad7 interacts with the surfaces of TGFBR type I preventing the phosphorylation of the R-Smads (62) (**Figure 3**).

TGF-β/BMP signaling is considered a fundamental key regulator for normal lung development and homeostasis (32). Insults during postnatal lung development, such as hyperoxia, alter the expression of TGF-β/BMP signaling and lead to impaired lung alveolarization (6, 93). In experimental animal models of BPD, perturbated TGF-β/BMP signaling disrupts alveologenesis. The restoration of TGF-β/BMP signaling by specific TGF-β antibodies neutralized the aberrant alveolarization (101). Moreover, the inhibition of TGF-β1 decreases apoptosis, inflammation, and mortality in newborn pups (141). TGF-β1 treatment promotes survival and repair in AEII cells that were previously damaged by hyperoxia exposure (17, 80). Hyperoxia alters lung architecture by modulating Smad3 expression during lung development. Treatment with rosiglitazone and curcumin improves Smad3 expression and alveolarization (29, 127). Increased TGF-β in preterm neonates causes damages to the alveolar epithelial cells associated with edema in the alveolar space (59). TGF-β modulates transglutaminase 2 (TGM-2) expression in clinical and experimental BPD. Blocking the TGF-β signaling restores TGM-2 levels (154) that are known to form aberrant extracellular matrix structure in BPD (90). Contrary to expectation, blockage of TGF-β signaling inhibits the secondary septation inducing alveolar simplification in BPD via the matricellular protein (TGFBI) (4). Another research article reports that hyperoxia induces alteration in the TGF-β-ALK1-Smad1/5 and TGF-β-TGFBR type II-Smad2/3 axes in lung endothelial cells leading to stunted alveolarization (60). Hyperoxia significantly decreased BMP-9, ALK1, ALK2, and BMPR type II expression during postnatal lung development leading to alveolar simplification and increased alveolar septum. However, BMP-9 induced overexpression in hyperoxic exposed mice improved lung alveolarization and prevented inflammation (25). Hyperoxia induces changes in Smad2 and Smad3 expression after hypermethylation of TFGBR type I suggesting epigenetic changes in hyperoxia exposed mice (15).

Taking these reports together, the TGF-β/BMP pathway is important for normal lung development. However, hyperoxia-driven disturbances to TGF-β/BMP signaling cause tremendously deleterious damage to lung architecture. Research demonstrated

that in the hyperoxia-based animal models of BPD, overexpression or neutralization of TGF-β/BMP signaling improved stunted alveolarization. Scientific reports have focused mainly on the activity of R-Smads such as Smad2 and Smad3 and the transduction to the nucleus by phosphorylation, but little is known for the other three members of the R-Smads, namely Smad1, Smad5, and Smad9. Studies on these R-Smads are mostly undertaken in prenatal lung development, where Smad1 and Smad5 deregulation affects early lung development (136) and might play a role in the mesenchymal-epithelial interaction (33). Smad1, Smad5, and Smad9 are crucial signal mediators during prenatal mouse development. Smad1 and Smad5 knockout mice are embryonic lethal (23, 143). Smad9 is still not fully studied but reports are showed that embryos and knockout mice survive (110). The use of conditional transgenic mice to study Smad1, Smad5, and Smad9 is an excellent genetic engineering tool to observe changes in postnatal lung development by knocking out the R-Smads. In fact, in the light of research findings, during normal postnatal lung development, Smad9 protein expression is not changed from P1 to P14, but the protein expression of Smad1 decreases over the same time frame and Smad5 protein expression instead increases (8). This reveals that Smad1, Smad5, and Smad9 are important players in prenatal and postnatal lung development. External insults might shift the tiny balance that exists among the R-Smads necessary for the signal transduction from the membrane to the nucleus. The miRs are emerging as a new class of modulators of gene and protein expression, which regulate and influence the balance of signal transduction. Microarray profiling revealed several deregulated miRs in a hyperoxia-based mouse model of BPD (124). An interesting deregulated miR found was miR-135b-5p. Bioinformatic tools, such as TargetScan, predicts miR targets by matching the miR seed sequence to the conserved untranslated region 3' (3'-UTR) as an 8-mer, 7-mer, and 6-mer matching sites (3, 40, 43), revealed that miR-135b-5p targets different members of the TGF-β/BMP signaling. Among these members are BMPR type I and type II, BMP10, Smad5, Smad4, TGFBR type I, and TGFBR type II. Some of the predicted targets were already validated such as Smad5, TGFBR type I, BMPR type II (14), and TGFBR type I (78). These reports demonstrated the importance of miR-135b-5p in regulating the TGF-β/BMP signaling, and this might implicate how miR-135b-5p could play an important role in normal and aberrant lung development.

1.5 The hypothesis and objective of the study

The hypothesis of this study was that miR-135b plays a central role in normal lung development, as well as in perturbed late lung development associated with BPD.

The objective of this study is to investigate the role of miR-135b-5p in clinical and experimental BPD, and the impact of deregulated miR-135b-5p expression on Smad5. Furthermore, to assess where miR-135b-5p is expressed in the lung, and function of the miR-135b-5p/Smad5 axis in normal and aberrant lung development.

The aims of the study were i) to assess changes in miR-135b-5p expression in experimental BPD and to apply treatments, such as antimiRs, to control miR-135b-5p expression; ii) to identify a specific target gene of miR-135b-5p; iii) to regulate and control the expression of the target gene after miR-135b-5p antimiR; and iv) to evaluate the lung architecture after miR-135b-5p antimiR; v) to observe changes in the lung architecture after ablation of miR-135b-5p and the identified target gene.

2 Material and Methods

2.1 Materials

2.1.1 Equipment

The equipment used in the study are reported below in table 1.

Table 1. Equipment used in the study.

The name of the equipment, the manufacturer and the location, and the catalogue number (#) used in the study. ##, no catalogue number available.

Name	Company, Location	Catalogue Number (#)
24 mm Transwell® with 0.4 µm Pore Polyester Membrane Insert	Corning Incorporated, USA	3450
Agar Cutting Mould	Made in House	##
Agar Mould	Made in House	##
Precision Balance	Merck, Germany	Z676152-1EA
Biorad PowerPac 200 Electrophoresis Power Supply	Bio-Rad, USA	BP-200
Blunt Needle G24	CML SUPPLY, USA	901-24-050
Boekel Scientific Slide Moat™ Slide Hybridizer	Boekel Industries, Inc., USA	240000
Brand™ Bürker Counting Chambers	Thermo Fisher Scientific, USA	10513451
SLR-Digital Reflex camera	Nikon Corporation, Japan	D5300
Cell Scraper 25 cm	Sarstedt AG & Co. KG, Germany	831830
CELLSTAR 96 Well Cell Culture Microplate	Greiner Bio-One GmbH, Germany	655098
CELLSTAR® 96 Well Plates	Greiner Bio-One GmbH, Germany	655180
CELLSTAR® multiwell culture plates	Merck, Germany	M8562
Cellulose Swabs Askina	B. Braun, Germany	9051015
Centrifuge MiniSpin®	Eppendorf, Germany	5452000018
Cryo.s™	Greiner Bio-One GmbH, Germany	1212XX
Digital Slide Scanner	Hamamatsu Photonics, Japan	NanoZoomer-XR C12000
Dynabeads® FlowComp™ Flexi	Thermo Fisher Scientific, USA	123.01
Easystrainer 100 µm	Greiner Bio-One GmbH, Germany	542000
Easystrainer 40 µm	Greiner Bio-One GmbH, Germany	542040
Greiner CELLSTAR® 96 well plates	Greiner Bio-One GmbH, Germany	655180
Heracell CO_2 Incubators	Thermo Fisher Scientific, USA	150i

Table 1-continued

Name	Company, Location	Catalogue Number (#)
Histobloc	Kulzer GmbH, Germany	64708995
Histoform Q Embedding Mould	Kulzer GmbH, Germany	12025
Homogenisator, Precellys® 24	VWR, USA	P000669PR240A
Hotplate/Stirrer	VWR, USA	5052000000
ImageQuant LAS 4000	GE Healthcare, United Kingdom	LAS4000
Infinite® 200 PRO	Tecan, Germany	M200PRO
Cast Iron Stand Base	VWR, USA	241-0090
Cast Iron Stand Base	VWR, USA	241-0091
Laminar Flow Cabinet	Thermo Fisher Scientific, USA	Safe 2020
Leica DMi1 Inverted Microscopes	Leica, Germany	DMi1
Leica Microtome	Leica, Germany	CM3050S
Macro Lens	Nikon Corporation, Japan	JAA637DA
Memmert Universal Oven UF30	Memmert GmbH + Co.KG, Germany	UF30
MicroAmp™ Fast Optical 96-Well Reaction Plate, 0.1 mL	Thermo Fisher Scientific, USA	4346907
Microcentrifuge, MiniStar Silverline	VWR, USA	16NK / 823
Microscope Slides	Thermo Fisher Scientific, USA	J3800AMNZ
Microtome	Leica, Germany	RM2255
Microtome Blades	Thermo Fisher Scientific, USA	MX35 ULTRA
Microtome Knife	Leica, Germany	14021604813
Mini-PROTEAN® Tetra Cell Casting Module	Bio-Rad, USA	1658024
NanoDrop One Microvolume UV-Vis Spectrophotometer	Thermo Fisher Scientific, USA	ND-ONE-W
Oxygen Chamber for Animal Cages	BioSpherix, Ltd., USA	##
Oxygen Chamber for Cell Culture	BioSpherix, Ltd., USA	C-374
Oxygen Controller	BioSpherix, Ltd., USA	ProOx 110
Pasteur Pipette, 3 ml, 5 ml	Sarstedt AG & Co. KG, Germany	##
PCR 8 Strips, 0,2 ml	Greiner Bio-One GmbH, Germany	673271
pH Meter	Mettler Toledo	MT30130863
Pipetboy	Eppendorf, Germany	4430000018
Pipettes, Automatic, 0.5-10 µl	Eppendorf, Germany	4861000015
Pipettes, Automatic, 15-300 µl	Eppendorf, Germany	4861000031
Pipettes, Automatic, 50-1000 µl	Eppendorf, Germany	4861000040
Pipettes, Manual, 0.1-2.5 µl	Eppendorf, Germany	3123000012
Pipettes, Manual, 0.5-10 µl	Eppendorf, Germany	3123000020
Pipettes, Manual, 2-20 µl	Eppendorf, Germany	3123000098
Pipettes, Manual, 10-100 µl	Eppendorf, Germany	3123000047

Table 1- continued

Name	Company, Location	Catalogue Number (#)
Pipettes, Manual, 20-200 µl	Eppendorf, Germany	3123000055
Pipettes, Manual, 100-1000 µl	Eppendorf, Germany	3123000063
Pipettes, Manual, 0.5-5 ml	Eppendorf, Germany	3123000071
Refrigerated Centrifuge	Heraeus, Germany	75004371
Refrigerated Microcentrifuge	VWR, USA	CT15RE
Rotiprotect®-Nitrile disposal gloves	Carl Roth, Germany	CPX8.1
Routine Stereo Microscopes	Leica, Germany	M50
Royal Bio-Imaging System-Intas Gel iX Imager	Intas Biopharmaceuticals, India	GP-07LED
Shakers & Mixers	Heidolph, Germany	Polymax2040
Snap-cap Vials	Carl Roth, Germany	LC84.1
Snap-on Lids	Carl Roth, Germany	LC87.1
StepOne™ Real-Time PCR System	Thermo Fisher Scientific, USA	4376357
Surgical Instruments	FST, Germany	15006-09
Surgical Instruments	FST, Germany	14058-09
Surgical Instruments	FST, Germany	15370-26
Surgical Instruments	FST, Germany	11063-07
Surgical Instruments	FST, Germany	11052-10
Surgical Instruments	FST, Germany	11651-10
Suture Thread	SMI, Belgium	4015X
Syringe, 10 ml	B. Braun, Germany	10BBRAINJV
Syringe, 30G	BD, USA	04144150
Syringe, 50 ml	B. Braun, Germany	8728844F
Thermal cyclers, ProFlex PCR System	Thermo Fisher Scientific, USA	4484073
Tissue Homogenizing CKMix - 2ml	Bertin GmbH, Germany	KT03961-1-009.2
Trans-Blot Turbo Transfer System	Bio-Rad, USA	1704150EDU
Trimming Blade	CellPath, United Kingdom	CAF-0113-09A
Tubes, 0.5 ml	Eppendorf, Germany	0030121023
Tubes, 1.5 ml	Eppendorf, Germany	0030120086
Tubes, 2.0 ml	Eppendorf, Germany	0030120094
Tubes, 5.0 ml	Eppendorf, Germany	0030119517
Tubes, 15 ml	Thermo Fisher Scientific, USA	339650
Tubes, 50 ml	Thermo Fisher Scientific, USA	339652
Tubing	Asid Bonz GmbH, Germany	NDCU 30
Ultra-Low Temperature Freezer	Eppendorf, Germany	Innova®U535
Vortex Mixer	VWR, USA	97043-562
Water Bath	Carl Roth, Germany	HAC3.1
White Light Transilluminator	UVP, LLC, Germany	TW-26

2.1.2 Reagents

The reagents used in the study are reported below in table 2.

Table 2. Reagents used in the study.

The name of the reagents, the manufacturer and the location, and the catalogue number (#) used in the study. ##, no catalogue number available.

Name	Company, Location	Catalogue Number (#)
2× Laemmli Sample Buffer	Bio-Rad, USA	1610737
2-Mercaptoethanol	Sigma-Aldrich, Germany	M6250
4′,6-diamidino-2-phenylindole	Thermo Fisher Scientific, USA	D3571
4× Laemmli Sample Buffer	Bio-Rad, USA	1610747
5× Green GoTaq® Flexi Buffer	Promega, USA	M891A
AccuStart™ II Mouse Genotyping Kit	Quantabio, USA	733-2236
Acetic Acid	Merck KGaA, Germany	100063
Acetic anhydride	Sigma-Aldrich, Germany	A6404
Acetone, > 99.7% (V/V)	Carl Roth, Germany	CP40.2
Agar	Sigma-Aldrich, Germany	05039
Agarose NEEO Ultra-Quality	Carl Roth, Germany	2267
Agarose, Low Gelling Temperatur	Sigma-Aldrich, Germany	A9414
Ammonium sulfate	Sigma-Aldrich, Germany	A2939
Anti-fluorescein-POD, Fab fragments	Hoffmann-La Roche, Switzerland	11426346910
Azure II	Sigma-Aldrich, Germany	861065
Blocking Reagent	Hoffmann-La Roche, Switzerland	11096176001
Bovine Serum Albumin	Thermo Fisher Scientific, USA	P/N 55213
Bovine Serum Albumin	Sigma-Aldrich, Germany	A3059
Caspase-Glo® 3/7 Assay Systems	Promega	G8091
Cell Proliferation ELISA, BrdU	Hoffmann-La Roche, Switzerland	11647229001
Cell Proliferation Kit I (MTT)	Merck KGaA, Germany	11465007001
Chloroform	Sigma-Aldrich, Germany	R2432
cOmplete™, Mini, EDTA-free Protease Inhibitor Cocktail	Merck KGaA, Germany	11836170001
Denhardt's Solution 50×	Sigma-Aldrich, Germany	D2532
Deoxyribonuclease I from bovine pancreas	Merck KGaA, Germany	260913
Dimethyl sulfoxide	Sigma-Aldrich, Germany	276855
Dispase	Corning Incorporated	354235
DMEM, high glucose, GlutaMAX™	Thermo Fisher Scientific, USA	61965
DMEM/F12	Thermo Fisher Scientific, USA	11320033
dNTP Mix (10 mM)	Promega, USA	U1511
Dynabeads™ Biotin Binder	Thermo Fisher Scientific, USA	11047
Eosin Y (yellowish)	Merck KGaA, Germany	45380
Ethanol ≥ 99.8 %	Carl Roth, Germany	K928.3

Table 2-continued

Name	Company, Location	Catalogue Number (#)
Ethidium Bromide Solution	Promega, USA	H5041
Fetal Bovine Serum	Thermo Fisher Scientific, USA	26140079
Fluoromount W	Serva Electroforesis, Germany	21634
Formamide	Sigma-Aldrich, Germany	47671
GeneAmp™ 10× PCR Buffer	Thermo Fisher Scientific, USA	4379878
Glutaraldehyde 50%	Serva Electroforesis, Germany	23116.02
Glycine	Carl Roth, Germany	3187.3
GoTaq® Hot Start Polymerase (500 u)	Promega, USA	M5005
HBSS – Hank's Balanced Salt Solution	Thermo Fisher Scientific, USA	14175-046
HEPES Solution	Sigma-Aldrich, Germany	H0887
Hydrochloric acid fuming 37%	Merck KGaA, Germany	100317
Hydrogen peroxide 30%	Merck KGaA, Germany	107209
Immobilon Western HRP Substrate	Merck KGaA, Germany	WBKLS0500
Lipofectamine™ 3000	Thermo Fisher Scientific, USA	L3000008
Liquid Nitrogen	Air Liquide, France	##
Magnesium chloride (25 mM)	Promega, USA	A351H
Methylene Blue	Carl Roth, Germany	A514.1
MicroAmp™ Optical Adhesive Film	Thermo Fisher Scientific, USA	4311971
miRNeasy® Mini kit	Qiagen, Germany	217004
miScript II RT Kit	Qiagen, Germany	218161
miScript SYBR Green PCR Kit	Qiagen, Germany	218073
M-MLV Reverse Transcriptase	Thermo Fisher Scientific, USA	28025-021
m-Xylol	Carl Roth, Germany	3791.1
N,N-Dimethylformamide	Sigma-Aldrich, Germany	494488
NARCOREN®, Pentobarbital-Natrium Injection Solution	Merial GmbH, Hallbergmoos, Germany	##
Nuclease-Free Water	Thermo Fisher Scientific, USA	AM9930
Opti-MEM™ Reduced Serum Medium	Thermo Fisher Scientific, USA	51985034
Osmiumtetroxide	Carl Roth, Germany	8371.3
Paraformaldehyde	Sigma-Aldrich, Germany	P6148
Penicillin-Streptomycin (10000 U/mL)	Thermo Fisher Scientific, USA	15140122
Phosphate Buffered Saline 1×	Sigma-Aldrich, Germany	D8537
Phosphate Buffered Saline 10×	Sigma-Aldrich, Germany	D1408
Platinum™ SYBR™ Green qPCR SuperMix-UDG	Thermo Fisher Scientific, USA	11733046
Ponceau S	Sigma-Aldrich, Germany	P3504
Potassium Ferrocyanide	Sigma-Aldrich, Germany	60279
Potassium Ferricyanide	Sigma-Aldrich, Germany	60299
Powdered Milk	Carl Roth, Germany	T145.5

Table 2-continued

Name	Company, Location	Catalogue Number (#)
Precision Plus Protein™ Dual Color Standards	Bio-Rad, USA	1610374
Quick Start™ Bradford 1× Dye Reagent	Bio-Rad, USA	5000205
Random Hexamers (50 µM)	Thermo Fisher Scientific, USA	N8080127
Restore™ PLUS Western Blot Stripping Buffer	Thermo Fisher Scientific, USA	46428
Restore™ Western Blot Stripping Buffer	Thermo Fisher Scientific, USA	21059
RIPA Buffer	Sigma-Aldrich, Germany	R0278
RNase Inhibitor	Applied Biosystems, USA	N8080119
RNaseZAP™	Sigma-Aldrich, Germany	R2020
Rotiphorese® 50x TAE Puffer	Carl Roth, Germany	CL86
Rotiphorese® Gel 30 (37,5:1)	Carl Roth, Germany	3029.1
SDS Solution, Molecular Biology Grade (10% w/V)	Promega, USA	V6553
Silica Gel	Carl Roth, Germany	P077.1
Sodium Cacodylate Trihydrate	Serva Electroforesis, Germany	15540.03
Sodium Chloride	Carl Roth, Germany	3957
Sodium Orthovanadate	Sigma-Aldrich, Germany	S6508
Sodium Tetraborate Decahydrate	Carl Roth, Germany	T880.1
SSC (20×), RNase-free	Thermo Fisher Scientific, USA	AM9763
Staurosporine	Cayman Chemical Company, USA	81590
SuperSignal™ West Femto Maximum Sensitivity Substrate	Thermo Fisher Scientific, USA	34096
Technovit® 3040 Powder, Yellow	Kulzer GmbH, Germany	64708806
Technovit® 7100	Kulzer GmbH, Germany	64709003
Technovit® Universal Liquid	Kulzer GmbH, Germany	66022678
TEMED	Bio-Rad, USA	1610800
Tissue-Tek® O.C.T.™ Compound	Science Services GmbH, Germany	4583
Trans-Blot Turbo Mini 0.2 µm Nitrocellulose Transfer	Bio-Rad, USA	1704158
Triethanolamine	Sigma-Aldrich, Germany	90279
TRIS	Carl Roth, Germany	4855.2
Triton™ X-100	Sigma-Aldrich, Germany	T8787
Trypan Blue Solution, 0.4%	Thermo Fisher Scientific, USA	15250061
Trypsin-EDTA (0.05%), Phenol Red	Thermo Fisher Scientific, USA	25300054
TSA Plus Fluorescence Systems	PerkinElmer, USA	NEL741
Tween® 20	Promega, USA	H5151
UltraPure™ DNase/RNase-Free Distilled Water	Thermo Fisher Scientific, USA	10977

Table 2-continued

Name	Company, Location	Catalogue Number (#)
Uranyl Acetate	Serva Electroforesis, Germany	77870.02
Water for Injection	Thermo Fisher Scientific, USA	A12873-01
5-Bromo-4-chloro-3-indoxyl-β-D-galactoside	Carl Roth, Germany	2315
Yeast tRNA	Thermo Fisher Scientific, USA	15401011

2.1.3 Software

The software used are reported below in table 3.

Table 3. Software used in the study.

The name of the software, the manufacturer and the location of the manufactuer.

Name	Company, Location
Camera Control Pro 2	Nikon Corporation, Japan
GraphPad Prism 7.0	GraphPad Software, USA
ImageJ	NIH, USA
ImageQuant LAS 4000	GE Healthcare, United Kingdom
IntasGelCaptureEntry	Intas Biopharmaceuticals, India
Microsoft Office	Microsoft, USA
NDP.scan	Hamamatsu Photonics, Japan
NDP.view2	Hamamatsu Photonics, Japan
StepOne™ and StepOnePlus™ Software v2.3	Thermo Fisher Scientific, USA
Visiopharm's newCAST™	Visiopharm A/S, Denmark

2.2 Approvals for animal studies

All animal experiments using an antimiR directed against miR-135b-5p were approved by the *Regierungspräsidium Darmstadt*, under the approval number B2/1002 and B2/1324.

2.3 Mice

2.3.1 C57BL/6J wild type mice

Mus musculus C57BL/6J wild type mice were purchased from The Jackson Laboratory.

2.3.2 The Mir135b^{tm1Mtm}/Mmjax mice

The Mir135b^{tm1Mtm}/Mmjax (miR-135b$^{lacZ,fl/lacZ,fl}$) conditional mutant mice (MGI: 4943943) are designed to generate a null allele or a *lacZ* tagged null allele when combined with recombinase flippase (Flp) or Cre recombinase (Cre) expressing strains (**Figure 4**). The target vector, to generate the miR-135b$^{fl/fl}$ mice, was designed to insert

a short flippase recognition target (FRT) site followed by a *lacZ* gene, a locus of X-over P1 (loxP) site, a neomycin cassette, an FRT site, and a loxP site upstream of the miR-135b gene and one loxP site after the miR-135b gene (112).

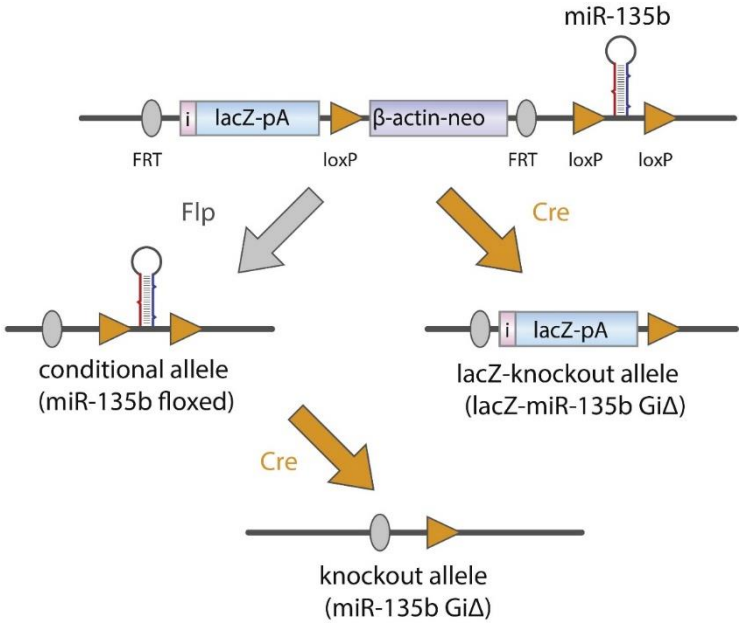

Figure 4. Schematic description of the miR-135b$^{lacZ,fl/lacZ,fl}$ mice before and after the Cre activation. Breeding strategies: the miR-135b$^{lacZ,fl/lacZ,fl}$ mice can be mated with germline deleter Flp mice, which removes the *lacZ* cassette and the neomycin cassette restoring the wild type loxP conditional miR-135b floxed allele (miR-135b$^{fl/fl}$). The conditional miR-135b floxed mice can be mated with germline- or tissue-specific Cre transgenic mice to generate miR-135b global induced deletion (miR-135b GiΔ). The miR-135b$^{fl/fl}$ mice can be crossed with germline deleter Cre mice to produce offspring with a reporter-tagged null allele (lacZ-miR-135b GiΔ). Picture modified and adapted from (112).

2.3.3 The B6.129-Gt(ROSA)26Sor$^{tm1(cre/ERT2)Tyj}$/J mice

The B6.129-Gt(ROSA)26Sor$^{tm1(cre/ERT2)Tyj}$/J (Cre-ER^{T2}) mice (MGI: 3790674) were purchased from The Jackson Laboratory. The Cre-ER^{T2} mice were used as germline deleter to control the temporal expression of floxed alleles by tamoxifen induction *in vivo (147)*.

2.3.4 The B6;SJL-Tg(ACTFLPe)9205Dym/J mice

The B6;SJL-Tg(ACTFLPe)9205Dym/J (Flp) mouse strain (MGI: 2174526) was purchased from The Jackson Laboratory. The Flp mouse expresses a FLP1 recombinase gene under the direction of the human ACTB promoter (121). The recombinase flippase recognizes and removes the FRT sites from the genome.

2.3.5 The Gt(ROSA)26Sor$^{tm4(ACTB-tdTomato,-EGFP)Luo/}$J mice

The Gt(ROSA)26Sor$^{tm4(ACTB-tdTomato,-EGFP)Luo/}$J (mTmG) mice (MGI: 3722404) were purchased from The Jackson Laboratory. These mice were generated by a target

vector designed to insert a CMV enhancer/chicken β-actin core promoter (pCA) driving expression, followed by a loxP site, an N-terminal membrane-tagged tdTomato (mT) cassette, a polyadenylation (pA) signal, a loxP site, an N-terminal membrane-tagged enhanced green fluorescent protein (mG) cassette and a pA signal.

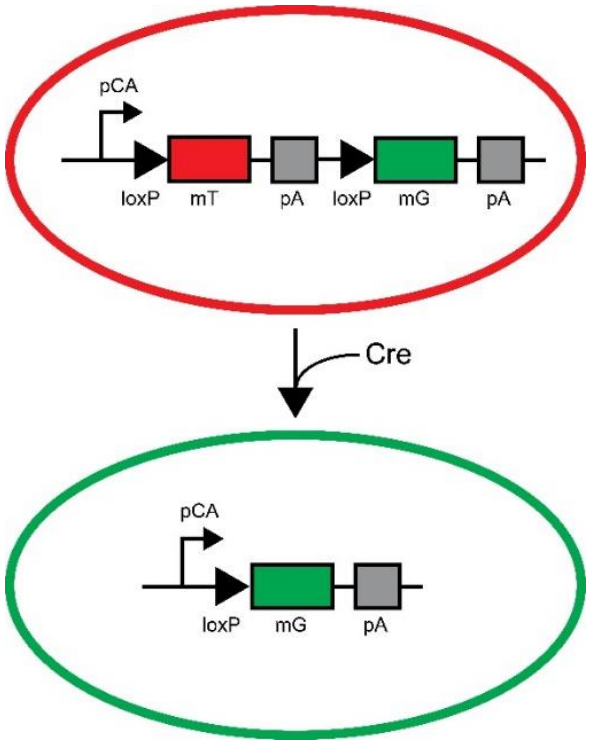

Figure 5. Schematic diagram of the mTmG construct before and after Cre activation.
The mTmG construct has a CMV enhancer/chicken beta-actin core promoter (pCA) driving expression followed by a loxP site, an N-terminal membrane-tagged tdTomato (mT) cassette, a polyadenylation (pA) signal, a loxP site, an N-terminal membrane-tagged enhanced green fluorescent protein (mG) cassette and a pA signal. Cells and tissue(s) express a strong red fluorescence. After delivery of tamoxifen Cre activation is achieved and the mT cassette and the pA are deleted, allowing the mG cassette and the second pA to be expressed. Cells and tissue(s), with active Cre, express a strong green fluorescence.

The mTmG mice express strong red fluorescence in all tissues and cell types, however when these mice are bred with Cre recombinase expressing mice and injected with tamoxifen, the resulting offspring have the mT cassette deleted in the Cre expressing tissue(s) and cells, allowing the expression of the mG cassette. These mice will express a strong green fluorescence (**Figure 5**) (100).

2.3.6 The Smad5$^{tm1.1Huy}$ mice

The Smad5$^{tm1.1Huy}$ (Smad5$^{fl/fl}$) conditional mutant mice (MGI: 2679443) were donated by Dr. An Zwijsen from the Katholieke Universiteit Leuven, Belgium. These mice are designed to generate a null allele when combined with germline deleter Cre strains.

The target vector to generate Smad5$^{fl/fl}$ was designed to insert a loxP site before and after the exon 2 of the Smad5 gene followed by a neomycin selection cassette in reverse orientation to the gene and a loxP site (**Figure 6**) (23, 146).

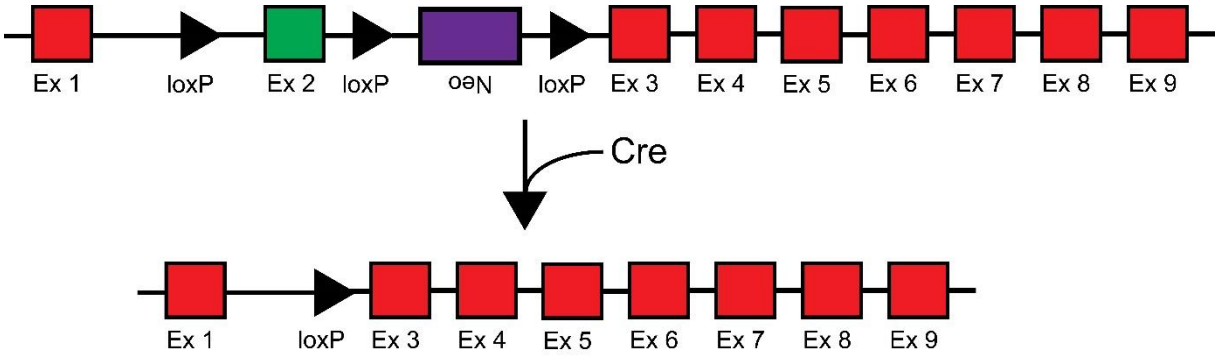

Figure 6. Schematic diagram of the Smad5$^{fl/fl}$ construct before and after the Cre-recombinase. Smad5$^{fl/fl}$ conditional mutant mice have a loxP site before and after the exon (Ex) 2 of the Smad5 gene followed by a neomycin (Neo) cassette in reverse orientation to the gene and a loxP site after the Neo cassette. Smad5$^{fl/fl}$ mice can be crossed with germline deleter Cre mice to produce offspring with a Smad*5* null allele.

2.3.7 Generation of knockout mice

The mTmG mice were crossed with the Cre-ER^{T2} mice to generate the Cre-ER^{T2}-mTmG mice. This strain was employed in the heterozygous state with a C57BL/6J background. The Smad5$^{fl/fl}$ conditional mutant mice were crossed with the Cre-ER^{T2} mice to generate Cre-ER^{T2}-Smad5$^{fl/fl}$ mice. This strain was used in the homozygous state with a C57BL/6J background. The miR-135b$^{lacZ,fl/lacZ,fl}$ mice were crossed with Flp mice, which removed the lacZ cassette and the neomycin cassette restoring the wild type loxP conditional miR-135b floxed allele to generate the miR-135b$^{fl/fl}$ mouse. The miR-135b$^{fl/fl}$ mice were crossed with the Cre-ER^{T2} mice to generate Cre-ER^{T2}-miR-135b$^{fl/fl}$ mice. This strain was always employed in the homozygous state with a C57BL/6J background. To induce tamoxifen-responsive genes, the newborn pups were injected intraperitoneal (IP) on postnatal day (P)1 and P2 with 0.1 mg/kg in 10 µl miglyol per gram of mouse. This protocol has been developed and validated because the tamoxifen treatment of newborn pups under hyperoxic conditions is poorly tolerated (125). The Cre-ER^{T2}-mTmG mice were injected with the vehicle miglyol, referred as mT mice, and with tamoxifen, referred as mG mice (**Figure 7A**). The Cre-ER^{T2}-Smad5$^{fl/fl}$ mice, which were injected with tamoxifen are referred as Smad5$^{Global\ induced\ Deletion}$ ($^{Gi\Delta}$) mice (**Figure 7B**). The Cre-ER^{T2}-miR-135b$^{fl/fl}$

mice, which were injected with tamoxifen are referred as miR-135b$^{Gi\Delta}$ mice (**Figure 7C**).

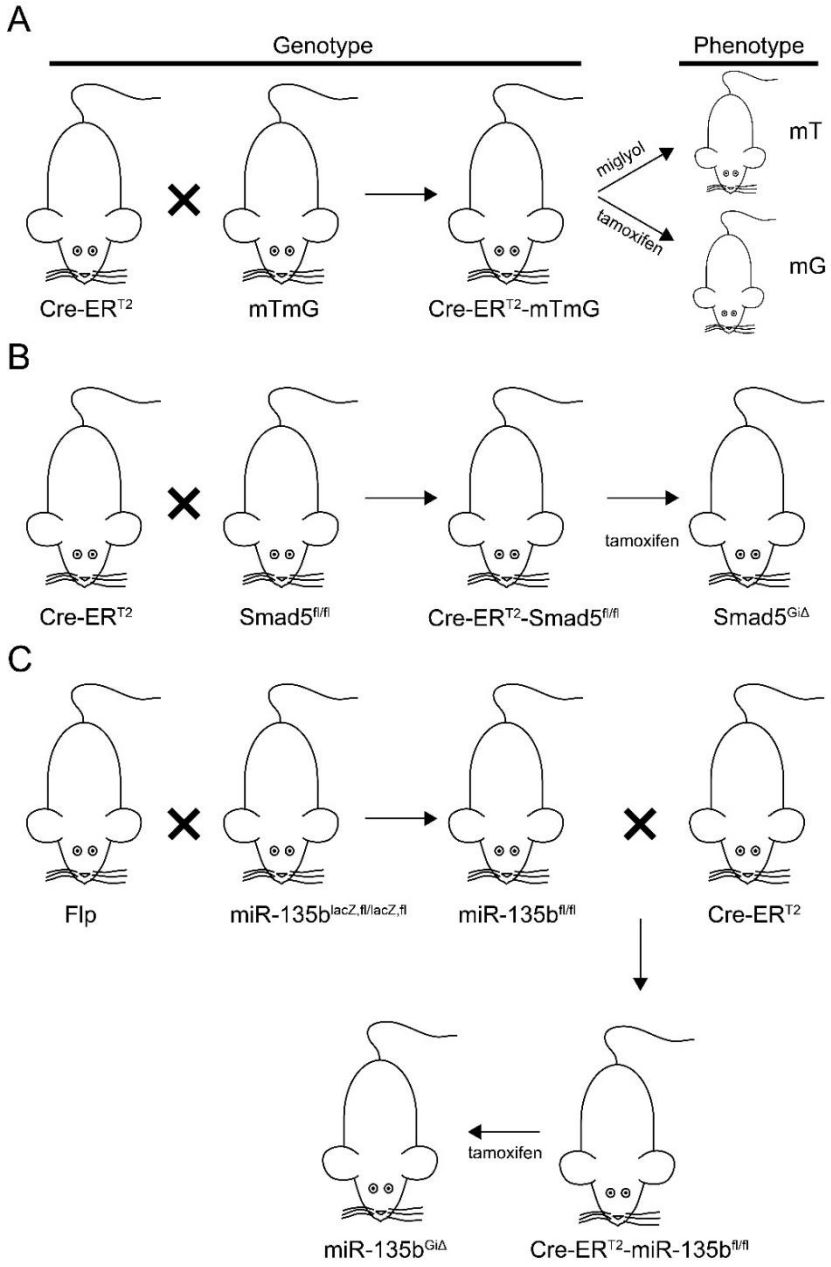

Figure 7. Generation of the knockout mice.

A) Germline deleter Cre-ER^{T2} mice were crossed with mTmG conditional mutant mice to generate the Cre-ER^{T2}-mTmG mice. Cre-ER^{T2}-mTmG mice were intraperitoneal (IP) injected on postnatal day (P)1 and P2 with miglyol or tamoxifen to generate the mT mutant mice or the mG mutant mice, respectively. B) Germline deleter Cre-ER^{T2} mice were crossed with Smad5$^{fl/fl}$ conditional mutant mice to generate the Cre-ER^{T2}-Smad5$^{fl/fl}$ mice. Cre-ER^{T2}-Smad5$^{fl/fl}$ mice were IP injected on P1 and P2 with tamoxifen to generate the Smad5$^{Gi\Delta}$ mice. C) Germline deleter Flp mice were crossed with miR-135b$^{lacZ,fl/lac,fl}$ conditional mutant mice to generate the miR-135b$^{fl/fl}$ conditional mutant mice. miR-135b$^{fl/fl}$ mice were crossed with germline deleter Cre-ER^{T2} mice to generate the mouse strain Cre-ER^{T2}-miR-135b$^{fl/f}$ conditional mutant mice. Cre-ER^{T2}-miR-135b$^{fl/fl}$ mice were IP injected on P1 and P2 with tamoxifen to generate the miR-135b$^{Gi\Delta}$ mice.

2.4 The hyperoxia-based mouse model of bronchopulmonary dysplasia

The newborn mouse pups were randomized to litters of equal size per nursing dam and placed into oxygen chambers (BioSpherix, Ltd., USA) under normoxic (21% O_2), hyperoxic (60% O_2) or severe hyperoxic (85% O_2) conditions within the first 4 h of birth from P1 to P14 in order to model BPD (103). The oxygen was maintained constant in the animal chambers using an oxygen control (BioSpherix, Ltd., USA, #ProOx 110) and daily monitored. All the mice were maintained on a 12 h:12 h dark:light cycle, and provided with food and water *ad libitum*. The nursing dams were rotated every 24 h to avoid oxygen toxicity (39). Newborn mouse lungs were collected at P2-P3, which is the phase prior the peak of the period of bulk secondary septation; at P5, which is the peak of the period of bulk secondary septation; at P7, which is directly after the peak of the period of bulk secondary septation; at P10, which is considered to be the time point when the bulk secondary septation has been ended; and at P14, which is the time point preceding microvasculature maturation (113, 129). The newborn mouse pups were killed by an overdose of 500 mg/kg Narcoren (Merial GmbH, Germany) with an IP injection.

2.5 Animal treatments

2.5.1 AntimiR treatment

The newborn mouse pups were randomized to litters of equal size per nursing dam on the day of birth and IP injected on P1 and P3 with locked-nucleic acid (LNA)-stabilized scrambled antimiR (5′-ACGTCTATACGCCCA-3′; Exiqon, Denmark) or an LNA-stabilized antimiR directed against miR-135b-5p (antimiR-135b-5p; 5′-AGGAATGAAAAGCCAT-3′; Exiqon, Denmark), at a dose of 10 mg/kg. The LNAs were diluted in nuclease-free water (Thermo Fisher Scientific, USA, #AM9930). The animals were exposed to 21%O_2, 60%O_2 and 85%O_2 and sacrificed at P14.

2.5.2 Target site blocker treatment

The newborn mouse pups were randomized to equal number of litter size per nursing dam on the day of birth and IP injected on P1 and P3 with target site blocker (TSB) control (Scrambled) (5′-TAACACGTCTATACGCCCA-3′; Exiqon, Denmark) and a TSB directed to target the interaction between the mmu-miR-135b-5p binding sites in the mouse Smad5 3′-UTR and miR-135b-5p (5′-AGTTATGGCTTTCAAAAGCACAATAT-3′, Exiqon, Denmark), at a dose of 10 mg/kg. The TSBs were diluted in nuclease-free water (Thermo Fisher Scientific, USA, #AM9930).

2.6 Total RNA isolation

Total RNA was isolated from mouse lungs, human alveolar epithelial (hAE) cells, mouse AEII cells, mouse AEI cells and A549 cells using the miRNeasy® Mini kit (Qiagen, Germany, #217004). Left lung was placed into 2 ml tubes containing ceramic beads (Bertin GmbH, Germany, #KT03961-1-009.2) and homogenized using a Precellys 24-Dual homogenizer (VWR, USA). The hAE, mouse AEII, mouse AEI and A549 cells were scraped in lysis buffer. Total RNA from lung tissue and from cells was resuspended in 50 µl and 30 µl nuclease-free water, respectively.

2.7 Gene expression analysis

The concentration of total RNA was determined using a NanoDrop One Microvolume UV-Vis Spectrophotometer (Thermo Fisher Scientific, USA, # ND-ONE-W). For miRs, 100 ng/µl total RNA was used to prepare cDNA using the miScript II RT Kit (Qiagen, Germany, # 218161). Below in table 4 are reported in detail the components used to prepare cDNA for miRs.

Table 4. Components used to prepare cDNA for miR analysis.

The listed components and volumes for one sample were suggested by the company**.**

Component	1 sample (µl)
Nuclease-free H_2O	10
5× miScript HiSpec Buffer	4
10× miScript Nucleics Mix	2
miScript Reverse Transcriptase Mix	2
RNA (100 ng/µl)	2
	Total 20

The samples were placed into a thermocycler (VWR, USA) and retrotranscribed with the following protocol listed in table 5.

Table 5. Procedure to prepare cDNA for miR gene analysis.

The steps, the reactions, the temperature, and the reaction time for one sample were suggested by the company.

Step	Reaction	Temperature	Time
1	Incubation	37 °C	60 min
2	Inactivation	95 °C	5 min
3	Storage	4 °C	∞

At the end of the procedure, the cDNA was diluted in 200 µl of nuclease-free water. For mRNA analysis, 1000 ng/µl of total RNA was used to prepare cDNA. In detail, the

first step was to prepare 20 µl containing 1000 ng/µl of total RNA and successively to denaturate into a thermocycler for 10 min at 70 °C. In the second step, the denatureted RNA was retrotranscribed in cDNA using the following components listed in table 6.

Table 6. Components used to prepare cDNA for gene expression analysis.

The steps, the reactions, the temperature, and the reaction time for one sample were previously established (6).

Component	1 sample (µl)
Nuclease-free H_2O	1
GeneAmp™ 10× PCR Buffer	4
Magnesium chloride solution (25 mM)	8
dNTP Mix (10 mM)	2
Random Hexamers (50 µM)	2
RNase Inhibitor (20 U/µl)	1
M-MLV Reverse Transcriptase (50 U)	2
RNA (1000 ng/µl)	20
	Total 40

Abbreviations: dNTP, Deoxynucleotide Triphosphates; M-MLV, Moloney Murine Leukemia Virus.

The samples were placed into a thermocycler and retrotranscribed with following protocol listed in table 7.

Table 7. Procedure to prepare cDNA for mRNA analysis.

The steps, the reactions, the temperature and the reaction time for one sample were previously established (6).

Step	Reaction	Temperature	Time
1	Incubation	21 °C	10 min
2	Extension	43 °C	75 min
3	Enzyme Inactivation	95 °C	5 min
4	Storage	4 °C	∞

At the end of the procedure, the cDNA was diluted in 60 µl of nuclease-free water. The real-time PCR or the quantitative polymerase chain reaction (qPCR) was performed using the Platinum™ SYBR™ Green qPCR SuperMix-UDG (Thermo Fisher Scientific, USA, #11733046) and the miScript SYBR Green PCR Kit (Qiagen, Germany, #218073) to study changes in gene expression for mRNA for miRs respectively. The qPCR was assessed in the StepOne™ Real-Time PCR System (Thermo Fisher Scientific, USA, #4376357) and the cycling conditions are reported in table 8.

Table 8. Real time PCR cycling conditions.

The steps, the reactions, the temperature, and the reaction time for one sample were previously established (6).

Step	Reaction		Temperature	Time
1	Denaturation		95 °C	5 min
2	Denaturation	40×	95 °C	5 s
3	Annealing		59 °C	5 s
4	Extension		72 °C	30 s
5	Final Extension		72 °C	5 min
6	Melting Curve Analysis			30 min
7	Storage		4 °C	∞

For qPCR analysis, ΔCt were assessed as mean Ct (reference gene) – Ct (gene of interest), where the Polr2a gene and the Rnu6 gene for mouse and the POLR2A gene and the RNU6 gene for human were used as reference genes for mRNA and miRs analysis respectively. Primers were purchased from Qiagen and Eurofins Scientific to study the expression levels of miRs and mRNA respectively. The primer pairs were designed intron-spanning and were validated. The primers and the primer sequences employed in in the mRNA analysis are listed in table 9 and the primers employed for the miRs study are listed in table 10.

Table 9. List of primers used for mRNA analysis.

mRNA analysis		
Mus musculus		
Gene	Forward (5′ - 3′)	Reverse (5′ - 3′)
Smad1	GCTTCGTGAAGGGTTGGGG	CGGATGAAATAGGATTGTGGGG
Smad5	TTGTTCAGAGTAGGAACTGCAAC	GAAGCTGAGCAAACTCCTGAT
Smad9	CGGGTCAGCCTAGCAAGTG	GAGCCGAACGGGAACTCAC
Polr2a	CTAAGGGGCAGCCAAAGAAAC	CCATTCAGCATACAACTCTAGGC
Homo sapiens		
SMAD5	CCAGCAGTAAAGCGATTGTTGG	GGGGTAAGCCTTTTCTGTGAG
POLR2A	GCGGAATGGAAGCACGTTAAT	CCCAGCACAAAACACTCCTC

Table 10. List of primers used for miR analysis.

miRs analysis *Mus musculus*		
Name	Sequence (5′ - 3′)	Catalogue number (Qiagen)
mmu-miR-135b-5p	UAUGGCUUUUCAUUCCUAUGUGA	MS00001575
hsa-Rnu6	CGCTTCGGCAGCACATATACTA	MS00033740
Homo sapiens		
Name	Sequence (5′ - 3′)	Catalogue number (Qiagen)
hsa-miR-135b-5p	UAUGGCUUUUCAUUCCUAUGUGA	MS00003472
hsa-Rnu6	CGCTTCGGCAGCACATATACTA	MS00033740

2.8 Total protein isolation

Total proteins were isolated from mouse lungs, hAE, mouse AEII and A549 cells using a protein lysis buffer composed of RIPA buffer (Sigma-Aldrich, Germany, #R0278), 1 mM of sodium orthovanadate (Sigma-Aldrich, Germany, #S6508) and cOmplete™, Mini, EDTA-free Protease Inhibitor Cocktail (Merck KGaA, Germany, #11836170001). Right lung was placed into 2 ml tubes containing ceramic beads and homogenized using a Precellys 24-Dual homogenizer. HAE, mouse AEII, mouse AEI and A549 cells were scraped in lysis buffer. The lungs and cell lysates were placed on ice for 10 min and transferred into a 1.5 ml tube. Tubes were centrifuged at 13000 rpm for 15 min using a refrigerated microcentrifuge (VWR, USA, # CT15RE) at 4 °C. The supernatant was transferred in a new tube. To measure protein concentration, sample and lysis buffer were diluted 1:50 in double distilled water (ddH_2O) if the proteins were extracted from lung tissue or 1:10 in ddH_2O if the proteins were extracted from cells. From the diluted proteins, 10 µl were pipetted in a 96-well plate (Greiner Bio-One GmbH, Germany, #655180). Bovine serum albumin (BSA) (Thermo Fisher Scientific, USA, # 11733046, P/N 55213) was prepared at different concentrations (0.05 µg, 0.10 µg, 0.20 µg, 0.30 µg, 0.40 µg and 0.50 µg) as protein standard and 10 µl was added to the 96-well plate. Moreover, 200 µl of Quick Start™ Bradford 1× Dye Reagent (Bio-Rad, USA, #5000205) was added to each well, left incubating for 5 min at room temperature and measured into a spectrophotometer Infinite® 200 PRO (Tecan, Germany, #M200PRO) at 570 nm wavelength. The protein concentration from each sample was calculated using the BSA standard curve as reference.

2.9 Electrophoresis and western blot

An amount of 25 µg of proteins was prepared for each sample and mixed with 2× (Bio-Rad, USA, #1610737) or 4× Laemmli sample buffer (Bio-Rad, USA, #1610747) containing 5% 2-Mercaptoethanol (Sigma-Aldrich, Germany, #M6250). Proteins were denatured for 6 min on 95 °C, loaded on a 10% sodium dodecyl sulphate (SDS) (Promega, USA, #V6553) polyacrylamyde gel (PAGE) and resolved at 100 mV in running buffer. After the Laemmli sample buffer has reached the end of the resolving gel, the SDS-PAGE was removed and proteins were transferred to a nitrocellulose membrane (Bio-Rad, USA, #1704158) using the Trans-Blot Turbo Transfer System (Bio-Rad, USA). The nitrocellulose membrane was incubated for 5 min with Ponceau S (Sigma-Aldrich, Germany, #P3504) to observe the correct loading and transfer. The membrane was washed for 2 min in ddH_2O and incubated for 1 h in 5% milk (Carl Roth,

Germany, #T145.5) used as blocking buffer. Successively, the membrane was incubated with primary antibody in blocking buffer over night at 4 °C. Afterward, the membrane was washed in washing buffer 6× for 5 min and incubated for 1 h at room temperature in horseradish-peroxidase-conjugated secondary antibody diluted in blocking buffer. Successively, the membrane was washed in washing buffer 6× for 5 min and incubated in SuperSignal® West Femto chemiluminescent substrate (Thermo Fisher Scientific, USA, #34096) for 5 min at room temperature. The proteins were visualized using the ImageQuant LAS 4000 (GE Healthcare, United Kingdom). After, the membrane was washed in washing buffer 6× for 5 minutes and stored or stripped using a Restore™ Western Blot Stripping Buffer (Thermo Fisher Scientific, USA, #21059) for removing the primary and secondary antibodies bound or a Restore™ PLUS Western Blot Stripping Buffer (Thermo Fisher Scientific, USA, #46428) for removing high-affinity primary and secondary antibodies bound. Gel and buffer preparation for western blot are listed in table 11. The primary antibodies used in western blot analysis are listed in table 12.

Table 11. Gel and buffer preparation during the western blot procedure.

Stacking Gel	Resolving Gel
5% Rotiphorese® Gel 30 (37,5:1) 125 mM Tris-Cl, pH=6.8 0.05% SDS 0.05% Ammonium persulfate 0.065% TEMED	10% Rotiphorese® Gel 30 (37,5:1) 375 mM Tris-Cl, pH=8.8 0.05% SDS 0.05% Ammonium persulfate 0.065% TEMED
Running Buffer	Blocking Buffer
250 mM Tris-Cl 2.5 M Glycine 1% SDS	1× PBS 0.2% Tween® 20 5% Powdered Milk
Washing Buffer	Ponceau S
1× PBS 0.2% Tween® 20	0.1% Ponceau S 0.87 M Acetic acid

Abbreviations: PBS, Phosphate buffered saline; SDS, sodium dodecyl sulphate; TEMED, N,N,N′,N′-tetramethylethylenediamine.

Table 12. Primary antibodies used in western blot analysis.

Antigen	Host Animal	Dilution	Catalogue Number	Company
Smad5	Goat	1:400	sc-7443	Santa Cruz Biotechnology
Smad1	Rabbit	1:1000	9743	Cell Signaling Technology, Inc.
Smad9	Rabbit	1:400	PA5-35162	Thermo Fisher Scientific
β-Actin	Rabbit	1:1000	4967	Cell Signaling Technology, Inc.
SP-C	Rabbit	1:1000	ab211326	Abcam
Aquaporin 5	Rabbit	1:500	ab78486	Abcam
Smad5	Mouse	1:400	sc-101151	Santa Cruz Biotechnology

Abbreviations: SP-C, Prosurfactant Protein C.

2.10 Designed-based stereology

The methods employed for the analysis of lung architecture were based on the American Thoracic Society and the European Respiratory Society recommendations (56). Newborn mouse pups were killed at P14 and mouse lungs were instilled and fixed though a blunt needle G24 (CML SUPPLY, USA, #901-24-050) applying a hydrostatic pressure of 20 cmH_2O. The fixative was prepared with 1.5% paraformaldehyde (PFA) (Sigma-Aldrich, Germany, # P6148), 1.5% glutaraldehyde 50% (Serva Electroforesis GmbH, Germany, #23116.02), 150 mM HEPES solution (Sigma-Aldrich, Germany, #H0887) dissolved in phosphate buffered saline 1× (PBS) (Sigma-Aldrich, Germany, #D1408) at pH 7.4 at 4 °C. The lungs were isolated intact with thymus, esophagus, trachea, and heart and kept in the fixative for 24 h at 4 °C. Thymus, esophagus, trachea, and heart were carefully removed. The next day, the lung was dried delicately with an askina cellulose swab (B. Braun, Germany, #9051015) and processed to measure lung volume applying the Archimede´s principle (128). Lungs were embedded in 2% agar (Sigma-Aldrich, Germany, #05039) and cut in 3-mm sections applying the random uniform sampling for stereology analysis (58, 130). Every section was pictured with same orientation over a millimeter paper using a camera (Nikon Corporation, Japan, #D5300). Successively, every section was used to estimate lung volume by the Cavalieri's principle using the software ImageJ (NIH, USA) (88). Every lung was placed into a glass vial under a fume hood to be embedded in plastic. In detail, the lungs were washed 4× for 5 min with 0.1 M sodium cacodylate trihydrate (Serva Electroforesis GmbH, Germany, #15540.03), then treated with 1% osmium tetroxide (Carl Roth,

Germany, #8371.3), washed again 4× for 5 min with 0.1 M sodium cacodylate trihydrate, washed then with ddH_2O 8× for 5 min, and treated with 2.5% uranyl acetate (Serva Electroforesis GmbH, Germany, #77870.02) over night. Next day, lungs were washed with ddH_2O for 4× for 5 min until the "yellowish" color of uranyl acetate went off. Lungs were treated 2× for 1 h with 70% acetone (Carl Roth, Germany, #CP40.2), 2× for 1 h with 90% acetone and 1× for 1 h with 100% acetone. Lungs were kept overnight with a 1:1 solution of 100% acetone:glycol methacrylate and hardener 1 (Technovit® 7100) (Kulzer GmbH, Germany, #64709003). The next day, the 1:1 solution of 100% acetone:glycol methacrylate and Technovit® 7100 was removed, and lungs were treated with Technovit® 7100 overnight. The Technovit® 7100 was removed and 3 ml of fresh Technovit® 7100 and 200 µl of hardener 2 were added to each lung. Every lung was mixed for 3 min and placed into the embedding mould (Kulzer GmbH, Germany, #12025). After 2 min, the 3 ml Technovit® 7100 and the 200 µl hardener 2 were added to each lung into the embedding mould. Lungs were kept in the fume hood for 48 h to allow the glycol methacrylate to solidify. Histoblocs (Kulzer GmbH, Germany, #64708995) were placed over each lung and a mixture of 10 g of Technovit® 3040 Powder and 5 ml of Technovit® Universal Liquid was poured slowly between the histobloc and the embedded lungs. The lung blocks were removed from the embedding mould and every block was sectioned using a microtome (Leica, Germany, #RM2255). To determine the total number of alveoli and the alveolar density, each lung block was cut into sections of 2 µm, and every first and third section of a consecutive series of sections throughout the block was used for analysis using the physical dissector approach (58, 138). For all other parameters, the mean linear intercept (MLI), the septal thickness and the total surface area of gas exchange, every tenth section of a consecutive series throughout the block was used for analysis (4 sections per block) (84, 85, 91, 97-99, 107, 130). Every section was stained with Richardson staining (117). Slides were scanned using digital slide scanner (Hamamatsu Photonics, Japan, #NanoZoomer-XR C12000). The analysis was assessed using the Visiopharm's newCAST™ computer-assisted stereology system (Visiopharm A/S, Denmark). MLI, septal thickness, total surface area of gas exchange, as well as alveolar number and alveolar density were estimated as described in previous scientific article (84, 91). In each case, 3-10% of each section was analysed. The coefficient of error (CE), the coefficient of variation (CV), as well as the squared

ratio between both (CE^2/CV^2) were measured for each stereological parameter. The quotient threshold was set at 0.5 to validate the precision of the measurements.

2.11 Cryosections

Mouse pups exposed to 21% O_2 and 85% O_2 for the first fourteen days of postnatal life were sacrificed at P14. The thoracic cavity was opened, and lungs were perfused with 1× PBS *via* the right ventricle. A tracheotomy was performed, and lungs were fixed with a solution 1:1 of Tissue-Tek® O.C.T.™ Compound (O.C.T.) (Science Services GmbH, Germany, #4583) and 1× PBS. Lungs were carefully removed and embedded in cryomolds (Thermo Fisher Scientific, USA, #1830TS) with O.C.T. and stored at -80 °C. The lung blocks were taken out from the cryomold and sectioned at 10 µm thickness using a cryomicrotome (Leica, Germany, #3050S). Sections were attached to glass slide and used to perform *in situ* hybridization and *in situ* β-galactosidase activity detection.

2.12 Fluorescent *in situ* hybridization

The fluorescent *in situ* hybridization (FISH) protocol was adapted using the protocol published by Silahtaroglu *et al.* (134). The lung sections were placed at room temperature under a fume hood for 3 min, and a circle was drawn around the lung tissue using a delimiting pen (Thermo Fisher Scientific, USA, #008899). Lung tissues were fixed with a 4% PFA for 10 min and successively were washed with diethyl pyrocarbonate (DEPC) (Sigma-Aldrich, Germany, #D5758)-PBS 3× for 5 min. Lung tissues were treated with acetylation buffer for 5 min to reduce background and increase permeability of the tissue and washed for 3× for 5 min in DEPC-PBS. Every section was treated with hybridization mixture for 30 min in a slide hybridizer (Boekel Industries, Inc., USA, #240000) at 56 °C. Successively, three different hybridization mixtures were prepared containing i) no probe, served as negative control, ii) 5 pmol locked nucleic acid (LNA) Rnu6 probe (Qiagen, Germany, #699002-310), served as positive control and iii) 5 pmol LNA miR-135b-5p probe (Qiagen, Germany, #616712-330). Lung sections were separately treated with the hybridization mixtures and incubated for 1 h at 56 °C in a slide hybridizer. Lung sections were washed with 0.1% Saline-sodium citrate (SSC) solution (Thermo Fisher Scientific, USA) for 10 min at 60 °C, to remove partially bound probes that could cause background staining, and a final wash with 5% SSC at room temperature for 5 min. Lung tissues were treated with 3% H_2O_2 (Merck KGaA, Germany, #107209) for 15 min to block endogenous peroxidases. Lungs were washed with Tris-Sodium Chloride (TN) buffer 3× for 5 min

and incubated in blocking buffer (Hoffmann-La Roche, Switzerland, #11096176001) for 30 min at room temperature. Every lung section was incubated with 150 µl of Anti-Fluorescein-Horseradish-peroxidase (POD), Fab fragments (Hoffmann-La Roche, Switzerland, #11426346910) for 30 min at room temperature and then washed with TNT buffer 3× for 5 min. Sections were incubated with 1:50 fluorescein isothiocyanate (FITC)-tyramide diluted in amplification buffer (PerkinElmer, USA, #NEL741) for 10 min at room temperature in darkness. Lung tissues were washed 3× for 5 min with Tris-Sodium Chloride-Tween (TNT) buffer and successively treated 1:5000 with 4′,6-diamidino-2-phenylindole (DAPI) (Thermo Fisher Scientific, USA, #D3571). Sections were washed 1× with 1× PBS, mounted with a cover slide using Fluoromount W (Serva Electroforesis GmbH, Germany, #21634) and stored over night at 4 °C to develop the signal. Every section was analyzed using a confocal microscope (Carl Zeiss, Germany, LSM710). The buffers used for *in situ* hybridization are listed in table 13.

Table 13. Buffer preparation for *in situ* hybridization.

Acetylation Buffer	Hybridization Mixture
6 M HCl 2 M Triethanolamine 0.6 M Acetic Anhydride in DEPC-PBS	50% Formamide 500 mg/ml Yeast tRNA 5× SSC 1× Denhardt's solution in DEPC-PBS
TN Buffer	TNT Buffer
0.1 M Tris-Cl, pH 7.5 0.15 M NaCl	0.1 M Tris-Cl, pH 7.5 0.15 M NaCl 0.3% Triton X-100

Abbreviations: DEPC, diethyl pyrocarbonate; PBS, Phosphate buffered saline; SSC, Saline-sodium citrate; TN, Tris-Sodium Chloride; TNT, Tris-Sodium Chloride-Tween.

2.13 *In situ* β-galactosidase activity detection

Sections with mouse lungs were fixed in 0.5% glutaraldehyde in 1× PBS for 10 min at 4 °C, washed in 1 mM $MgCl_2$ (Sigma-Aldrich, Germany, #208337) in 1× PBS for 2× for 15 min and incubated in 5-bromo-4-chloro-3-indolyl-β-D-galactopyranoside (X-Gal) (Carl Roth, Germany, #2315) buffer for 10 s. Sections were incubated with 1 mg/ml X-Gal in X-Gal buffer at 37 °C overnight in darkness. The sections were washed with 1 mM $MgCl_2$ in 1×PBS 1× for 15 min at room temperature and, successively, fixed in

4% PFA in 1× PBS for 4 min. Sections were dehydrated in a graduated ethanol in series (100%, 96% and 70%) for 5 min each, washed in 1× PBS for 5 min at room temperature, followed by 1% eosin (Merck KGaA, Germany, #45380) staining in 1:4 solution ddH_2O and 100% ethanol for 1 min at room temperature. Sections were observed using a light microscope (Leica, Germany, #DM6000B). The preparation of the X-Gal is described in table 14.

Table 14. Buffer preparation for *in situ* β-galactosidase activity detection.

X-Gal Buffer
5 mM potassium ferrocyanide (II)
5 mM potassium ferricyanide (III)
1 mM $MgCl_2$ in 1× PBS, pH 7.0

Abbreviations: PBS, Phosphate buffered saline; X-Gal, 5-bromo-4-chloro-3-indolyl-β-D-galactopyranoside.

2.14 Fluorescence-activated cell sorting

Lungs from P14 wild type mice exposed to 21% O_2 and 85% O_2 were prepared by instilling approximately 300 µl of dispase into the lung, followed by incubation for 30 min at 37 °C. Lungs were placed in tubes with DMEM medium (Thermo Fisher Scientific, USA, #61965), 10 mM HEPES, 1% penicillin-streptomycin (P/S) (Thermo Fisher Scientific, USA, #15140122) and 0.01% Deoxyribonuclease I (DNase) from bovine pancreas (Merck KGaA, Germany, #260913), and homogenized using the gentleMACS™ dissociator. The homogenized mixture was filtered using as first a 100 µm filter (Greiner Bio-One GmbH, Germany, #542000) and as second a 40 µm filter (Greiner Bio-One GmbH, Germany, #542040). The filtered lung cell suspension was washed with 1×PBS and centrifuged at 1300 g for 15 min at 4 °C. The pellet was resuspended in Fluorescence-activated cell sorting (FACS) buffer and prepared for FACS. The gating strategy started with back gating, doublets exclusion, live cells selection, Epithelial cell adhesion molecule ($EpCAM^+$) cell selection, alveolar epithelial cell selection and selection of the AEI and AEII cells is illustrated in Figure 8. The AEI and AEII cells were sorted using the antibodies listed in table 15.

Table 15. Antibody used in fluorescence-activated cell sorting.

Antibody	Color	Clone	Company
Live dead stain	Pacific Blue		Thermo Fisher Scientific
CD31	FITC	390	BioLegend
CD45	FITC	30-F11	BioLegend
EpCAM	APC-Cy7	G8.8	BioLegend
CD49f	PE	GoH3	BioLegend
T1α	APC	8.1.1	BioLegend

Abbreviations: CD31, Platelet endothelial cell adhesion molecule; CD45, Protein tyrosine phosphatase, receptor type, C; CD49f, Integrin alpha-6; EpCAM, Epithelial cell adhesion molecule; FITC, Fluorescein isothiocyanate; T1α, Podoplanin.

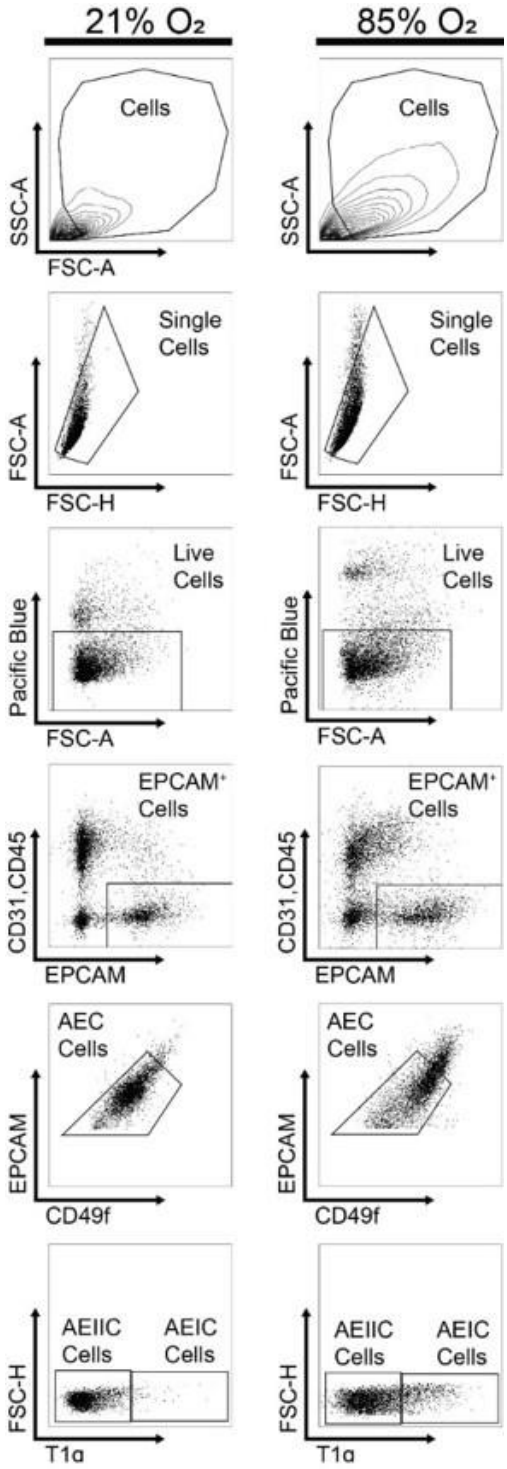

Figure 8. Gating strategy for fluorescence-activated cell sorting of alveolar epithelial type I and type II cells in lung tissue.

Illustration of alveolar epithelial type I (AEI) cells and alveolar epithelial type II (AEII) cells isolation from P14 mouse lungs. The gating strategy begins with back gating, doublets exclusion, live cells selection, $EpCAM^+$ cell selection, alveolar epithelial cell selection and selection of the AEI cells and AEII cells. AEC, Alveolar epithelial cells; AEIC, Alveolar epithelial type I cells; AEIIC, Alveolar epithelial type II cells; CD31, Platelet endothelial cell adhesion molecule; CD45, Protein tyrosine phosphatase, receptor type, C; CD49f, Integrin alpha-6; EpCAM, Epithelial cell adhesion molecule; FSC-A, forward scatter area; FSC-H, forward scatter height; SSC-A, side scatter area; T1α, Podoplanin.

2.15 Cell culture

2.15.1 Mouse alveolar epithelial type II cells

Primary mouse AEII cells were isolated using a modified isolation protocol from Corti *et al*. (27). The thoracic cavity was opened, and lungs were perfused with Hank´s Balanced Salt Solution (HBSS) (Thermo Fisher Scientific, USA, #14175-046) *via* the right ventricle. The *Vena cava* was cut, and lungs were perfused again with HBSS. A tracheotomy was performed, and lungs were instilled with a 37 °C pre-hit 1:1 mixture of dispase (Corning Incorporated, USA, #354235) and low melting point agar (Sigma-Aldrich, Germany, #A9414) using a blunt needle G24 (CML SUPPLY, USA, #901-21-050). After 5 min, the lungs were carefully removed and incubated in 2 ml of dispase at room temperature for 45 min. Under a laminar flow cabinet (Thermo Fisher Scientific, USA, #Safe2020), every lung was dissected in a Petri dish with 7 ml of DMEM medium (Thermo Fisher Scientific, USA, #61965), 10 mM HEPES, 1% P/S (Thermo Fisher Scientific, USA, #15140122) and 0.01% DNase (Merck KGaA, Germany, #260913), and then incubated for 10 min. The cells were filtered in series through a 100 µm filter (Greiner Bio-One GmbH, Germany, #542000), a 40 µm filter (Greiner Bio-One GmbH, Germany, #542040) and a 20 µm nylon filter (Merck, Germany, #NY2004700). The filtered cell suspension was centrifuged at 800 rpm for 8 min at 4 °C. The pellet was resuspended in DMEM medium containing 10% fetal bovine serum (FCS) (Thermo Fisher Scientific, USA, #26140079). The cells were stained with trypan blue solution (Thermo Fisher Scientific, USA, #15250061) and living cells were counted using a Neubauer chamber. The cells were centrifuged at 800 rpm for 8 min at 4 °C, were resuspended in DMEM without FCS and incubated with biotinylated anti-CD45 (0.9 µl per million cells) [BD (Becton Dickinson, #553078)], biotinylated anti-CD16/32 (0.7 µl per million cells) [BD (Becton Dickinson, #553143)] and biotinylated anti-CD31 (0.4 µl per million cells) [BD (Becton Dickinson, #553371)] for 30 min at 37 °C. The Dynabeads™ biotin binder (2.45 µl per million cells) (Thermo Fisher Scientific, USA, #11047) were added to the cell suspension and incubated for 30 min at room temperature, where the AEII cells were negatively selected. The cell suspension was placed into a magnetic separator (Thermo Fisher Scientific, USA, #123.01) for 15 min. The cells were collected and i) resuspended in DMEM with 10% FCS and 1% P/S, and cultured on a 6-well plate containing a 24 mm Transwell® with 0.4 µm pore polyester membrane insert (Corning Incorporated, USA, #3450) in an air-liquid; or ii) resuspended in protein lysis buffer to study protein expression.

2.15.2 Human alveolar epithelial cells

The hAE cells (Cell Biologics Inc, USA, #H-6053) were isolated from normal human lung tissue and were cultured in human epithelial cell medium supplement kit (Cell Biologics Inc, USA, #H6621).

2.15.3 A549 cells

A549 cell line (American Type Culture Collection, USA) is an adenocarcinoma human alveolar basal epithelial cell line. These cells were cultured in DMEM/F-12 (Thermo Fisher Scientific, USA, #11320033) medium with 10% FCS and 1% P/S.

2.15.4 Hyperoxia treatment

The mouse AEII, hAE and the A549 cells were exposed to 21% O_2 and 85% O_2 conditions for 24 h or 48 h and total RNA and proteins were isolated.

2.15.5 Mimic treatment

The A549 cells were seeded at a concentration of 1×10^5 in 2 ml in a 6-well plate for cell culture (Greiner Bio-One GmbH, Germany, #657160) and incubated overnight. When the cell confluence was 70%, cells were transfected with a synthetic scrambled miR mimic (Qiagen, Germany, #SI03650318) and a miR-135b-5p mimic (Qiagen, Germany, #MSY0000758) for 48 h with 80 nM; using Lipofectamine™ 3000 (Thermo Fisher Scientific, USA, #L3000008) and Opti-MEM™ Reduced Serum Medium (Thermo Fisher Scientific, USA, #51985034) following the manufacture´s guidelines. Briefly, scrambled miR mimic and miR-135b-5p mimic, respectively, were incubated with i) lipofectamine™ 3000, ii) P™ 3000 and iii) Opti-MEM™ Reduced Serum Medium for 15 min to form the mimic-lipid complex. The mimic-lipid complex was added to the cells and incubated for 6 h. After, DMEM/F12 medium (Thermo Fisher Scientific, USA, #11320033) was added and cells could grow for 48 h. Efficiency of cell transfection was analyzed *via* qPCR. Total proteins were isolated and analyzed *via* western blot.

2.15.6 Cell proliferation assay

The A549 cells were seeded at a concentration of 8000 cells in 100 µl per well of a 96-well plate for cell culture (Greiner Bio-One GmbH, Germany, #655180) and incubated overnight. Cells were transfected with 80 nM scrambled miR mimic and 80 nM miR-135b-5p mimic as described before. The proliferation was observed by 5-Bromo-2'-deoxyuridine (BrdU) integration using the colorimetric cell proliferation ELISA kit (Hoffmann-La Roche, Switzerland, #11647229001). Cells were starved for 1 h in Opti-MEM™ Reduced Serum Medium, followed by 24 h of DMEM/F12 medium

with 10% FCS and 1% P/S. The signal was developed at 450 nm every 5 min for 30 min using a spectrophotometer Infinite® 200PRO.

2.15.7 Apoptosis assay

The A549 cells were seeded at a concentration of 8000 cells in 100 µl per well of a 96-well plate for cell culture (Greiner Bio-One GmbH, Germany, #655098) and incubated overnight. Cells were transfected with 80 nM scrambled miR mimic and 80 nM miR-135b-5p mimic as described before. Cells were starved for 1 h in Opti-MEM™ Reduced Serum Medium, followed by 24 h of DMEM/F12 medium with 10% FCS and 1% P/S. The apoptosis was detected by caspase 3 and caspase 7 activity using a Caspase-Glo® 3/7 Assay System (Promega, USA, #G8091) after 24 h. For a positive control, 0.5 µM of staurosporine (Cayman Chemical Company, USA, #62996-74-1) was added to the medium for the last 6 h of 24 h period. The signal was developed at 30 min using a spectrophotometer Infinite® 200PRO.

2.15.8 Viability assay

The A549 cells were seeded at a concentration of 8000 cells in 100 µl per well of a 96-well plate for cell culture (Greiner Bio-One GmbH, Germany, #655180) and incubated overnight. Cells were transfected with 80 nM scrambled miR mimic and 80 nM miR-135b-5p mimic as described before. Cells were starved for 1 h in Opti-MEM™ Reduced Serum Medium, followed by 24 h of DMEM/F12 medium with 10% FCS and 1% P/S. The cell viability was observed by the yellow tetrazolium dye 3-(4,5-dimethylthiazol-2-yl)-2,5-diphenyltetrazolium bromide (MTT) reduced to insoluble formazan with purple color using the MTT assay (Merck KGaA, Germany, #11465007001). The signal was developed at 550 nm using a spectrophotometer Infinite® 200PRO.

2.15.9 Target site blocker treatment

The A549 cells were seeded at a concentration of 1×10^5 in 2 ml in a 6-well plate for cell (Greiner Bio-One GmbH, Germany, #657160) and incubated overnight. When the cell confluence was 70%, the cells were transfected as described before with miRCURY LNA™ microRNA target site blockers (TSB) control and a TSB directed to target the interaction between the hsa-miR-135b-5p binding sites in the human SMAD5 3′-UTR and miR-135b-5p: (TSB-Smad5) for 48 h with 80 nM.

2.16 Microarray

Primary mouse AEII cells were isolated as described before and exposed to room air and 85% O_2 for 6 h and 24 h. The miRs were isolated with miRNeasy® Mini kit (Qiagen,

Germany, #217004) and the microRNA expression was performed using Agilent-035430 mouse miRNA array. Microarray analysis (GEO accession number GSE92551) were accomplished by IMGM Laboratories GmbH, Munich, Germany.

2.17 Genotyping

2.17.1 Sex genotyping

Tail biopsies were collected from newborn mice and genomic DNA was isolated using AccuStart™ II Mouse Genotyping Kit (Quantabio, USA, #733-2236). The sex of each mouse was determined by PCR, screening for the male-specific sex determining region of Chr Y (Sry) locus together with the interleukin 3 (Il3) gene present in male and female sex (72). Amplicons were resolved in a 1.5% agarose gel (Agarose NEEO Ultra-Quality, Carl Roth, Germany, #2267) prepared in 1× Tris-acetate-EDTA (TAE) buffer (Carl Roth, Germany, #CL86) and visualized by ethidium bromide (Promega, USA, #H5041). The amplification protocol, the primers and the PCR cycling conditions are listed respectively in table 16, table 17 and table 18.

Table 16. Components used to amplify genomic DNA for sex genotyping.

Component	1 sample (µl)
Nuclease-free H_2O	31.15
5× Green GoTaq® Flexi Buffer	10
Magnesium chloride solution (25 mM)	4
dNTP Mix (10 mM)	1
Primer pair Il3 (1 mM)	0.6
Primer pair Sry (1 mM)	1
GoTaq® Hot Start Polymerase (500 U)	0.25
Genomic DNA	2
	Total 50

Abbreviations: dNTP, Deoxynucleotide Triphosphates; *Il3*, interleukin 3; *Sry*, sex determining region of Chr Y.

Table 17. List of primers used for sex genotyping.

Gene	Forward (5′ - 3′)	Reverse (5′ - 3′)
Il3	GGGACTCCAAGCTTCAATCA	TGGAGGAGGAAGAAAAGCAA
Sry	TGGGACTGGTGACAATTGTC	GAGTACAGGTGTGCAGCTCT

Abbreviations: Il3, interleukin 3; Sry, sex determining region of Chr Y.

Table 18. PCR cycling conditions for sex genotyping.

Step	Reaction		Temperature	Time
1	Denaturation		95 °C	4.30 min
2	Denaturation	33×	95 °C	35 s
3	Annealing		50 °C	1 min
4	Extension		72 °C	1 min
5	Final Extension		72 °C	5 min
6	Storage		4 °C	∞

2.17.2 Smad5$^{fl/fl}$ mouse genotyping

Tail biopsies were collected from newborn mice and genomic DNA was isolated using AccuStart™ II Mouse Genotyping Kit (Quantabio, USA, #733-2236). The wild type allele and the mutant allele were determined by PCR, screening the Smad5 locus. Amplicons were resolved in a 1.5% agarose gel (Agarose NEEO Ultra-Quality, Carl Roth, Germany, #2267) prepared in 1× TAE buffer and visualized by ethidium bromide (Promega, USA, #H5041). The amplification protocol, the primers and the PCR cycling conditions are listed respectively in table 19, table 20 and table 21.

Table 19. Components used to amplify genomic DNA for genotyping Smad5$^{fl/fl}$ mice.

Component	1 sample (µl)
Nuclease-free H_2O	29.75
5× Green GoTaq® Flexi Buffer	10
Magnesium chloride solution (25 mM)	6
dNTP Mix (10 mM)	1
Primer Pair Smad5 (1 mM)	2
GoTaq® Hot Start Polymerase (500 U)	0.25
Genomic DNA	1
	Total 50

Abbreviations: dNTP, Deoxynucleotide Triphosphates.

Table 20. List of primer used for genotyping Smad5$^{fl/fl}$ mice.

Gene	Forward (5′ - 3′)	Reverse (5′ - 3′)
Smad5	CACTGGCAAAGCAGAGGTTCAGA	GAGCGTCTTCCTTAGCTAATGTG

Table 21. PCR cycling conditions for genotyping Smad5$^{fl/fl}$ mice.

Step	Reaction		Temperature	Time
1	Denaturation		95 °C	5 min
2	Denaturation	39×	95 °C	20 s
3	Annealing		58 °C	40 s
4	Extension		72 °C	1 min
5	Final Extension		72 °C	10 min
6	Storage		4 °C	∞

2.17.3 Cre-ER^{T2} mouse genotyping.

Tail biopsies were collected from newborn mice and genomic DNA was isolated using AccuStart™ II Mouse Genotyping Kit (Quantabio, USA, #733-2236). The presence of the Cre was determined by PCR, screening the Cre locus. Amplicons were resolved in a 1.5% agarose gel (Agarose NEEO Ultra-Quality, Carl Roth, Germany, #2267) prepared in 1× TAE buffer and visualized by ethidium bromide (Promega, USA, #H5041). The amplification protocol, the primers and the PCR cycling conditions are listed respectively in table 22, table 23 and table 24.

Table 22. Components used to amplify genomic DNA for genotyping Cre-ER^{T2} mice.

Component	1 sample (µl)
Nuclease-free H_2O	28.75
5× Green GoTaq® Flexi Buffer	10
Magnesium chloride solution (25 mM)	6
dNTP Mix (10 mM)	1
Primer Pair Cre (1 mM)	3
GoTaq® Hot Start Polymerase (500 U)	0.25
Genomic DNA	1
	Total 50

Abbreviations: dNTP, Deoxynucleotide Triphosphates.

Table 23. List of primers used for genotyping Cre-ER^{T2} mice.

Primer	(5′ - 3′)
Mutant reverse	CGGTTATTCAACTTGCACCA
Wild type forward	AAGGGAGCTGCAGTGGAGTA
Wild type reverse	CCGAAAATCTGTGGGAAGTC

Table 24. PCR cycling conditions for genotyping Cre-ER^{T2} mice.

Step	Reaction		Temperature	Time
1	Denaturation		94 °C	10 min
2	Denaturation	35×	94 °C	15 s
3	Annealing		65 °C	1 min
4	Extension		72 °C	30 s
5	Final Extension		72 °C	2 min
6	Storage		4 °C	∞

2.17.4 MiR-135b$^{lacZ,fl/lacZ,fl}$ mouse genotyping.

Tail biopsies were collected from newborn mice and genomic DNA was isolated using AccuStart™ II Mouse Genotyping Kit (Quantabio, USA, #733-2236). The wild type allele and the mutant allele were determined by PCR, screening the miR-135b locus. Amplicons were resolved in 1.5% agarose gel (Agarose NEEO Ultra-Quality, Carl Roth, Germany, #2267) prepared in 1× TAE buffer and visualized by ethidium bromide (Promega, USA, #H5041). The amplification protocol, the primers and the PCR cycling conditions are listed respectively in table 25, table 26 and table 27.

Table 25. Components used to amplify genomic DNA for genotyping miR-135b$^{lacZ,fl/lacZ,fl}$ mice.

Component	1 sample (µl)
Nuclease-free H_2O	10.3
5× Green GoTaq® Flexi Buffer	4
Magnesium Chloride Solution (25 mM)	2
dNTP Mix (1 mM)	1.6
Primer Pair miR-135b (1 mM)	1
GoTaq® Hot Start Polymerase (500 U)	0.1
Genomic DNA	1
	Total 20

Abbreviations: dNTP, Deoxynucleotide Triphosphates.

Table 26. List of primers used for genotyping miR-135b$^{lacZ,fl/lacZ,fl}$ mice.

Gene	Forward (5′ - 3′)	Reverse (5′ - 3′)
miR-135b	GGTCTTATTTAGGGCTTTTTCCTC	GTTTCAGAGTGGGAATAGAACCAG

Table 27. PCR cycling conditions for genotyping miR-135b$^{lacZ,fl/lacZ,fl}$ mice.

Step	Reaction		Temperature	Time
1	Denaturation		94 °C	10 min
2	Denaturation	35×	94 °C	15 s
3	Annealing		65 °C	1 min
4	Extension		72 °C	30 s
5	Final Extension		72 °C	2 min
6	Storage		4 °C	∞

2.18 Human lung material

Total RNA from human lung tracheal aspirates was obtained from premature infants that were or not mechanically ventilated in the first weeks of life. The infants were diagnosed with or without BPD (table 28). This material was donated from Dr. Gloria Pryhuber from the University of Rochester School of Medicine and Dentistry, Rochester, USA.

Table 28. The characteristics of control and BPD infants.

	Sex	FiO_2 > 0.21 (Days)	Body mass on birth (g)
Ctrl	F	0	4300
	F	1	2035
	F	0	2580
	F	0	3480
BPD	F	5	540
	F	102	575
	M	13	1021
	M	30	520
	M	96	825
	F	23	520
	M	13	965
	F	23	910
	M	***	***
	M	60	490

Abbreviations: BPD, Bronchopulmonary dysplasia; Ctrl: Control; F, Female; M, Male; ***, no information available.

2.19 Statistical analysis

Statistics were performed using GraphPad Prism 7.0 (GraphPad Software, USA). Values are presented as mean ± SD. Differences between groups were evaluated by one-way ANOVA with Tukey's *post hoc* test. Differences between two groups comparisons were performed with an unpaired Student's *t*-test or a nonparametric

Mann–Whitney *U* test. The presence of outliers was verified by Grubbs' test. *P* values below 0.05 were considered as significant.

3 Results

3.1 MiR-135b-5p expression in the lungs of premature infants with BPD

Gene expression obtained from human lung tracheal aspirates was analyzed by qPCR. Levels of miR-135b-5p were compared between four control lungs and 10 BPD infant lungs. The gene expression of miR-135b-5p was significantly increased in BPD lungs compared to control lungs (**Figure 9**).

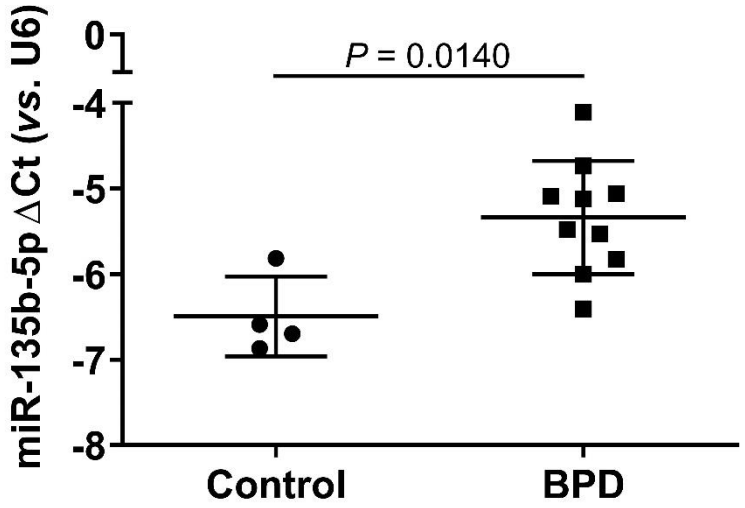

Figure 9. MiR-135b-5p gene expression in human BPD lungs.

The gene expression levels of miR-135b-5p were assessed by qPCR from four control and ten BPD lungs. Data represent mean ± SD. *P* value was determined by nonparametric Mann-Whitney *U* test (*n*=4-10).

3.2 MiR-135b-5p expression in an experimental animal model of BPD

Newborn mice were exposed to hyperoxic conditions to model BPD (103). Changes in the expression of miRs during 85% O_2 exposure were detected at P2, P3, P5 and P14 by microarray published previously (124). (GEO accession number GSE89666). MiR-135b-5p was increased on P3, P5 and P14, suggesting this miR as a candidate and potential regulator for arrested alveolarization. Validation of miR-135b-5p expression was achieved by qPCR on P2, P3, P5, P7, P10 and P14, revealing increased gene expression at P3, P5, P7, P10 and P14 in hyperoxia-exposed lungs. There were no changes observed at P2 (**Figure 10**).

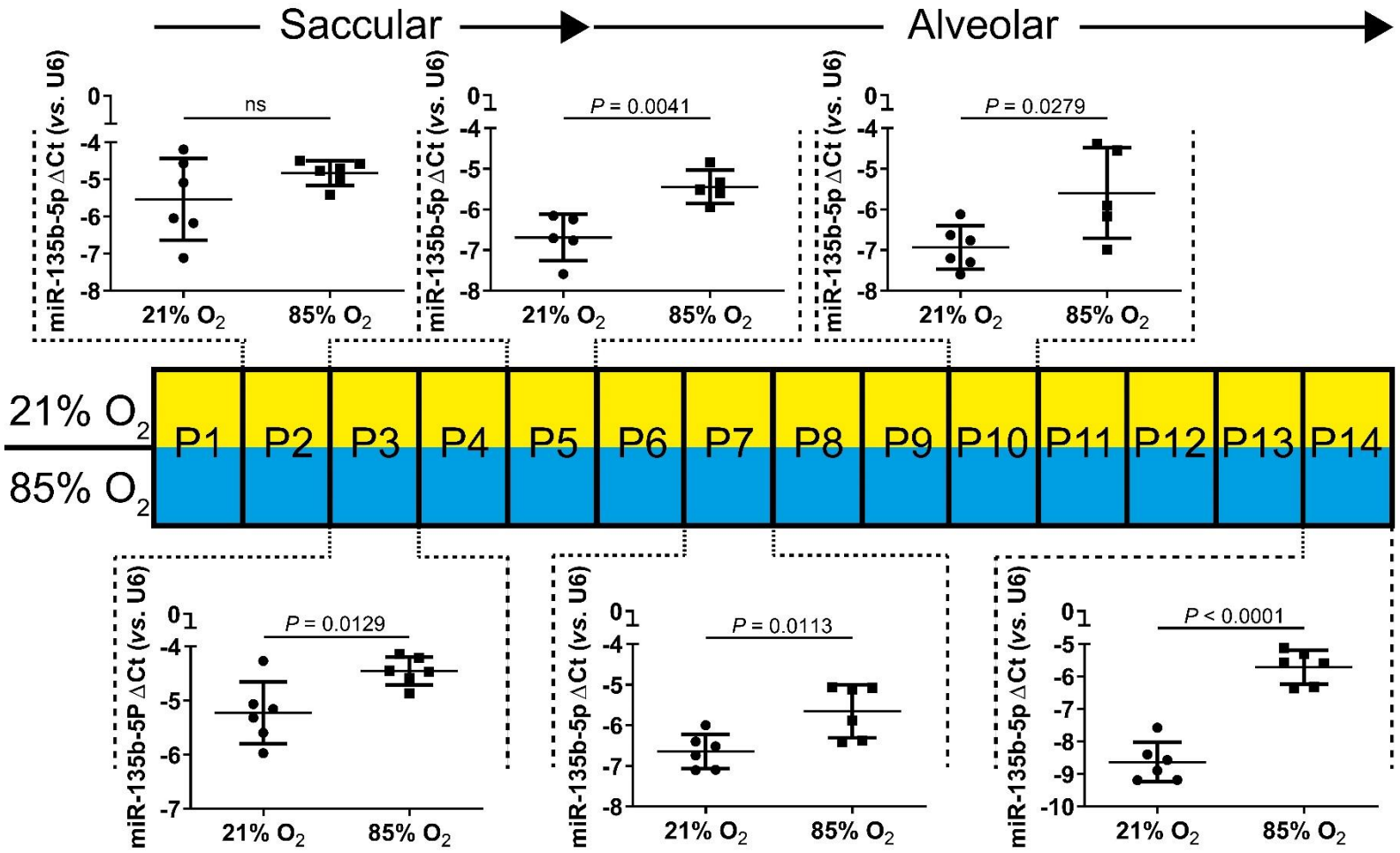

Figure 10. MiR-135b-5p expression in newborn mice over the course of postnatal lung alveolarization.

Newborn mice were randomized to normoxic (21% O_2) or hyperoxic (85% O_2) conditions on postnatal day (P)1, within 4 h of birth. Newborn mouse lungs were collected at P2-P3-P5, which is the saccular phase and at P7-P10-P14, which is the alveolar phase. The gene expression of the mir-135b-5p was assessed by qPCR at P2, P3, P5, P7, P10 and P14 from newborn mice exposed to 21% O_2 or 85% O_2. Data represent mean ± SD. *P* values were determined by unpaired Student´s *t*-test (*n*=5-6).

3.3 Global deletion of miR-135b-5p in normal and aberrant lung development

The germline deleter Cre-ER^{T2} mice were crossed with mTmG mice in order to test the efficiency of the Cre activity in the miR135b$^{Gi\Delta}$ mice. To investigate the activity and efficiency of Cre, the Cre-ER^{T2}-mTmG newborn mice were injected IP on P1 and P2 with miglyol to generate mT mice, and with 0.1 mg/kg tamoxifen to generate the mG mice (**Figure 7A**). Lungs were collected at P14 and analyzed with confocal microscope. In mT mice, the Cre activity was not expressed and the red fluorescence from the reporter gene rfp was the only fluorescence detectable. Instead, in mG mice, the Cre activity was active and the green fluorescence from the reporter gene gfp was predominant and replaced most of the red fluorescence (**Figure 11**).

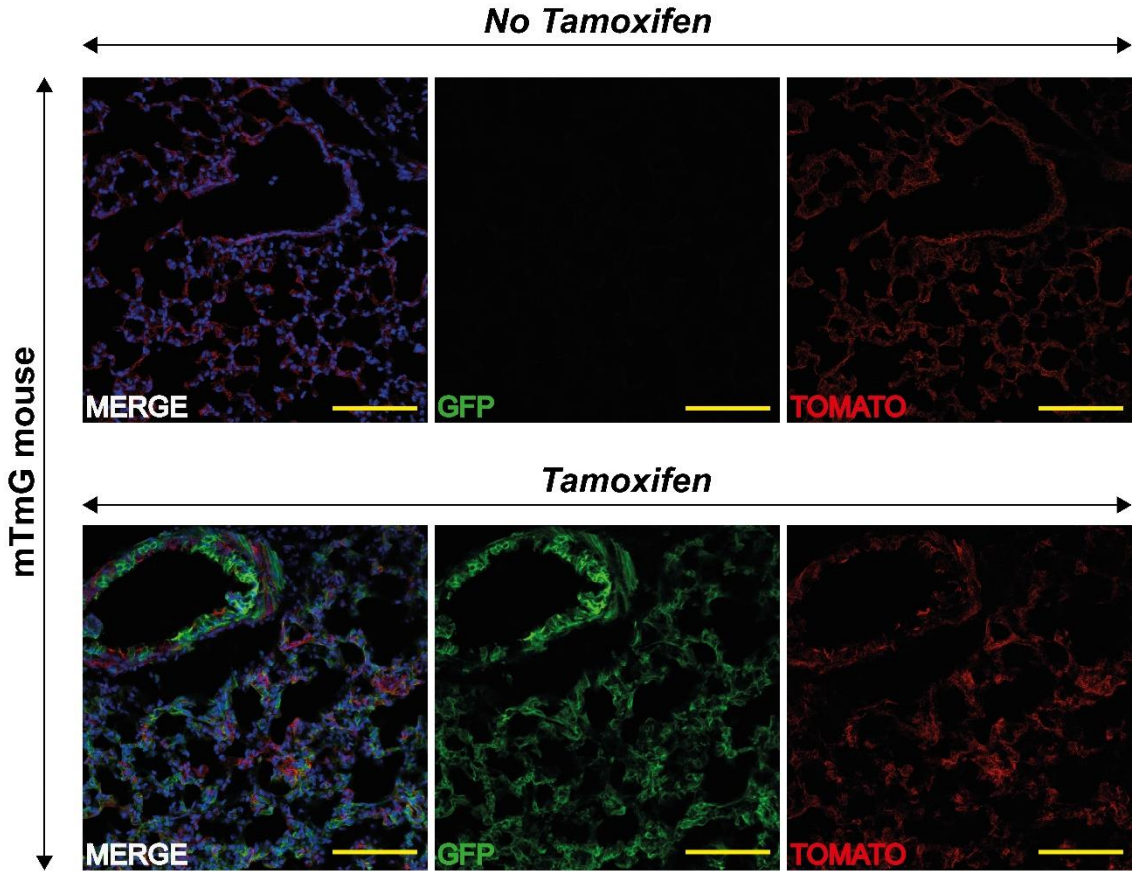

Figure 11. Detection and efficiency of Cre activity in the postnatal lung.

The Cre-ER^{T2}-mTmG (mTmG) newborn mice were injected on P1 and P2 with miglyol (no tamoxifen) and with 0.1 mg/kg tamoxifen. Lungs were analyzed at P14. The miglyol-injected animals expressed the rfp reporter gene (TOMATO) and did not express the gfp reporter gene (GFP) because the Cre was not expressed. In the tamoxifen-injected animals (Tamoxifen) the Cre was activated, removed the rfp reporter gene and expressed the gfp reporter gene (GFP). DAPI staining (blue) revealed nuclei of all cells present in the section. *n* = 12 fields for each group, trends are representative of those observed in two other experiments. Scale bar: 100 µm; GFP: green fluorescent protein.

The Cre activity was detected after tamoxifen injection in the Cre-ER^{T2}-mTmG mice. The Cre-ER^{T2}-miR-135b^{wt} and Cre-ER^{T2}-miR-135b$^{fl/fl}$ newborn mice were injected IP on P1 and P2 with 0.1 mg/kg tamoxifen to generate miR-135b^{wt} mice and miR-135b^{GiΔ} mice. Lungs were collected on P14 for lung architecture analysis by stereology and or gene expression analysis. The miR-135b-5p gene expression was assessed by qPCR in left lung homogenate. The miR-135b-5p gene expression was significantly downregulated in the miR-135b^{GiΔ} mice compared to Cre-ER^{T2}-miR-135b^{wt} mice (**Figure 12**).

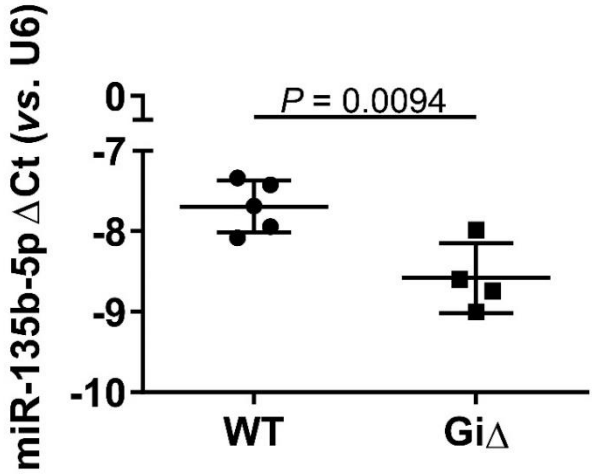

Figure 12. MiR-135b-5p expression in lung homogenates after tamoxifen treatment at P14.
The gene expression levels of miR-135b-5p were assessed by qPCR in left lung homogenates. Cre-ER^{T2}-miR-135b^{wt} newborn mice (WT) and miR-135b^{GiΔ} newborn mice (GiΔ) were exposed to 21% O_2 for the first 14 days of postnatal life and injected IP on P1 and P2 with 0.1 mg/kg tamoxifen. Data represent mean ± SD. Statistical comparisons were made by Student's *t*-test (*n*=4-5, per group)

The global induced deletion of miR-135b slightly improved lung architecture over the period P1 to P14 in miR-135b^{GiΔ} mouse pups (*n*=5 per group) exposed to 85% O_2 compared to Cre-ER^{T2}-miR-135b^{wt} mouse pups exposed to 85% O_2 (**Figure 13G, H** *versus* **13E, F**; complete data set in table 29). In fact, comparing Cre-ER^{T2}-miR-135b^{wt} mice exposed to 85% O_2 *versus* miR-135b^{GiΔ} mice, total number of alveoli was increased from 1.6×10^6 alveoli to 1.9×10^6 alveoli (**Figure 13I**), alveolar density was increased from 6.9×10^6 alveoli/cm^3 to 8.5×10^6 alveoli/cm^3 (**Figure 13J**) and surface area of gas exchange was increased from 97.08 cm^2 to 111.40 cm^2 (**Figure 13K**). MLI was decreased from 70.58 µm to 57.41 µm (**Figure 13N**). Instead, lung volume (**Figure 13L**) and septal thickness (**Figure 13M**) were not affected (table 29). Moreover, the global induced deletion of miR-135b did not impact the structural development in miR-135b^{GiΔ} mouse pups (*n*=5 per group) exposed under 21% O_2 compared to

Cre-ER^{T2}-miR-135b^{wt} mouse pups exposed to 21% O_2 (**Figure 13C, D** *versus* **13A, B**). These data indicate the miR-135b as a crucial player in aberrant lung development.

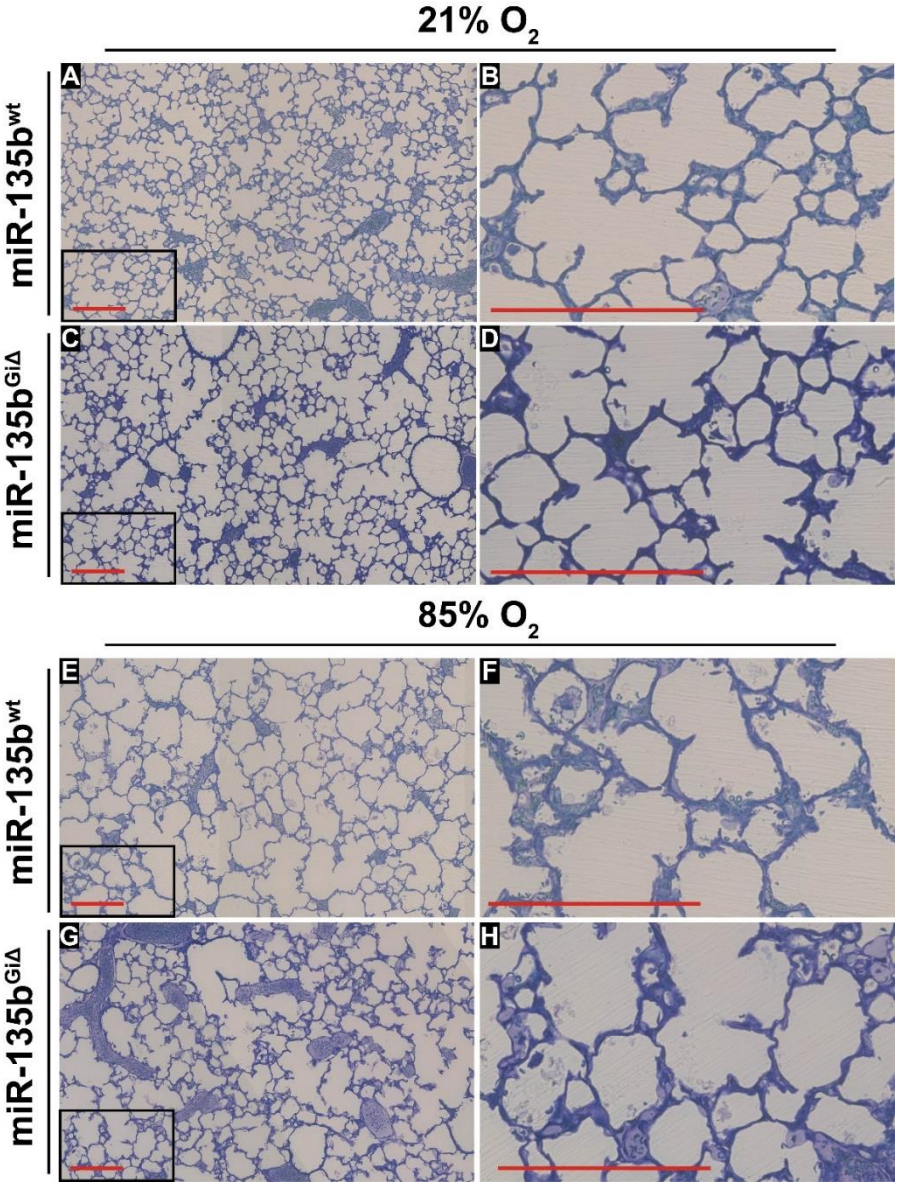

Figure 13. Stereological analysis of lung structure in wild type and miR-135b^{GiΔ} mice at postnatal day 14.

Cre-ER^{T2}-miR-135b^{wt} newborn mice (WT) and miR-135b^{GiΔ} newborn mice (GiΔ) were exposed to 21% O_2 and 85% O_2 from the day of birth until P14. Lungs were harvested and processed for analysis of the lung structure by design-based stereology on P14. (A, C, E, G) Lower magnification images from lungs. (B, D, F, H) Higher magnification images derived from the black rectangle on the corresponding image on the bottom left, to highlight changes in septal thickness. Each image is representative of images of lung sections obtained from four other mice within each experimental group (*n*=5, per experimental group). Scale bars in photomicrographs represent 200 µm. Design-based stereology was employed to assess (I) alveoli number, (J) alveolar density, (K) surface area of gas exchange, (L) lung volume, (M) septal thickness and (N) mean linear intercept. Data represent mean ± S.D. Data comparisons were made by one-way ANOVA with Tukey's *post hoc* test. Sex: blue square denotes males and red circle denotes females.

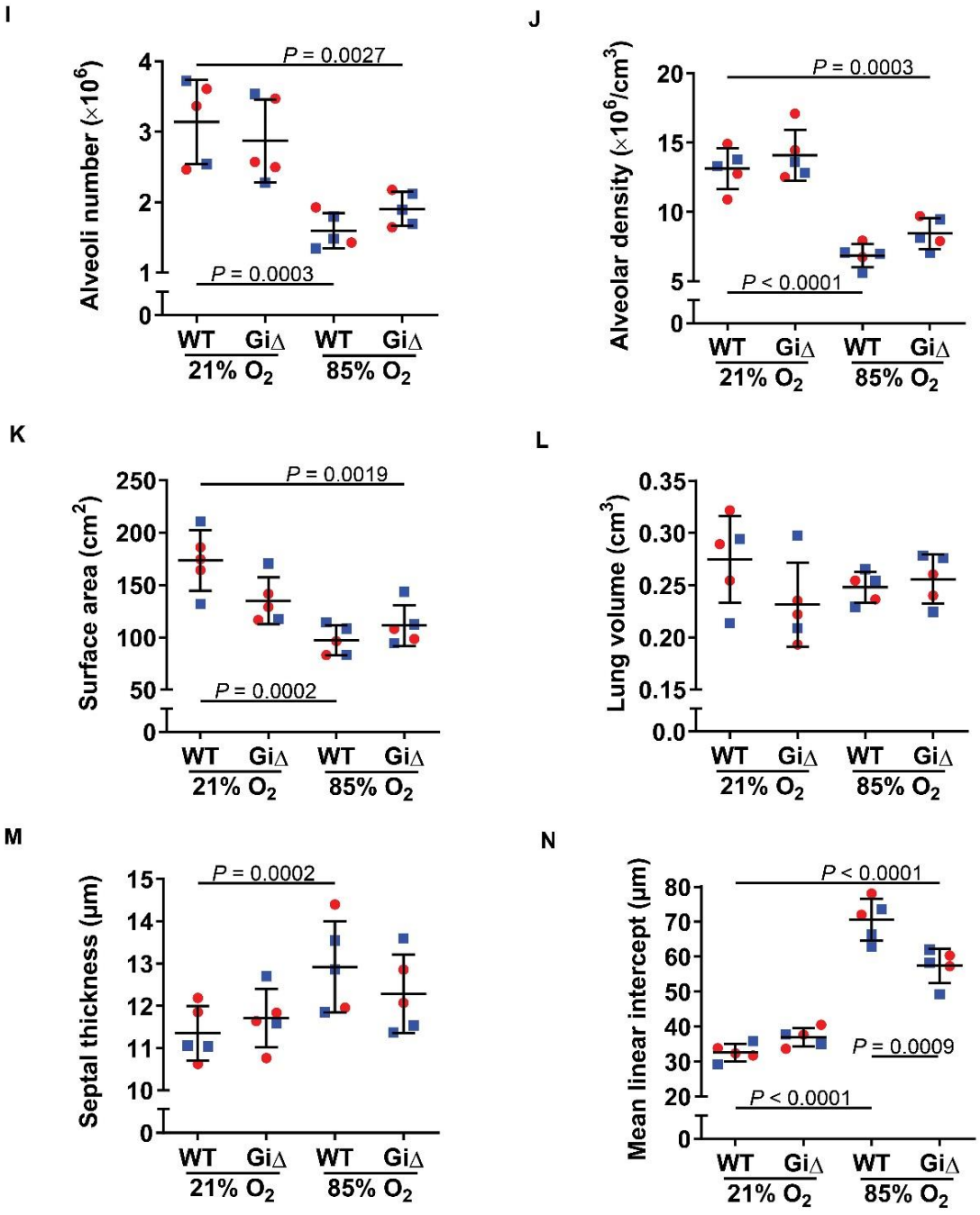

Figure 13-continued

Table 29. Stereology analysis of lung structure in wild type and miR-135b^{GiΔ} mice at postnatal day 14.

Parameter	21% O_2		85% O_2			
	Cre-ER^{T2}-miR-135b^{wt}	miR-135b^{GiΔ}	Cre-ER^{T2}-miR-135b^{wt}		miR-135b^{GiΔ}	
	mean ± SD	mean ± SD	mean ± SD	*P* value *vs.* Cre-ER^{T2}-miR-135b^{wt} /21% O_2	mean ± SD	*P* value *vs.* Cre-ER^{T2}-miR-135b^{wt} /85% O_2
V (lung) [cm^3]	0.27 ± 0.04	0.23 ± 0.04	0.25 ± 0.01	0.5673	0.26 ± 0.02	0.9790
CV [*V* (lung)]	0.15	0.17	0.06		0.09	
V_V (par/lung) [%]	87.18 ± 4.15	88.13 ± 2.40	93.57 ± 3.06	0.0343	88.40 ± 3.37	0.1032
N (alv, lung) 10^6	3.14 ± 0.59	2.87 ± 0.59	1.60 ± 0.25	0.0003	1.90 ± 0.24	0.7089
N_V (alv/par) 10^6 [cm^{-3}]	13.13 ± 1.48	14.10 ± 1.84	6.87 ± 0.84	< 0.0001	8.46 ± 1.12	0.2933
CV [N (alv/lung)]	0.19	0.20	0.15		0.13	
S_V [cm^{-1}]	724.70 ± 33.67	663.60 ± 25.97	416.40 ± 28.91	< 0.0001	489.80 ± 35.62	0.0092
S (alv epi, lung) [cm^2]	173.50 ± 28.99	135.10 ± 22.35	97.08 ± 14.32	0.0002	111.40 ± 19.38	0.7347
CV [S (alv epi, lung)]	0.17	0.16	0.15		0.17	
τ (sep) [µm]	10.00 ± 0.43	9.84 ± 1.07	10.18 ± 0.42	0.0463	11.97 ± 0.86	0.6484
CV [τ (sep)]	0.04	0.11	0.04		0.07	
MLI [µm]	32.59 ± 2.44	36.94 ± 2.66	70.58 ± 6.02	< 0.0001	57.41 ± 4.90	0.0009
CV [MLI]	0.07	0.07	0.08		0.08	

Abbreviations: *alv*, alveoli; *alv air*, alveolar airspaces; *alv epi*, alveolar epithelium; *CV*, coefficient of variation; MLI, mean linear intercept; *N*, number; N_V, numerical density; *par*, parenchyma; *S*, surface area; S_V, surface density; *τ* (sep), arithmetic mean septal thickness; *V*, volume; V_V, volume density; WT, wild type. Values are presented as mean ± SD, *n* = 4-5 lungs for each group. A one-way ANOVA with Tukey's *post-hoc* analysis was used to determine *P* values.

To validate the induced global deletion of miR-135b in the newborn mice employed in the lung structure analysis, tail biopsies were collected, and genomic DNA was isolated. The wild type allele and the mutant allele were determined by end point PCR, screening the miR-135b locus. Amplicons were resolved in 1.5% agarose gel. All the miR-135b$^{Gi\Delta}$ mice presented a slightly or did not present the miR-135b fragment (**Figure 14**).

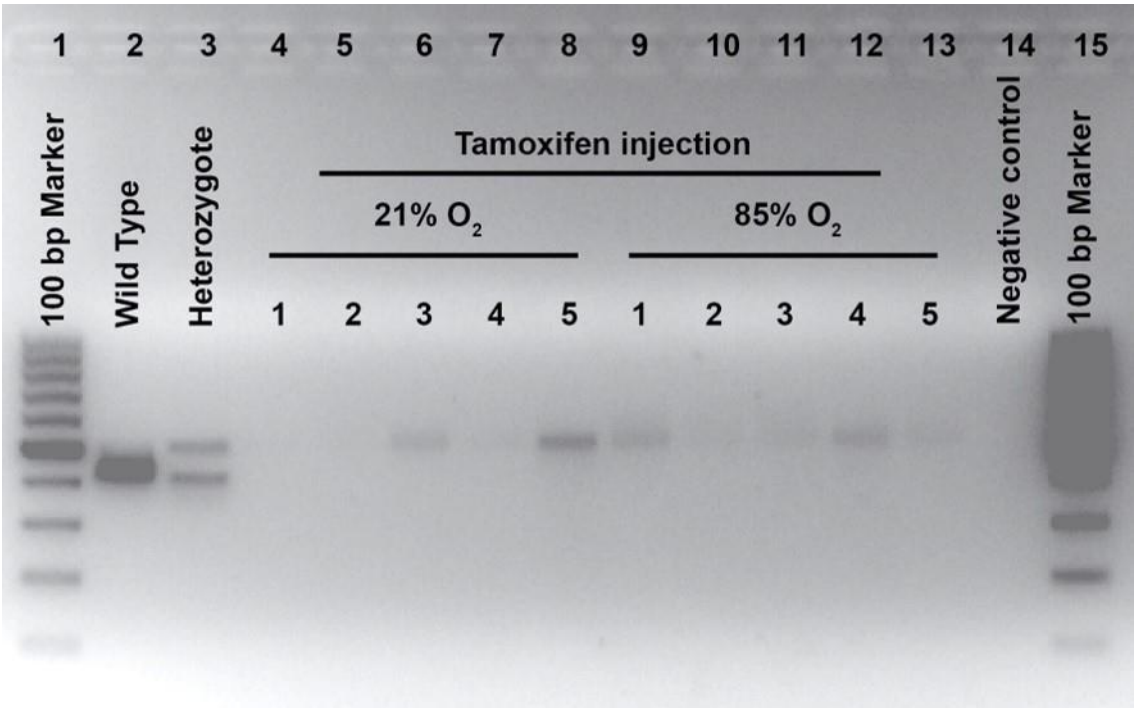

Figure 14. PCR amplification of genomic DNA isolated from tail biopsies of miR135b$^{Gi\Delta}$ mice. Tail biopsies were collected from miR135b$^{Gi\Delta}$ mice at P14 prior stereology analysis. Genomic DNA was isolated, and the wild type and mutant allele were determined by end point PCR screening the miR-135b locus. Amplicons were resolved in 1.5% agarose gel and visualized by ethidium bromide. Lane 1: 100 bp marker. Lane 2: wild type control. Lane 3: heterozygote control. Lane 4-8: miR135b$^{Gi\Delta}$ mice injected IP with 0.1 mg/kg tamoxifen exposed under 21% O_2. Lane 9-13: miR135b$^{Gi\Delta}$ mice injected IP with 0.1 mg/kg tamoxifen exposed to 85% O_2. Lane 14: negative control. Lane 15: 100 bp marker.

3.4 Antagonizing gene expression of miR-135b-5p

Newborn wild type C57BL/6J mice were injected IP on P1 and P3 with 10 mg/kg scrambled control and 10 mg/kg antimiR-135b-5p. Pups were kept from the day of birth until P14 to 21% O_2 or 85% O_2. Lungs were collected at P14 for detection of the antimiR-135b-5p in the mouse lung by qPCR and for analysis of the lung structure by design-based stereology. The expression levels of miR-135b-5p in antimiR-135b-5p treated animals were not detectable in 21% O_2 and significant reduced in 85% O_2 compared to the scrambled treated animals (**Figure 15**).

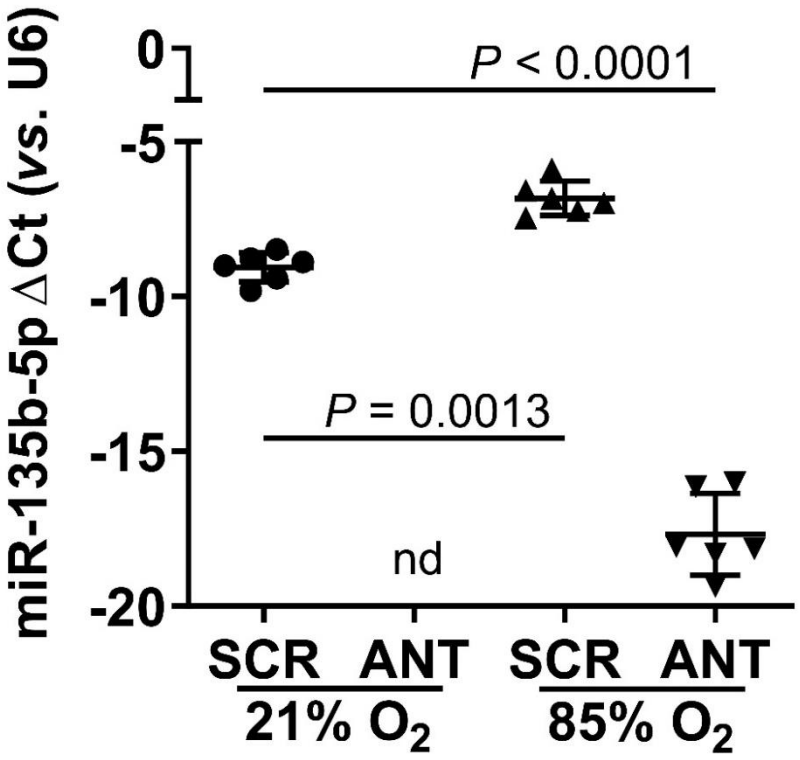

Figure 15. MiR-135b-5p expression in lung homogenates after antimiR-135b-5p treatment.
The miR-135b-5p levels were assessed by qPCR in left lung homogenates in 21% O_2 scrambled control (SCR) and antimiR-135b-5p treated (ANT) and 85% O_2 scrambled control (SCR) and antimiR-135b-5p treated (ANT) groups at P14. Data represent mean ± SD. Statistic comparison were made using one-way ANOVA with Tukey's *post hoc* test (*n*=6, per group). nd, no detected.

The antimiR-135b-5p treatment modest improved the lung structure in the first 14 days of postnatal life in 85% O_2 treated animals (*n*=5, per group) compared to 85% O_2 control mice (**Figure 16G, H** *versus* **16E, F**; complete data set in table 30). In detail, comparing antimiR-135b-5p treated animals exposed to 85% O_2 *versus* control animals exposed to 85% O_2, total number of alveoli was increased from 1.8×10^6 alveoli to 2.2×10^6 alveoli (**Figure 16I**), alveolar density was increased from 7.3×10^6 alveoli/cm^3 to 9.3×10^6 alveoli/cm^3 (**Figure 16J**), and MLI was decreased from 54.10 µm to 46.71 µm (**Figure 16N**). Lung volume (**Figure 16L**), surface area of gas-exchange (**Figure 16K**) and septal thickness (**Figure 16M**) were not changed (table 30). Moreover, the antimiR-135b-5p did not affect the structural development in 21% O_2 exposed mouse pups (*n*=5, per group) compared to antimiR-135b-5p mouse pups exposed to 21% O_2 (**Figure 16A, B,** *versus* **16C, D**).

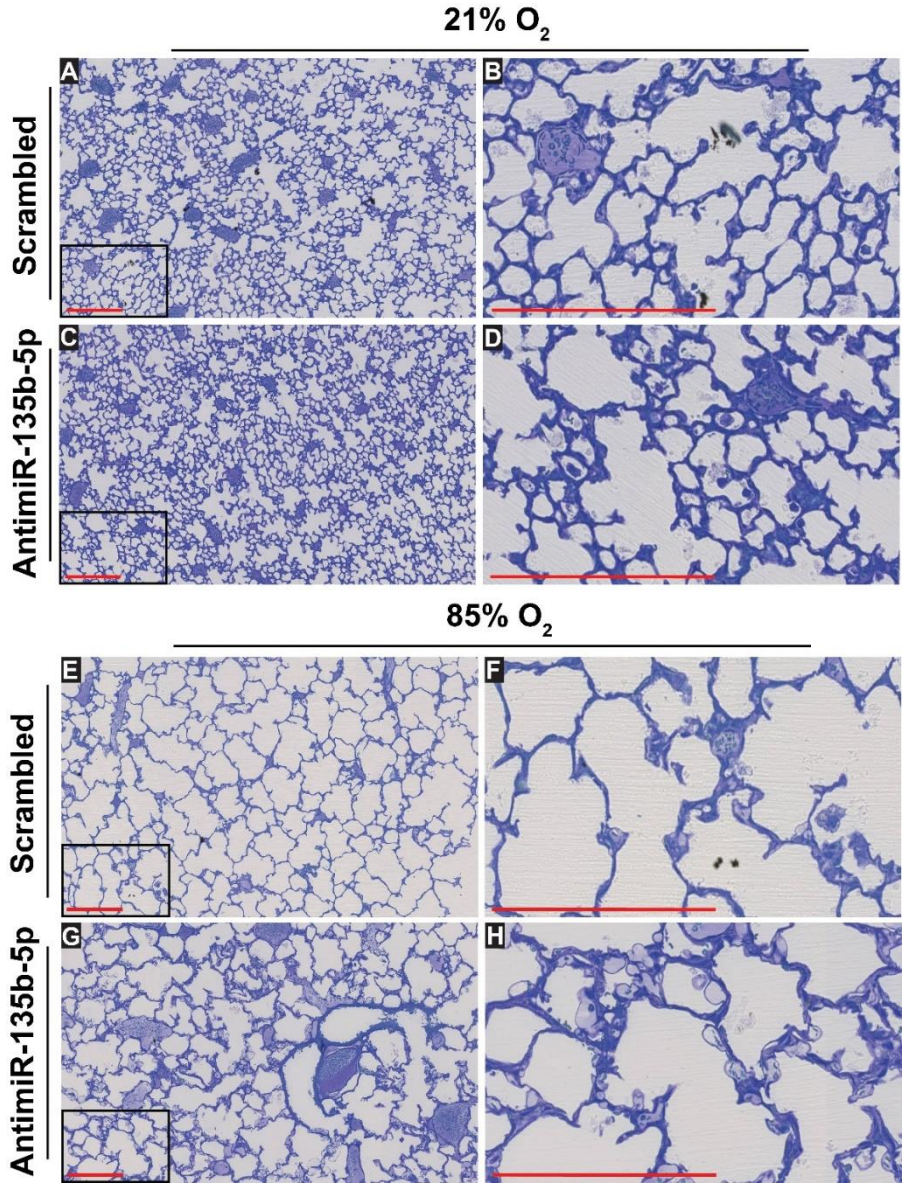

Figure 16. Stereological analysis of lung structure in C57BL/6J pups after antimiR-135b-5p treatment.

Newborn mice were IP injected on P1 and P3 with scrambled (SCR) and antimiR-135b-5p (ANT) and exposed to 21% O_2 and 85% O_2 from the day of birth until P14. Lungs were harvested and processed for analysis of the lung structure by design-based stereology on P14. (A, C, E, G) Lower magnification images from lungs. (B, D, F, H) Higher magnification images derived from the black rectangle on the corresponding image on the bottom left, to highlight changes in the septum. Each image is a representative of images of lung sections obtained from four other mice within each experimental group (*n*=5, per group). Scale bars in photomicrographs represent 200 μm. Design-based stereology was employed to assess (I) alveoli number, (J) alveolar density, (K) surface area of gas-exchange, (L) lung volume, (M) septal thickness and (N) mean linear intercept. Data represent mean ± S.D. Data comparisons were made by one-way ANOVA with Tukey's *post hoc* test. Sex: blue square denotes males and red circle denotes females.

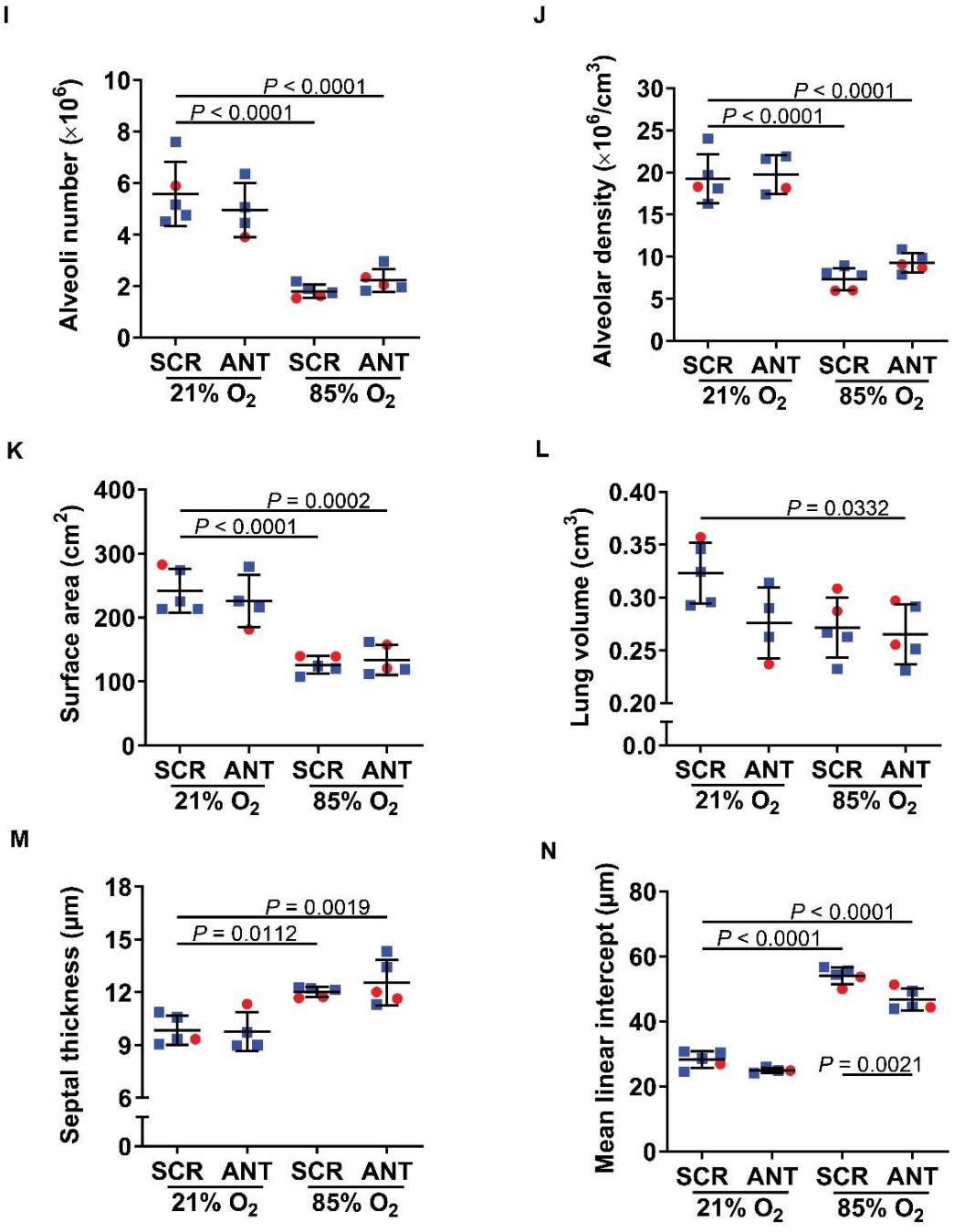

Figure 16-continued

Table 30. Stereological analysis of lungs from P14 antimiR-135b-5p treated mice exposed either to normoxia or to severe hyperoxia compared to scrambled controls.

Parameter	21% O_2		85% O_2			
	scrambled	antimiR-135b-5p	scrambled		antimiR-135b-5p	
	mean ± SD	mean ± SD	mean ± SD	*P* value *vs.* scrambled/21% O_2	mean ± SD	*P* value *vs.* scrambled/85% O_2
V (lung) [cm^3]	0.32 ± 0.03	0.28 ± 0.03	0.27 ± 0.03	0.0627	0.26 ± 0.03	0.9862
CV [*V* (lung)]	0.089	0.121	0.105		0.106	
V_V (par/lung) [%]	89.10 ± 2.42	90.29 ± 2.57	90.77 ± 2.57	0.7655	90.03 ± 3.15	0.9722
N (alv, lung) 10^6	5.58 ± 1.24	4.95 ± 1.05	1.79 ± 0.26	< 0.0001	2.22 ± 0.45	0.8490
N_V (alv/par) 10^6 [cm^{-3}]	19.28 ± 2.89	19.76 ± 2.33	7.35 ± 1.31	< 0.0001	9.28 ± 1.15	0.4608
CV [N (alv/lung)]	0.10	0.08	0.11		0.12	
S_V [cm^{-1}]	836.80 ± 43.54	901.70 ± 49.40	512.60 ± 20.70	< 0.0001	558.80 ± 34.33	0.2545
S (alv epi, lung) [cm^2]	241.70 ± 33.92	225.70 ± 40.59	126.60 ± 13.54	< 0.0001	134.10 ± 23.56	0.9717
CV [S (alv epi, lung)]	0.140	0.180	0.107		0.176	
τ (sep) [µm]	9.84 ± 0.82	9.76 ± 1.10	12.01 ± 0.28	0.0112	12.54 ± 1.28	0.8076
CV [τ (sep)]	0.084	0.112	0.023		0.102	
MLI [µm]	28.23 ± 2.57	24.94 ± 0.74	54.10 ± 2.56	< 0.0001	46.71 ± 3.40	0.0021
CV [MLI]	0.091	0.030	0.047		0.073	

Abbreviations: *alv*, alveoli; *alv air*, alveolar airspaces; *alv epi*, alveolar epithelium; *CV*, coefficient of variation; MLI, mean linear intercept; *N*, number; N_V, numerical density; *par*, parenchyma; *S*, surface area; S_V, surface density; *τ* (sep), arithmetic mean septal thickness; *V*, volume; V_V, volume density. Values are presented as mean ± SD, *n* = 4-5 lungs for each group. A one-way ANOVA with Tukey's *post-hoc* analysis was used to determine *P* values.

Moreover, the exposure to 85% O_2 from P1 to P14 generated a pronounced deleterious effect on lung structure to mimic the two hallmark of human BPD, increased septal thickness and blunted alveolarization (12). The problem of this severe hyperoxia-based model of BPD, is that it might cover positive effects of intervention candidates such as the antimiR-135b-5p (103). For this reason, newborn C57BL/6J mice were injected IP on P1 and P3 with 10 mg/kg scrambled control and 10 mg/kg antimiR-135b-5p and kept from the day of birth until P14 to 21% O_2 and 60% O_2. Lungs were collected at P14 for detection of the antimiR-135b-5p in the mouse lung by qPCR and for analysis of the lung structure by design-based stereology. The antimiR-135b-5p was successfully delivered to the lung; the expression levels of miR-135b-5p were not detectable in 21% O_2 exposed animals and significant reduced in 60% O_2 exposed animals compared to the scrambled treated animals (**Figure 17**).

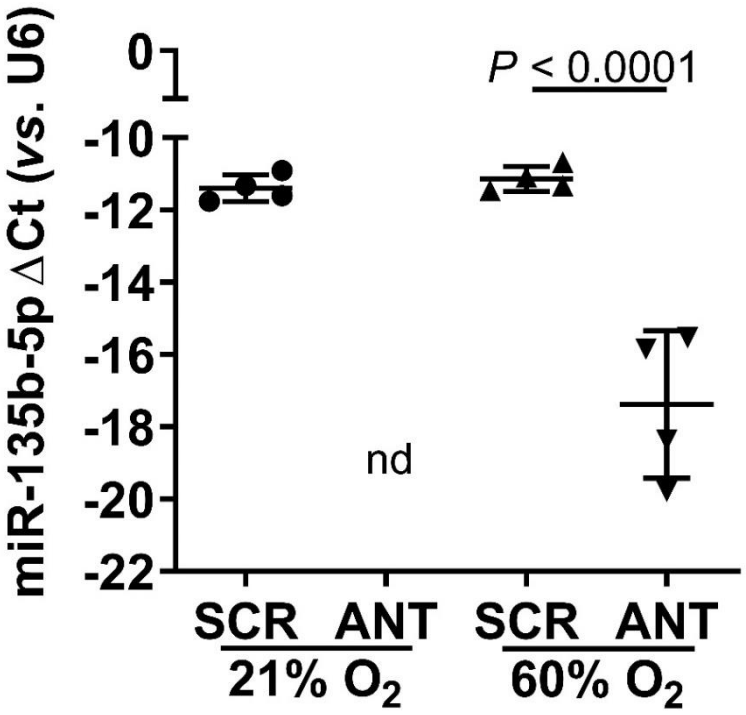

Figure 17. MiR-135b-5p expression in lung homogenates after antimiR-135b-5p treatment.
MiR-135b-5p levels were assessed by qPCR in left lung homogenates in 21% O_2 and 60% O_2 treated with scrambled (SCR) and antimiR-135b-5p (ANT) at P14. Data represent mean ± SD. Statistic comparison were made using one-way ANOVA with Tukey's *post hoc* test (*n*=4, per group). nd, not detected.

The antimiR-135b-5p treatment restored the lung structure in the first 14 days of postnatal life in 60% O_2 antimiR-135b-5p treated animals (*n*=6, per group) compared to 60% O_2 scrambled control mice (**Figure 18G, H** *versus* **18E, F**; complete data set in

table 31). The antimiR-135b-5p treated mouse pups exposed to 60% O_2 had a normalized total number of alveoli (**Figure 18I**), alveolar density (**Figure 18J**), surface area of gas exchange (**Figure 18K**) and lung volume (**Figure 18L**), when compared to 21% O_2 exposed control animals. Septal thickness (**Figure 18M**) was not changed. MLI was increased from 26.94 µm in 21% O_2 scrambled control group to 39.00 µm in antimiR-135b-5p treated animals (**Figure 18N**) (table 31). The antimiR-135b-5p treatment did not affect the development of lung architecture in 21% O_2 exposed mouse pups (*n*=5, per group) compared to antimiR-135b-5p mouse pups exposed to 21% O_2 (**Figure 18A, B** *versus* **18C, D**).

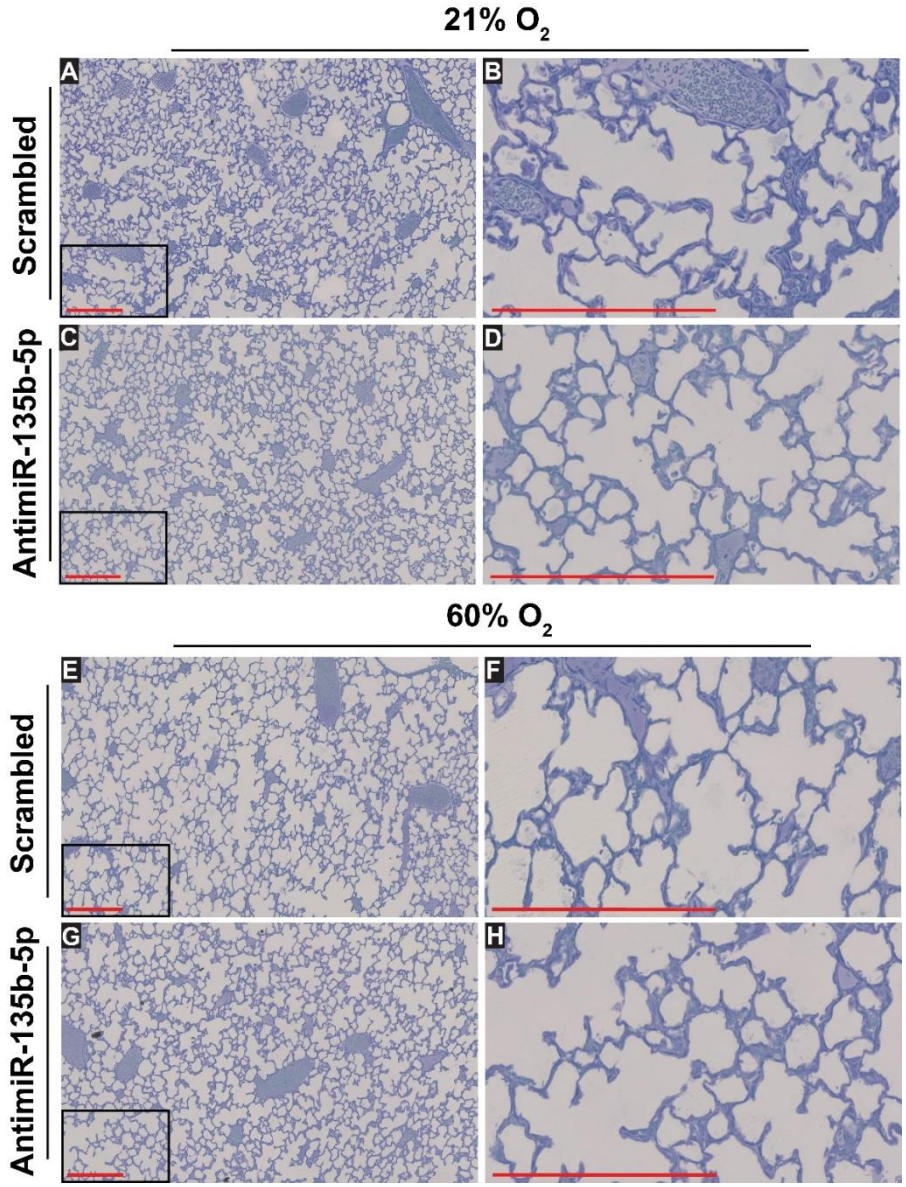

Figure 18. Stereological analysis of lung structure in newborn pups after antimiR-135b-5p treatment.

Newborn mice were IP injected on P1 and P3 with scrambled (SCR) and antimiR-135b-5p (ANT) and exposed to 21% O_2 and 60% O_2 from the day of birth until P14. Lungs were harvested and processed for analysis of the lung structure by design-based stereology on P14. (A, C, E, G) Lower magnification images from lungs. (B, D, F, H) Higher magnification images derived from the black rectangle on the corresponding image on the bottom left, to highlight changes in the septum. Each image is a representative of images of lung sections obtained from four other mice within each experimental group (*n*=5, per group). Scale bars in photomicrographs represent 200 μm. Design-based stereology was employed to assess (I) alveoli number, (J) alveolar density, (K) surface area of gas-exchange, (L) lung volume, (M) septal thickness and (N) mean linear intercept. Data represent mean ± S.D. Data comparisons were made by one-way ANOVA with Tukey's *post hoc* test. Sex: blue square denotes males and red circle denotes females.

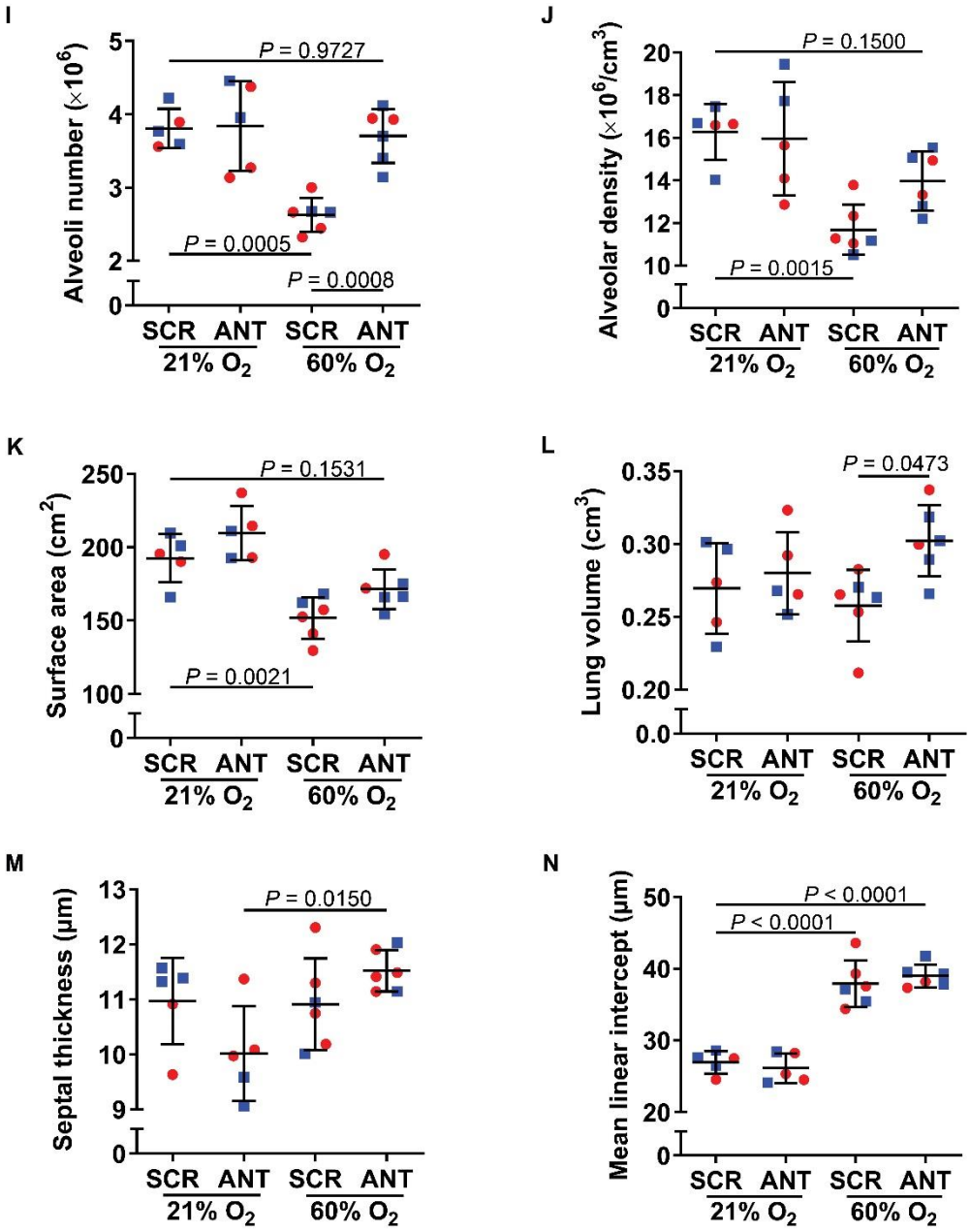

Figure 18-continued

Table 31. Stereological analysis of lungs from P14 antimiR-135b-5p treated mice exposed either to normoxia or to moderate hyperoxia compared to scrambled controls.

Parameter	21% O_2		60% O_2			
	scrambled	antimiR-135b-5p	scrambled		antimiR-135b-5p	
	mean ± SD	mean ± SD	mean ± SD	*P* value *vs.* scrambled/21% O_2	mean ± SD	*P* value *vs.* Scrambled/85% O_2
V (lung) [cm^3]	0.26 ± 0.03	0.28 ± 0.03	0.26 ± 0.02	0.8875	0.30 ± 0.02	0.0473
CV [*V* (lung)]	0.12	0.10	0.09		0.08	
V_V (par/lung) [%]	87.37 ± 2.73	86.36 ± 1.94	87.83 ± 3.18	0.9886	88.03 ± 1.35	0.9990
N (alv, lung) 10^6	3.81 ± 0.27	3.84 ± 0.61	2.63 ± 0.23	0.0005	3.71 ± 0.37	0.0008
N_V (alv/par) 10^6 [cm^{-3}]	16.28 ± 1.31	15.96 ± 2.67	11.68 ± 1.19	0.0015	13.97 ± 1.39	0.1266
CV [N (alv/lung)]	0.08	0.17	0.10		0.10	
S_V [cm^{-1}]	821.00 ± 52.97	868.70 ± 47.57	672.40 ± 47.58	< 0.0001	645.00 ± 12.37	0.6821
S (alv epi, lung) [cm^2]	192.40 ± 16.45	209.60 ± 18.35	151.70 ± 14.18	0.0021	171.40 ± 13.53	0.1621
CV [S (alv epi, lung)]	0.08	0.09	0.09		0.08	
τ (sep) [µm]	10.36 ± 0.78	10.01 ± 0.86	10.91 ± 0.83	0.9994	11.52 ± 0.38	0.4933
CV [τ (sep)]	0.07	0.08	0.08		0.03	
MLI [µm]	26.94 ± 1.55	26.13 ± 2.06	37.91 ± 3.26	< 0.0001	39.00 ± 1.59	0.8389
CV [MLI]	0.06	0.08	0.08		0.04	

Abbreviations: *alv*, alveoli; *alv air*, alveolar airspaces; *alv epi*, alveolar epithelium; *CV*, coefficient of variation; MLI, mean linear intercept; *N*, number; N_V, numerical density; *par*, parenchyma; *S*, surface area; S_V, surface density; *τ* (sep), arithmetic mean septal thickness; *V*, volume; V_V, volume density. Values are presented as mean ± SD, *n* = 4-5 lungs for each group. A one-way ANOVA with Tukey's *post-hoc* analysis was used to determine *P* values.

3.5 MiR-135b-5p interaction with Smad5 mRNA in normal and aberrant lung development

The miR-135b-5p was identified (**Figure 19**) and verified *in silico* analysis to target Smad5 by bioinformatics tools such as target scan and verified by Bhinge *et al.* (14).

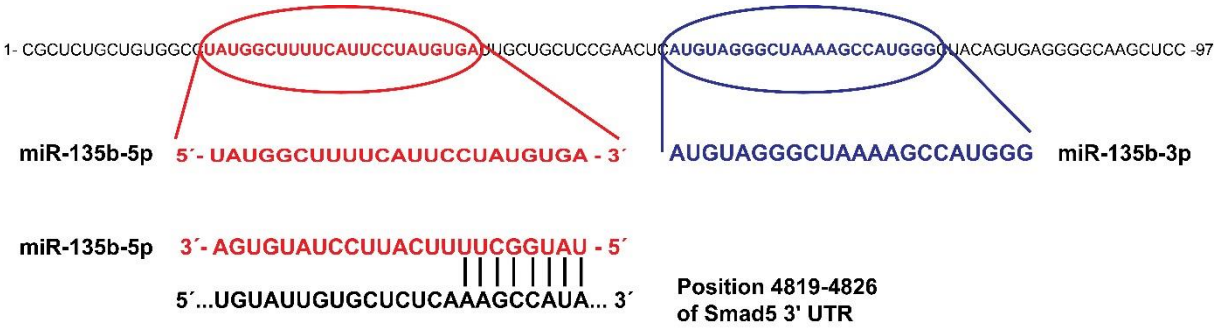

Figure 19. MiR-135b-5p binding sites in the Smad5 3′-UTR mRNA region.

The precursor microRNA is a sequence of 97 base pairs (bp) that contains the mature sequence for the miR-135b-5p (Red) and the mature sequence for the miR-135b-3p (Blue). The mature miR-135b-5p can bind 8-mer complementary the 3′-UTR mRNA region of Smad5.

The R-Smads gene expression and protein expression were analyzed respectively by qPCR and western blot in lung homogenates at P14 from newborn C57BL/6J mice injected IP with scrambled control and antimiR-135b-5p and exposed to 21% O_2 or 85% O_2. The Smad1 gene expression was increased in control animals exposed to 85% O_2 *versus* scrambled control animals exposed to 21% O_2. The antimiR-135b-5p treatment did not impact Smad1 gene expression levels in animals exposed to 85% O_2 but impacted with two-fold change increase the 21% O_2 exposed antimiR-135b-5p treated animals. (**Figure 20A**). The Smad5 gene expression was decreased in scrambled treated animals exposed to 85% O_2 *versus* scrambled treated animals exposed to 21% O_2. After antimiR-135b-5p treatment, animals exposed to 85% O_2 had Smad5 gene expression levels identically to scrambled control animals exposed to 21% O_2 (**Figure 20B)**. The gene expression of Smad9 was not changed (**Figure 20C**).

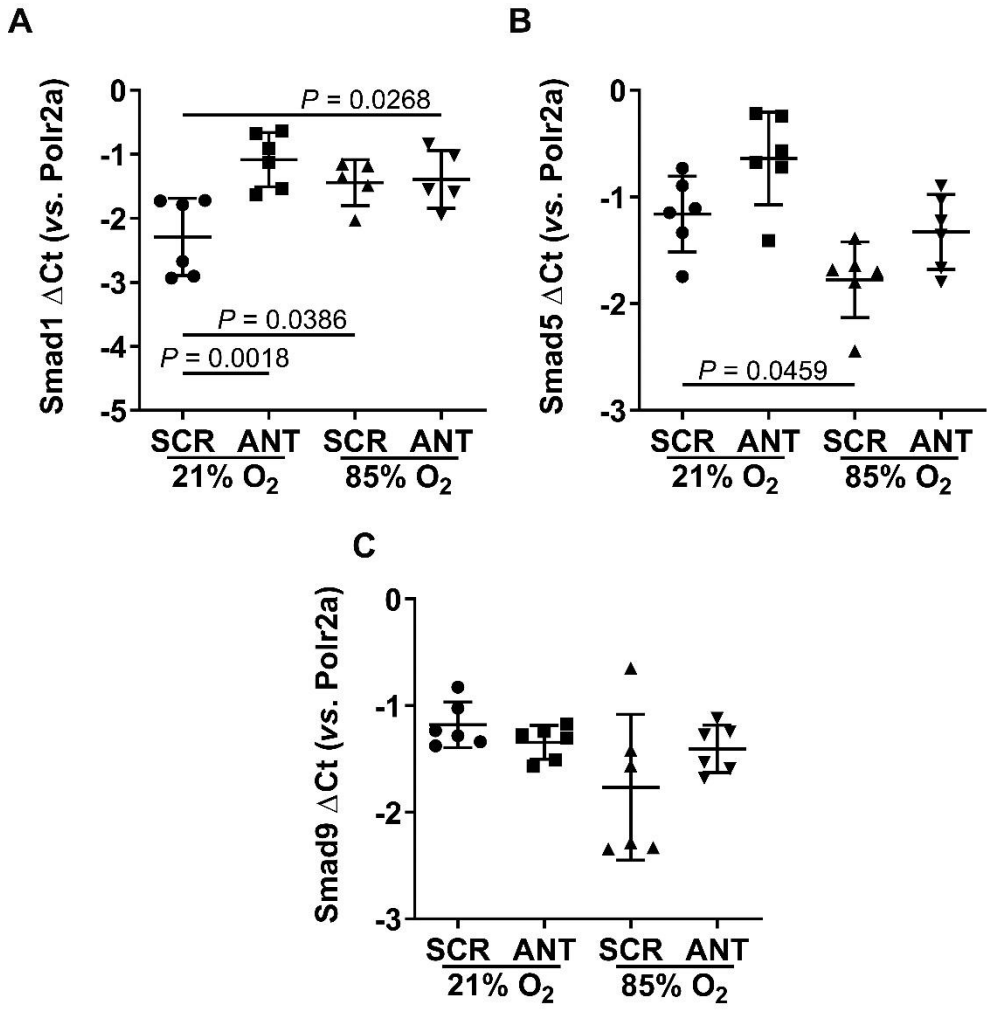

Figure 20. R-Smad gene expressions in lung homogenates after antimiR-135b-5p treatment at P14.

R-Smads gene expressions in lung homogenates after antimiR-135b-5p treatment at P14. (A) Smad1, (B) Smad5 and (C) Smad9 levels were assessed by qPCR in lung homogenates of newborn mice exposed to 21% O_2 scrambled control (SCR) and antimiR-135b-5p treated (ANT) and in 85% O_2 scrambled control (SCR) and antimiR-135b-5p treated (ANT). Data represent mean ± SD. Statistic comparison were made using one-way ANOVA with Tukey's *post hoc* test (*n*=5-6, per group).

The protein expression analysis by western blot revealed that Smad1 protein expression was not changed in lung homogenates between groups. The Smad9 protein expression was decreased in lung homogenates of control animals exposed to 85% O_2 compared to 21% O_2 exposed animals. The Smad5 protein expression was decreased in lung homogenates of control animals exposed to 85% O_2 *versus* control animals exposed to 21% O_2. Moreover, Smad5 expression appeared restored to 21% O_2 levels in the antimiR-135b-5p treated animals exposed to 85% O_2 (**Figure 21A**). To investigate further the effect of antimiR-135b-5p treatment in the hyperoxic group, a higher number of animals was employed. Six newborn mice for the scrambled control

group and six newborn mice for the antimiR-135b-5p treatment group were used. The Smad5 protein expression was significantly higher in the antimiR-135b-5p treatment group compared to the scrambled group after 85% O_2 exposure (**Figure 21B**). The Smad5 protein expression was quantified by densitometry (**Figure 21C**).

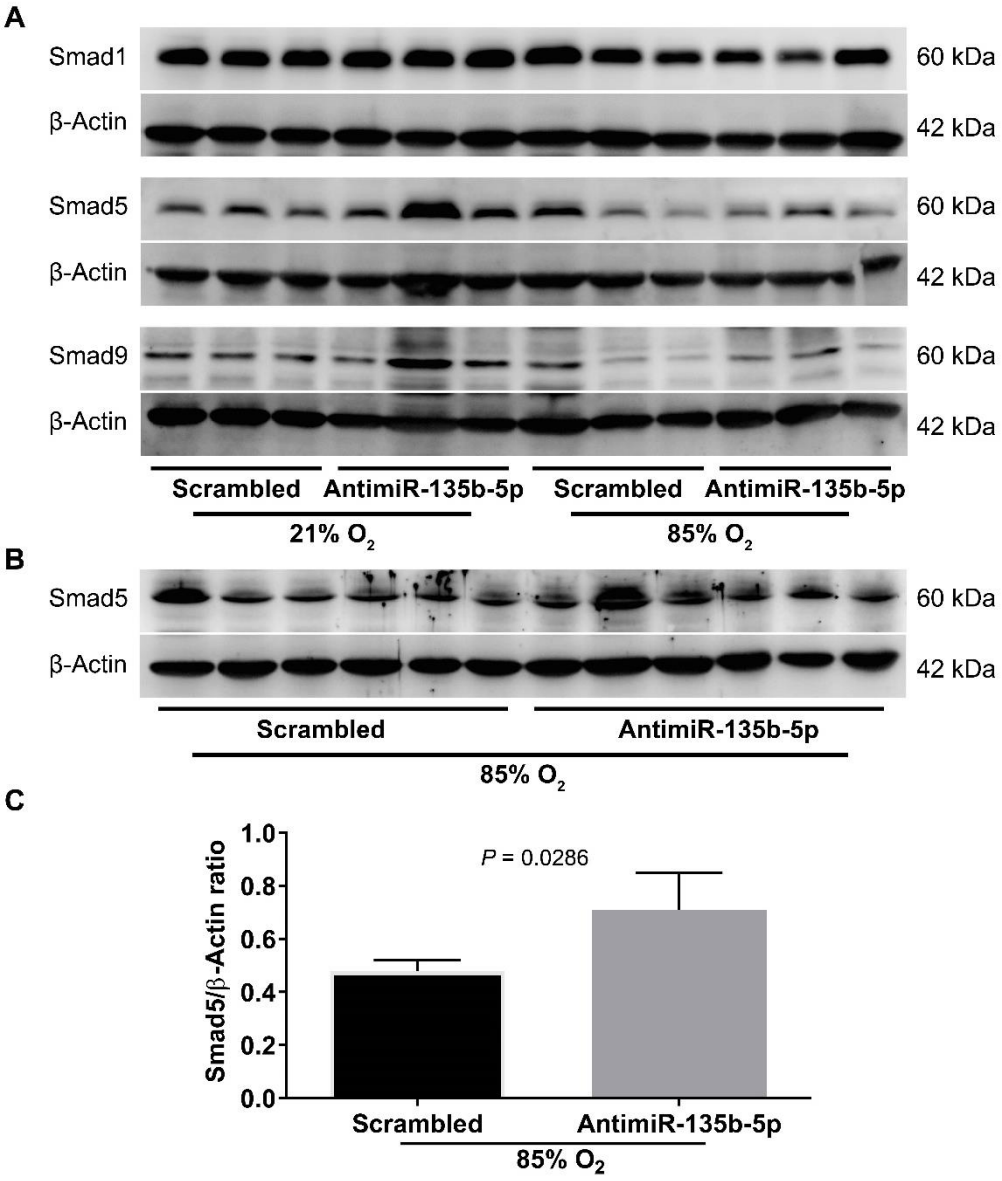

Figure 21. R-Smad protein expression in lung homogenates after antimiR-135b-5p treatment at P14.

(A) Smad1, Smad5 and Smad9 levels were assessed by western blot in lung homogenates of P14 newborn mice exposed to 21% O_2 scrambled control and antimiR-135b-5p treated and in 85% O_2 scrambled control and antimiR-135b-5p treated (*n*=3, per group). (B) Smad5 protein levels assessed by Western Blot in lung homogenates in 85% O_2 scrambled control and treated antimiR-135b-5p treated animals (*n*=6, per group). (C) Smad5 protein expression was quantified by the ratio of Smad5 to total β-Actin (*n*=6, per group). Data represent mean ± SD. *P* values were determined by unpaired Student's *t*-test.

3.6 Expression and localization of miR-135b-5p

The impact of a deregulated miR in lung development could cause a cascade of events that can lead to aberrant lung development (57, 124, 142, 163) and it is crucial to find and demonstrate the causes and the effects of deregulated miRs (104). For this reason, an important aspect was to elucidate where the miR-135b-5p is mainly expressed in the lung. Newborn miR-135b$^{lacZ,fl/lacZ,fl}$ mice were exposed to normixic and hyperoxic conditions. Lungs were harvest at P14 and embedded in OCT. MiR-135b-5p expression was detected mainly in the septa of developing lungs using β-galactosidase activity staining to detect the lacZ reporter gene (**Figure 22C, D, G, H**). The expression of lacZ reporter gene was not detectable in newborn wildtype mice (**Figure 22A, B, E, F**).

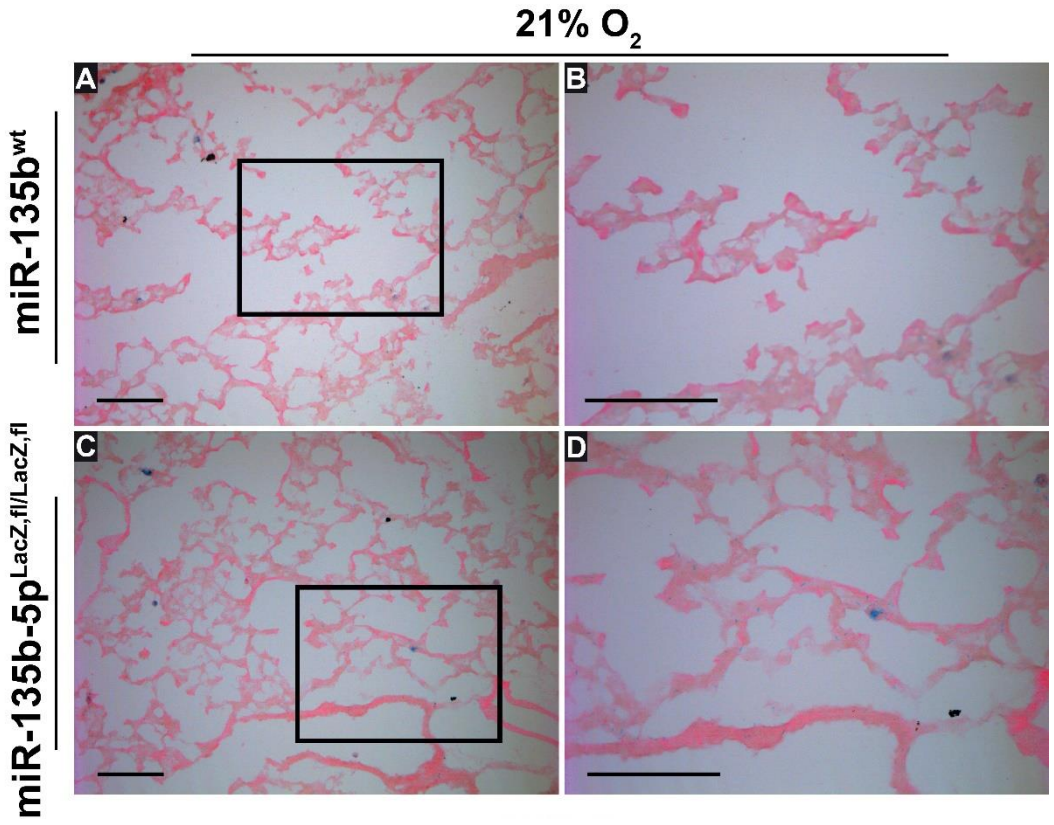

Figure 22. Expression and localization of miR-135b-5p by β-galactosidase activity staining in P14 newborn mice.

The miR-135b$^{lacZ,fl/lacZ,fl}$ newborn mice were used to observe the expression of the lacZ reporter gene by β-galactosidase activity staining. C57BL/6J (miR-135b^{wt}) newborn mice and miR-135b$^{lacZ,fl/lacZ,fl}$ newborn mice were exposed to 21% O_2 and to 85% O_2 for the first 14 days of postnatal life. Lungs were collected at P14. (A, C, E, G) Lower magnification images from lungs. (B, D, F, H) Higher magnification images derived from the black rectangle on the corresponding image on the left, to highlight the β-galactosidase activity staining in the septum. Each image is a representative of images of lung sections obtained from two other mice within each experimental group (*n*=3, per group). Scale bars in photomicrographs represent 50 μm. β-galactosidase activity staining (blue) and eosin counterstaining (pink).

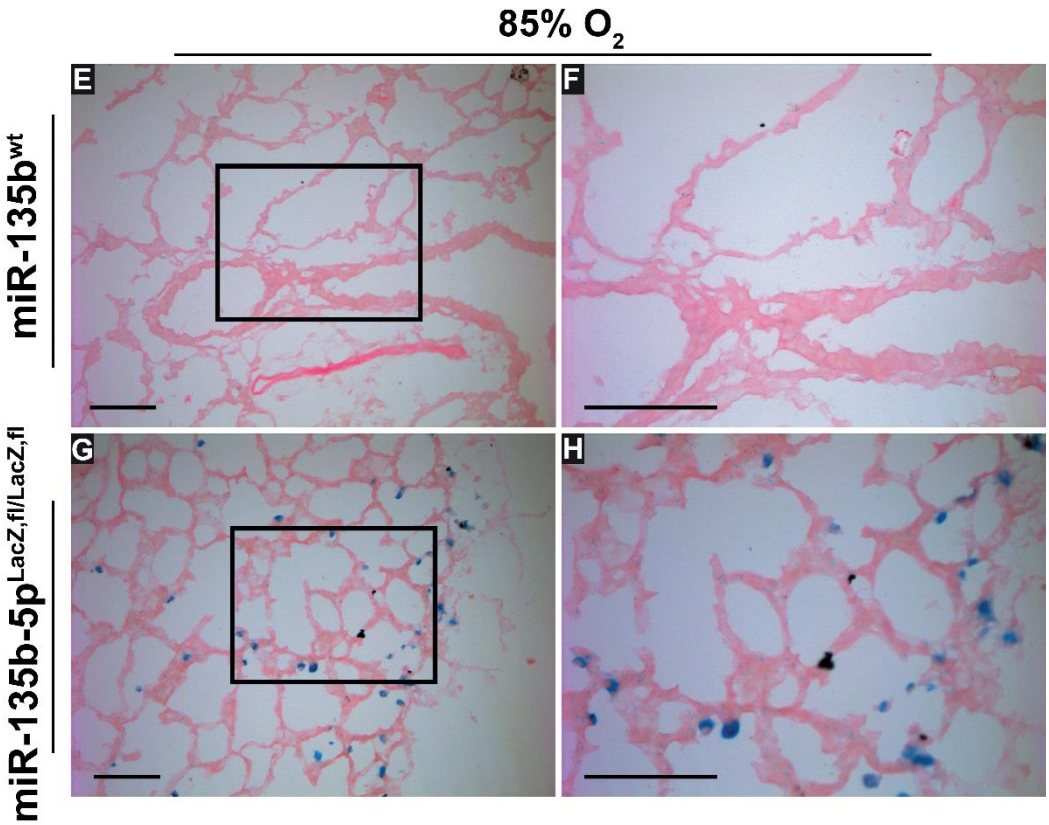

Figure 22-continued

To confirm the previous results, newborn wild type mice were exposed to normoxic or hyperoxic conditions for the first fourteen days of postnatal life and lungs were harvest at P14 and embedded in OCT. The miR-135b-5p localization was performed by FISH using LNA miR-135b-5p probe. The miR-135b-5p expression and localization was detected in the septa of developing lung with higher fluorescence in the 85% O_2 exposed lungs (**Figure 23**).

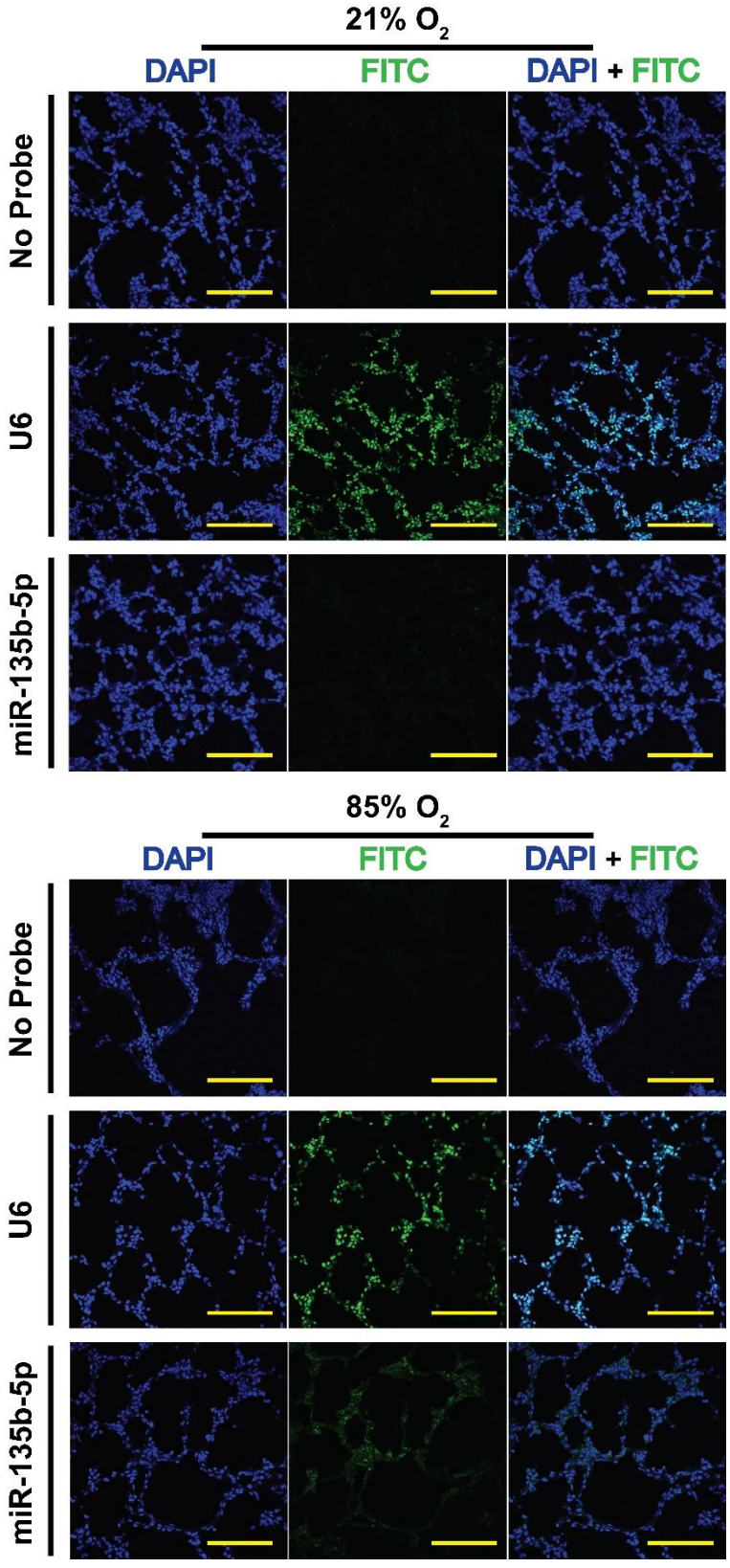

Figure 23. Expression and localization of miR-135b-5p by FISH in P14 newborn mice.

The miR-135b-5p expression localization was performed by FISH using a specific LNA miR-135b-5p probe in cryosection of mouse lungs exposed to 21% O_2 and to 85% O_2 at P14. No Probe was used as negative control probe. The LNA Rnu6 probe (U6) was used as a positive LNA control probe. Positive *in situ* hybridization signals are visualized in green [fluorescein isothiocyanate (FITC)], while blue depicts diamidino-2-phenylindole (DAPI) nuclear stain. Scale bars in photomicrographs represent 50 µm.

The next step was to identify the exact cell population where the miR-135b-5p is expressed. CD31$^+$ cells, CD45$^+$ cells, EpCAM$^+$ cells and the mesenchymal cell fraction were sorted by FACS from P14 mouse lungs. Total miRs were isolated and the miR-135b-5p expression was analyzed by qPCR. On basal levels, the EpCAM$^+$ cells expressed the highest miR-135b-5p expression levels (**Figure 24A**).

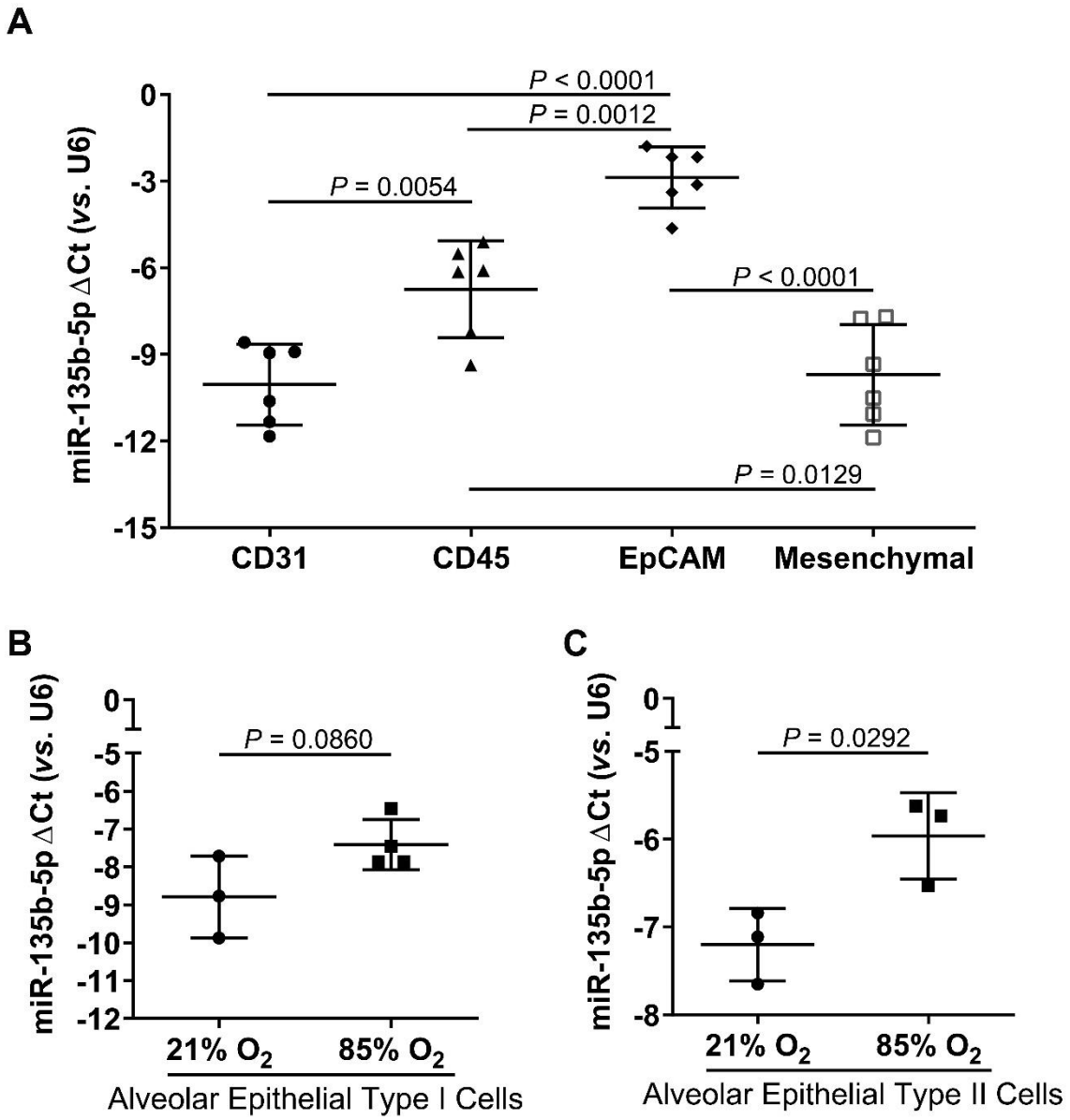

Figure 24. MiR-135b-5p expression in different sorted cell type of newborn mouse lung at P14. (A) miR-135b-5p levels were assessed by qPCR in CD31$^+$ cells, CD45$^+$ cells, EpCAM$^+$ cells and mesenchymal cells isolated by FACS from 21% O_2 exposed mouse lungs at P14. Data represent mean ± SD. Statistical comparison were made using one-way ANOVA with Tukey's *post hoc* test (*n*=6, per group). (B) The miR-135b-5p levels were assessed by qPCR in primary mouse alveolar type I cells sorted by FACS from 21% O_2 exposed mouse lungs *versus* 85% O_2 exposed mouse lungs at P14. (C) miR-135b-5p levels were assessed by qPCR in primary mouse alveolar type II cells isolated by FACS from 21% O_2 exposed mouse lungs *versus* 85% O_2 exposed mouse lungs at P14. Data represent mean ± SD. *P* values were determined by unpaired Student's *t*-test.

To investigate more in detail which cell type of the $EpCAM^+$ cells expressed the miR-135b-5p, mouse AEI and mouse AEII cells were sorted from P14 mouse lungs exposed to 21% O_2 and 85% O_2 by FACS. The miR-135b-5p expression was not significantly changed in mouse AEI cells isolated from normoxic *versus* hyperoxic exposed lungs (**Figure 24B**). Instead, miR-135b-5p expression was 5.6-fold change higher in mouse AEII sorted from lungs exposed to 85% O_2 *versus* lungs exposed to 21% O_2 (**Figure 24C**).

3.7 MiR-135b-5p interaction with Smad5 mRNA in primary mouse alveolar epithelial type II cells

Protein from primary mouse AEII cells were isolated from P14 normoxic and hyperoxic exposed mouse pups and analyzed by western blot. The protein expression of Smad1 and Smad9 was not changed between the normoxic and hyperoxic lungs. The protein expression of Smad5 was significantly decreased in 85% O_2 exposed mouse lungs *versus* 21% O_2 exposed mouse lungs (**Figure 25A**) and was estimated by densitometry (**Figure 25B**). To verify the purity of the mouse AEII cell population, Sftpc protein expression confirmed the presence of mouse AEII cells and aquaporin 5 confirmed the absence of mouse AEI cells (**Figure 25C**).

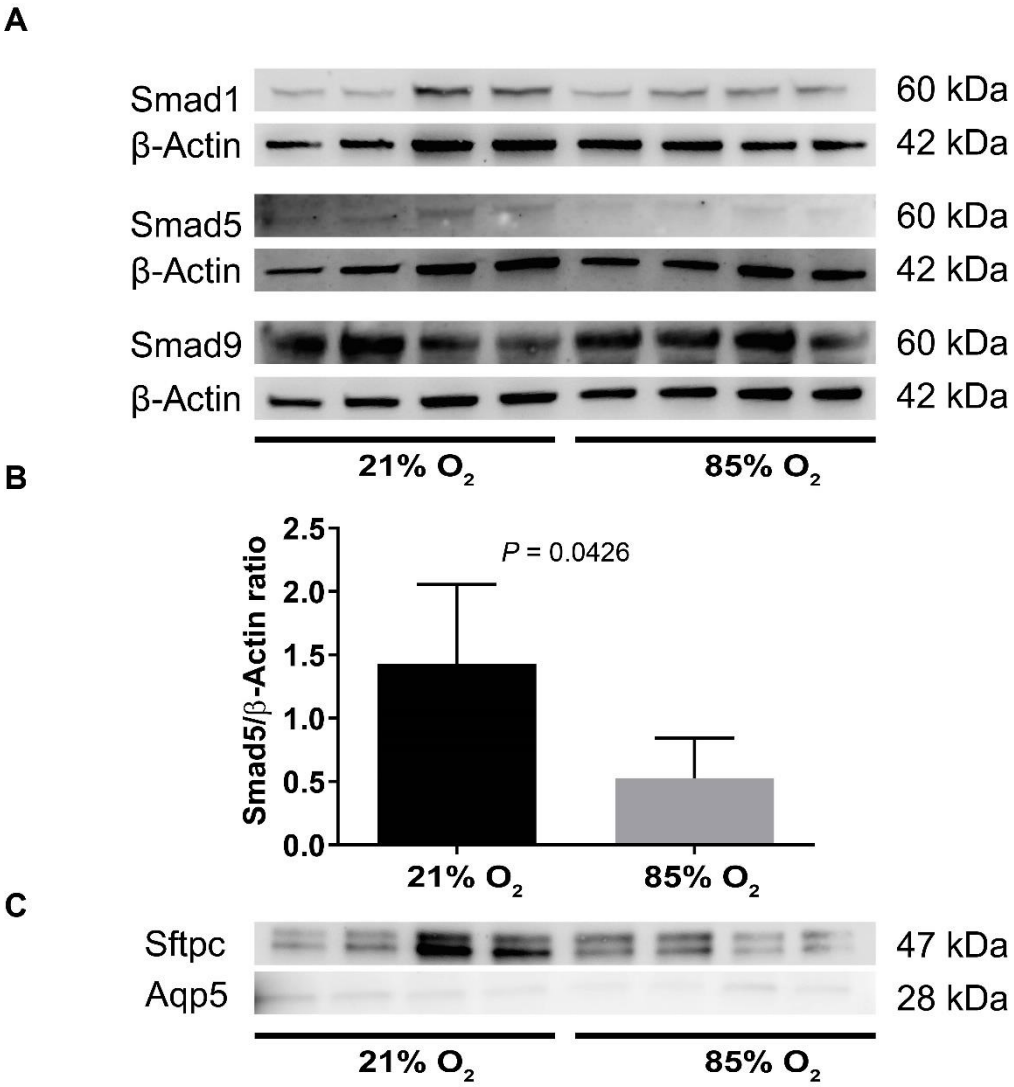

Figure 25. R-Smad protein expression in primary mouse alveolar type II cells at P14.

(A) Smad1, Smad5 and Smad9 levels were assessed by western blot in primary mouse alveolar epithelial type II cells isolated from mice exposed to 21% O_2 and 85% O_2 (*n*=4, per group). (B) Smad5 protein expression was quantified by the ratio of Smad5 to total β-Actin (*n*=4, per group). Data represent mean ± SD. *P* values were determined by unpaired Student's *t*-test. (C) Sftpc and Aqp5 levels were assessed by western blot in primary mouse epithelial type II cells isolated from mice exposed to 21% O_2 and 85% O_2 (*n*=4, per group).

3.8 MiR-135b-5p expression in mouse alveolar epithelial type II cells *in vitro*

The mouse AEII cells were isolated from 3 to 6 months old C57BL/6J wild type mice. A total number of 1×10^6 cells were cultured on an air liquid interface 6-well plate and exposed under 21% O_2 and 85% O_2 for 24 h. Changes in miRs were detected by microarray (GEO accession number GSE92551) and miR-135b-5p was found as significantly upregulated miR (**Figure 26**).

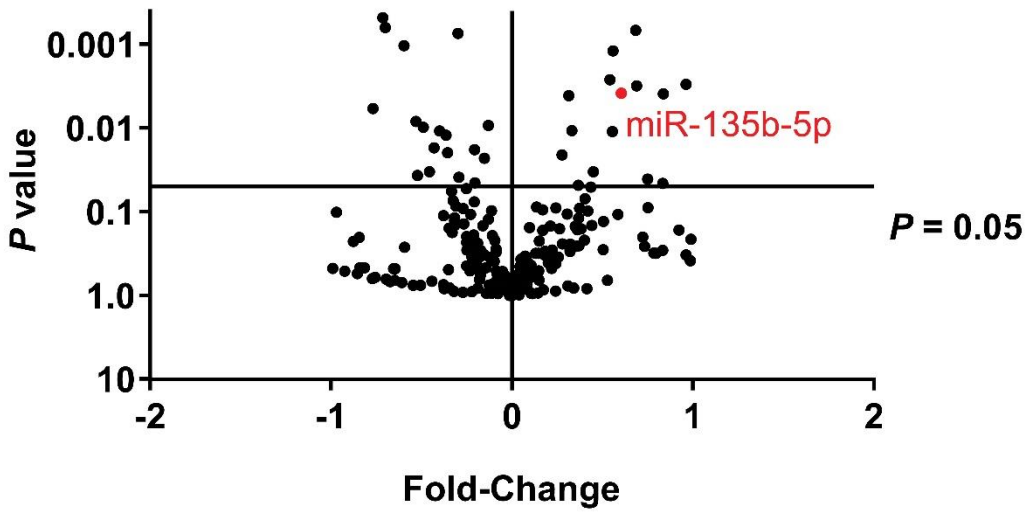

Figure 26. Microarray analysis of miRs in primary mouse alveolar type II cells.
Microarray analysis of miR expression changes in primary mouse alveolar type II cells exposed to 21% O_2 *versus* 85% O_2 for 24 h. Microarray data are available at the GEO database under accession number GSE92551. A one-way ANOVA with Tukey's post-hoc analysis was used to determine *P* values. MiR-135b-5p expression is demarcated in red.

Validation of the microarray was performed independently by qPCR and revealed no changes in the first 24 h of exposure to 85% O_2, but a significant increase of 2.6-fold changes after 48 h exposure to 85% O_2 (**Figure 27**).

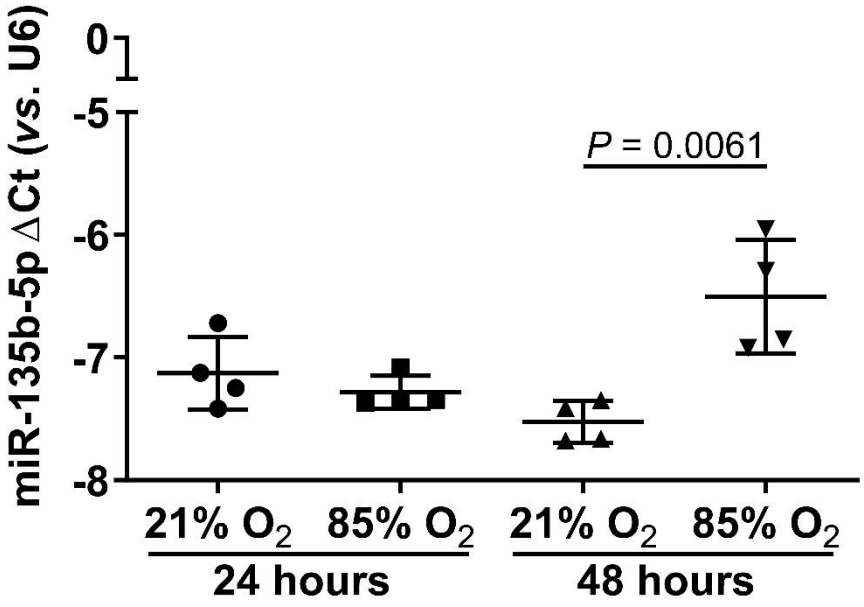

Figure 27. MiR-135b-5p expression in primary mouse alveolar type II cells exposed to 85% O_2.
MiR-135b-5p levels were assessed by qPCR in primary mouse alveolar type II cells exposed to 21% O_2 and 85% O_2 for 24 h and 48 h. Data represent mean ± SD. Statistic comparison were made using unpaired Student's *t*-test (*n*=4 per group).

3.9 Smads regulation in alveolar epithelial cells exposed to hyperoxia

Primary mouse alveolar epithelial type II cells were isolated from three to six months old C57BL/6J wild type and cultured under room air and 85% O_2 for 48 h. The Smad5 gene and protein expression were analyzed respectively by qPCR and western blot. The Smad5 gene expression was not changed (**Figure 28**); however, Smad5 protein expression was significant downregulated in 85% O_2 conditions (**Figure 29**).

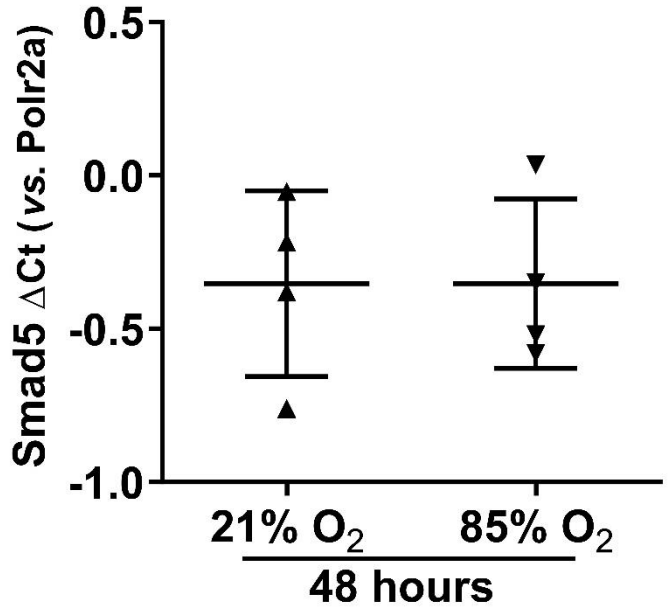

Figure 28. Smad5 gene expression primary mouse alveolar epithelial type II cells.
Smad5 levels were assessed by qPCR in primary mouse alveolar epithelial type II cells exposed to 21% O_2 and 85% O_2. Data represent mean ± SD. Statistic comparison were made using unpaired Student's *t*-test (*n*=4, per group).

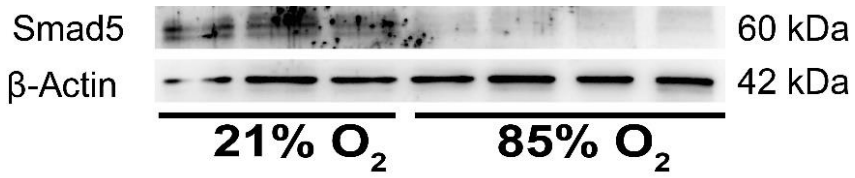

Figure 29. Smad5 protein expression in primary mouse alveolar type II cells.
The Smad5 levels were assessed by western blot in primary mouse alveolar type II cells exposed to 21% O_2 and 85% O_2 for 48 h. (*n*=3-4, per group).

HAE cells were cultured in 21% O_2 and in 85% O_2 for 48 h. Total RNA was isolated and miR-135b-5p gene expression was analyzed by qPCR. The miR-135b-5p was significantly increased in 85% O_2 exposed cells (**Figure 30**).

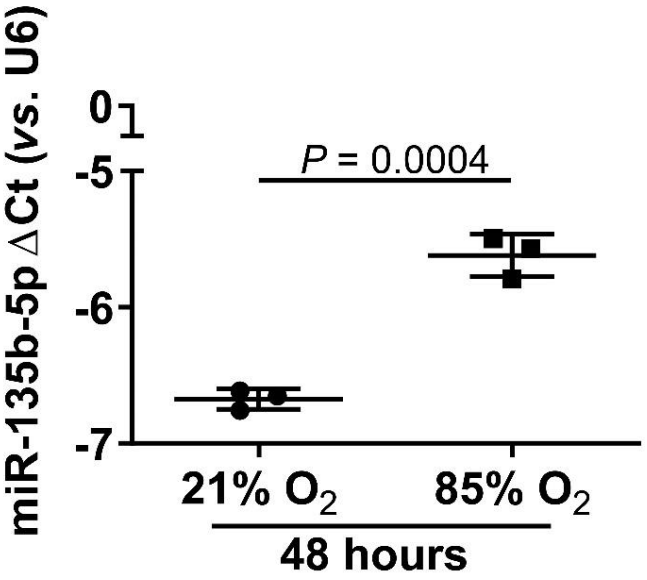

Figure 30. MiR-135b-5p expression human alveolar epithelial cells.

MiR-135b-5p levels were assessed by qPCR in human alveolar epithelial cells exposed to 21% O_2 and 85% O_2. Data represent mean ± SD. Statistic comparison were made using unpaired Student's *t*-test (*n*=3, per group).

The R-Smads levels were analyzed in hAE cells exposed to 21% O_2 and 85% O_2 by western blot. The protein expressions of Smad1, Smad5 and Smad9 were significantly downregulated (**Figure 31A**). Smad5 protein expression was increased and quantified by densitometry (**Figure 31B**).

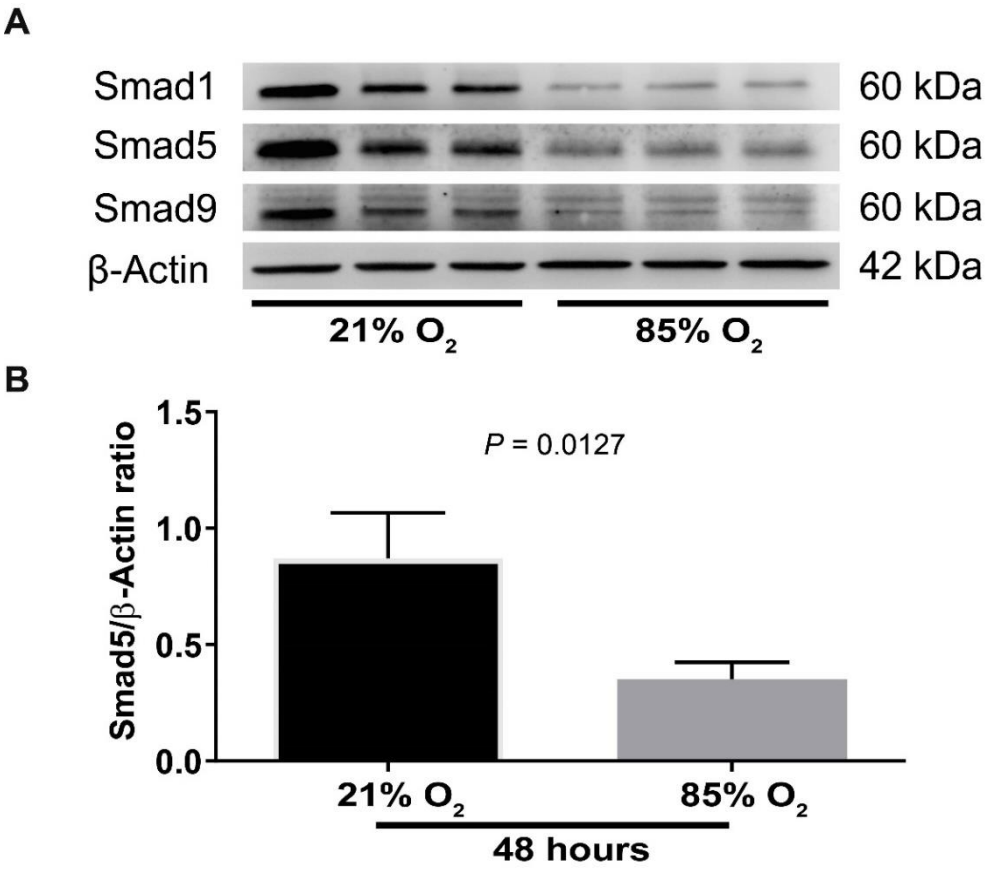

Figure 31. R-Smads protein expression in human alveolar epithelial cells.

(A) Smad1, Smad5 and Smad9 protein expressions were assessed by western blot in human alveolar epithelial cells exposed to 21% O_2 and 85% O_2 (*n*=3, per group). (B) Smad5 protein expression was quantified by the ratio of Smad5 to total β-Actin (*n*=3, per group). Data represent mean ± SD. *P* values were determined by unpaired Student's *t*-test.

3.10 Smad5 expression in A549 cells exposed to hyperoxia and transfected with a synthetic mimic-135b-5p

A549 cells were exposed to 21% O_2 and 85% O_2 for 48 h. R-Smads protein expression was analyzed by western blot. The Smad1 and Smad9 protein expression was not changed, instead the protein expression of Smad5 was reduced in the A549 cells exposed to 85% O_2 (**Figure 32A**). The Smad5 protein expression was quantified by densitometry and was reduced under hyperoxic conditions (**Figure 32B**).

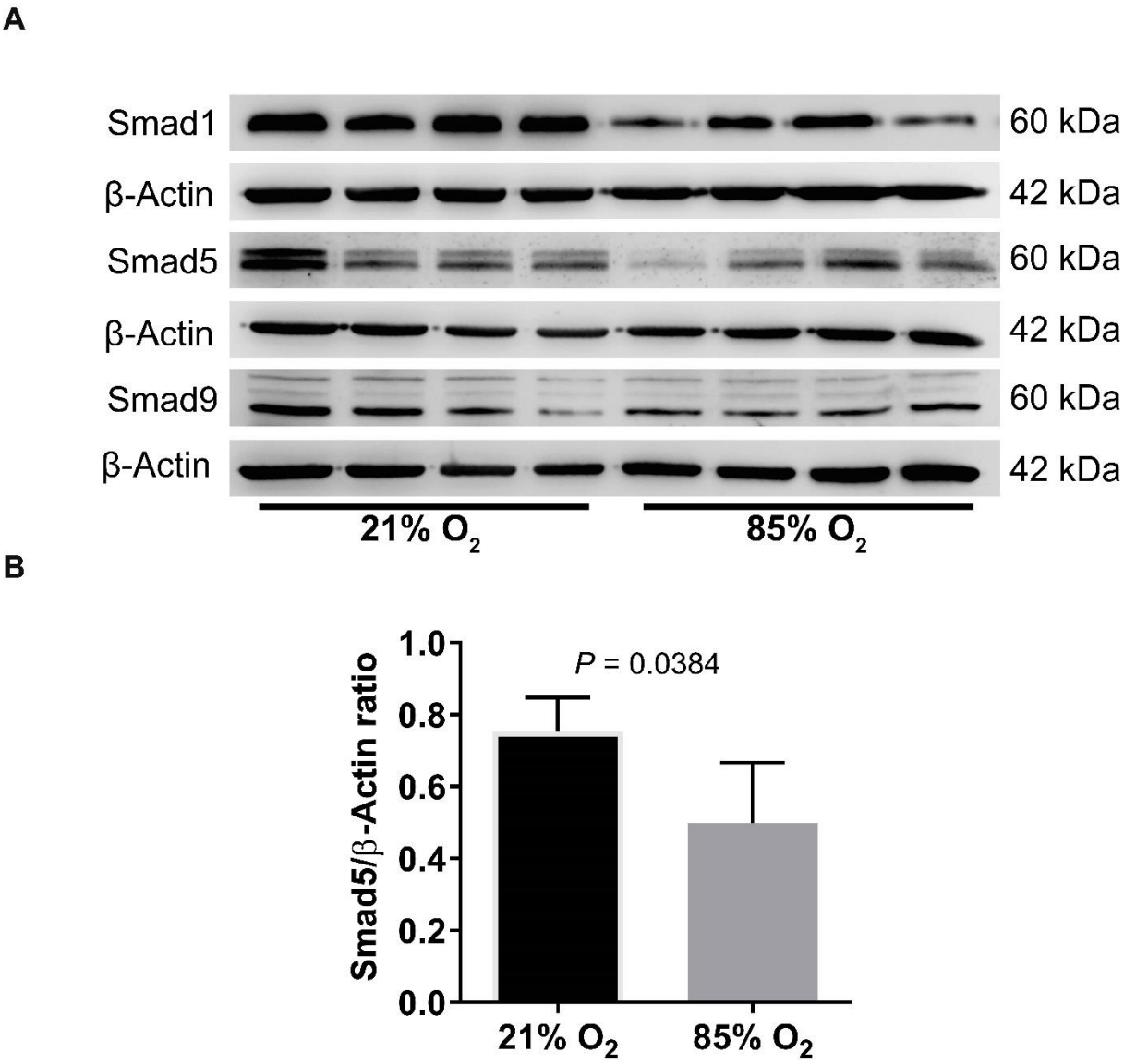

Figure 32. R-Smad protein expression in A549 cells exposed to 21% O_2 and 85% O_2.
(A) Smad1, Smad5 and Smad9 levels were assessed by western blot in A549 cells exposed to 21% O_2 and 85% O_2 for 48 h (*n*=4, per group). (B) Smad5 protein expression was quantified by the ratio of Smad5 to total β-Actin (*n*=4, per group). Data represent mean ± SD. *P* values were determined by unpaired Student's *t*-test.

Moreover, A549 cells were transfected with a synthetic scrambled miR mimic and a synthetic miR-135b-5p mimic for 48 h with a concentration of 80 nM. Smad5 protein expression was analyzed by western blot confirming that the synthetic miR-135b-5p mimic was able to knockdown the Smad5 protein expression. The Smad1 and Smad9 proteins were not changed in expression, confirming that the miR-135b-5p interacts only with Smad5 (**Figure 33**).

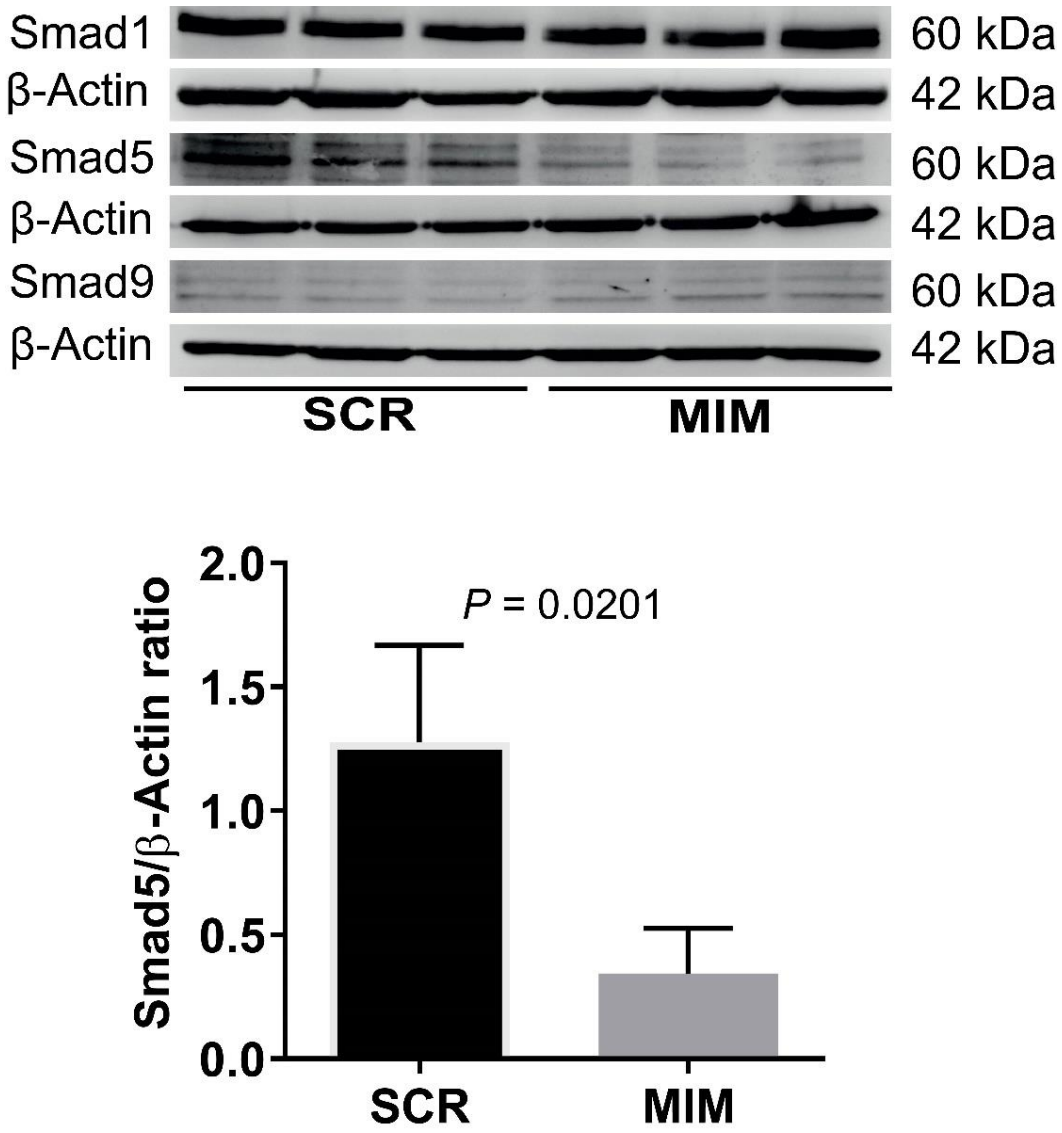

Figure 33. Smad1, Smad5 and Smad9 protein expression in A549 cells transfected with synthetic miR mimics.

Smad1, Smad5 and Smad9 levels were assessed by western blot in A549 cells transfected with a synthetic scrambled miR mimic (SCR) and a synthetic miR-135b-5p mimic (MIM) for 48 h at 80 nM (*n*=3, per group). Smad5 protein expression was quantified by the ratio of Smad5 to total β-Actin (*n*=4, per group). Data represent mean ± SD. *P* values were determined by unpaired Student's *t*-test.

To prove the transfection of the 80 nM of synthetic miR-135b-5p mimic, the expression of miR-135b-5p was analyzed by qPCR. MiR-135b-5p gene expression was significantly increased meaning that the synthetic miR-135b-5p mimic was successfully delivered to the A549 cells (**Figure 34**).

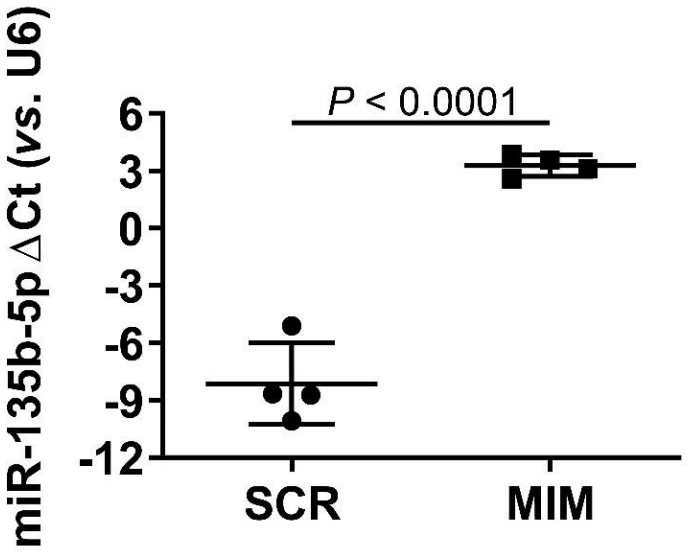

Figure 34. MiR-135b-5p gene expression in A549 cells transfected with synthetic miR-135b-5p mimic.

MiR-135b-5p levels were assessed by qPCR in A549 cells transfected with synthetic scrambled miR mimic (SCR) and a synthetic miR-135b-5p mimic (MIM) for 48 h at 80 nM. Data represent mean ± SD. Statistical comparisons were made using unpaired Student's *t*-test (*n*=4, per group).

3.11 The impact of synthetic miR-135b-5p mimic on proliferation, apoptosis, and viability in A549 cells

The impact of synthetic miR-135b-5p mimic on cell proliferation was assessed by BrdU assay in untransfected cells, mock, synthetic scrambled miR mimic and synthetic miR-135b-5p mimic. Absorption of 450 nm was significant lower in the synthetic miR-135b-5p mimic treated cells, demonstrating an important role of the miR-135b-5p in cell proliferation (**Figure 35A**). Furthermore, the impact of synthetic miR-135b-5p mimic treatment was analyzed in the apoptosis assay and in the viability assay, with no significant changes (**Figure 35B** and **35C**).

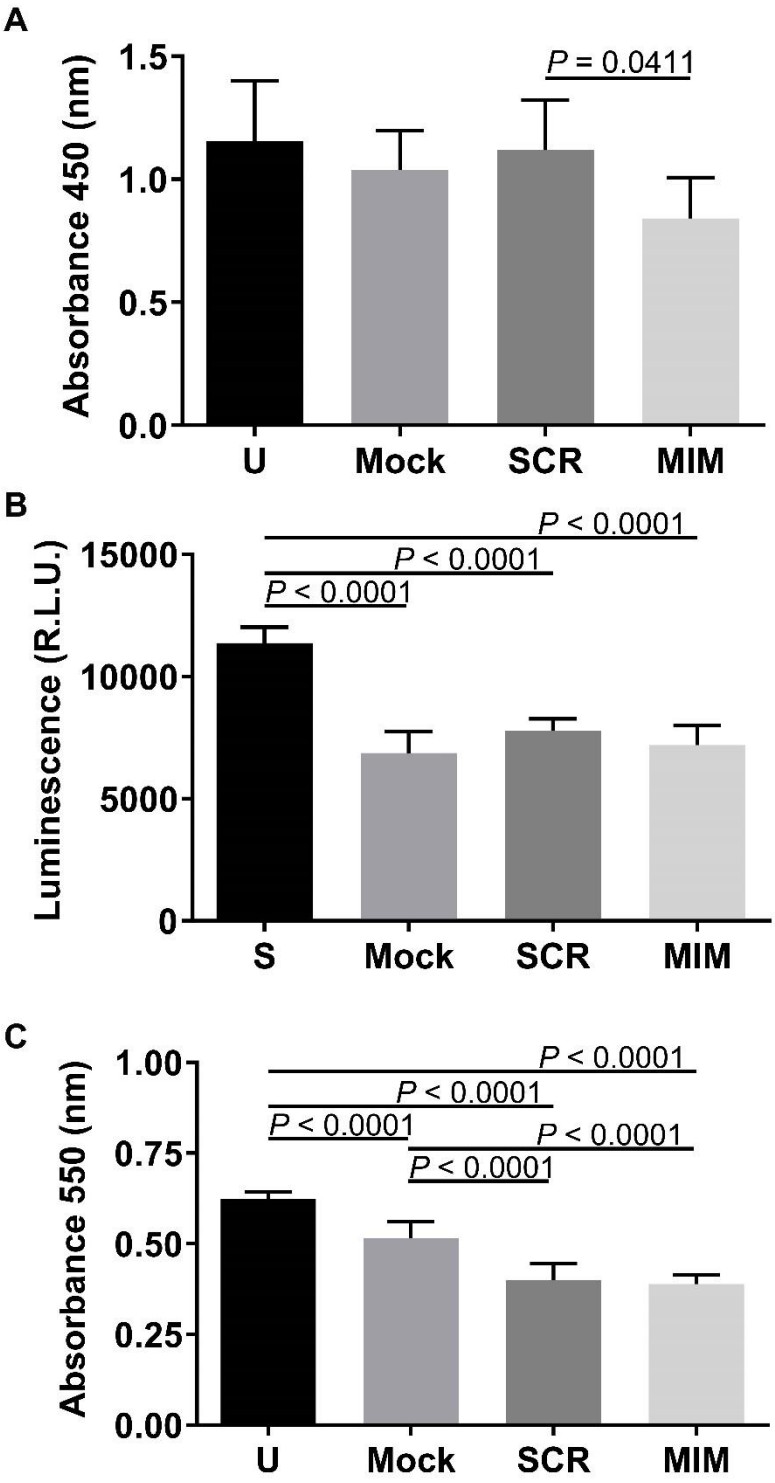

Figure 35. Determination of the impact of synthetic miR-135b-5p mimic on proliferation, apoptosis, and viability in A549 cells.

The impact of synthetic miR-135b-5p mimic application in A549 cells was assessed in untransfected cells (U), mock, synthetic scrambled miR mimic treated cells (SCR) and synthetic miR-135b-5p mimic treated cells (MIM) by measuring (A) cell proliferation, (B) cell apoptosis and (C) cell viability. Data represent mean ± SD. Statistic comparison were made using one-way ANOVA with Tukey's *post hoc* test (*n*=12, per group). R.L.U., relative luminescence units; S, Staurosporine.

3.12 The effects of induced global deletion of Smad5

The germline deleter Cre-ER^{T2} mice were crossed with Smad5$^{fl/fl}$ conditional mutant mice to generate the Cre-ER^{T2}-Smad5$^{fl/fl}$ mice. The Cre-ER^{T2}-Smad5^{wt} and Cre-ER^{T2}-Smad5$^{fl/fl}$ mice were IP injected on P1 and P2 with tamoxifen to generate the Cre-ER^{T2}-Smad5^{wt} mice and the Smad5^{GiΔ} mice respectively (**Figure 7B**). Lungs were harvest on P14 to analyze R-Smads protein expression and to study lung architecture by design-based stereology. Smad1 and Smad9 protein expression was not changed between groups. The Smad5 protein expression, as expected, was significantly lower in the Smad5^{GiΔ} mice compared to the Cre-ER^{T2}-Smad5^{wt} mice. The presence of Smad5 protein in the Smad5^{GiΔ} mice was due to the incomplete Cre driver employed in the study (**Figure 36**).

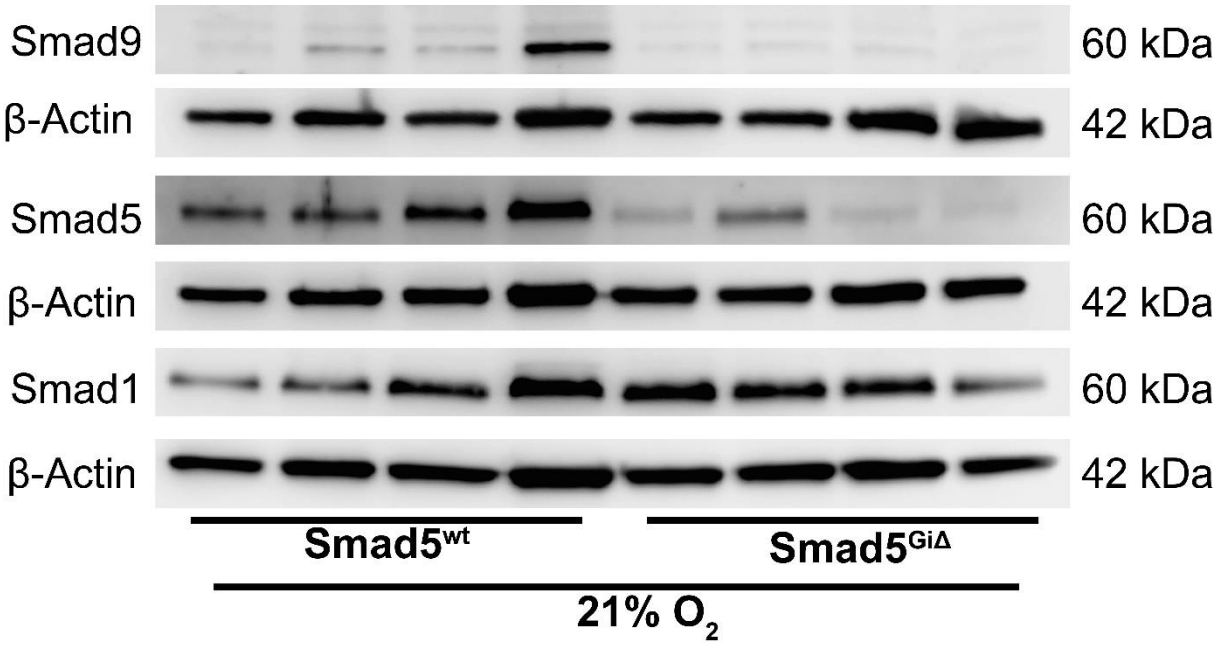

Figure 36. R-Smad protein expression in lung homogenates in Cre-ER^{T2}-Smad5^{wt} mice and Smad5^{GiΔ} mice.

Smad1, Smad5 and Smad9 levels were assessed by western blot in lung homogenates in Cre-ER^{T2}-Smad5^{wt} (Smad5^{wt}) mice and Smad5^{GiΔ} mice exposed to 21% O_2 at P14 (*n*=4, per group).

The global induced deletion of the Smad5 worsened the lung architecture over the period from P1 to P14 in Smad5^{GiΔ} pups (*n*=5, per group) compared to Cre-ER^{T2}-Smad5^{wt} pups (**Figure 37A, B** *versus* **37C, D**; complete data set in table 32). In fact, comparing Cre-ER^{T2}-Smad5^{wt} mice *versus* Smad5^{GiΔ} mice, total number of alveoli was decreased from 2.61×10^6 alveoli to 1.78×10^6 alveoli (**Figure 37E**), alveolar density was decreased from 13.60×10^6 alveoli/cm^3 to 10.97×10^6 alveoli/cm^3 (**Figure**

37F), surface area of gas exchange was decreased from 139.40 cm^2 to 116.60 cm^2 (**Figure 37G**) and lung volume was decreased from 0.22 cm^3 to 0.18 cm^3 (**Figure 37I**). MLI (**Figure 37J**) and septal thickness (**Figure 37H**) were not affected. These data indicate that Smad5 is a crucial player in normal lung development.

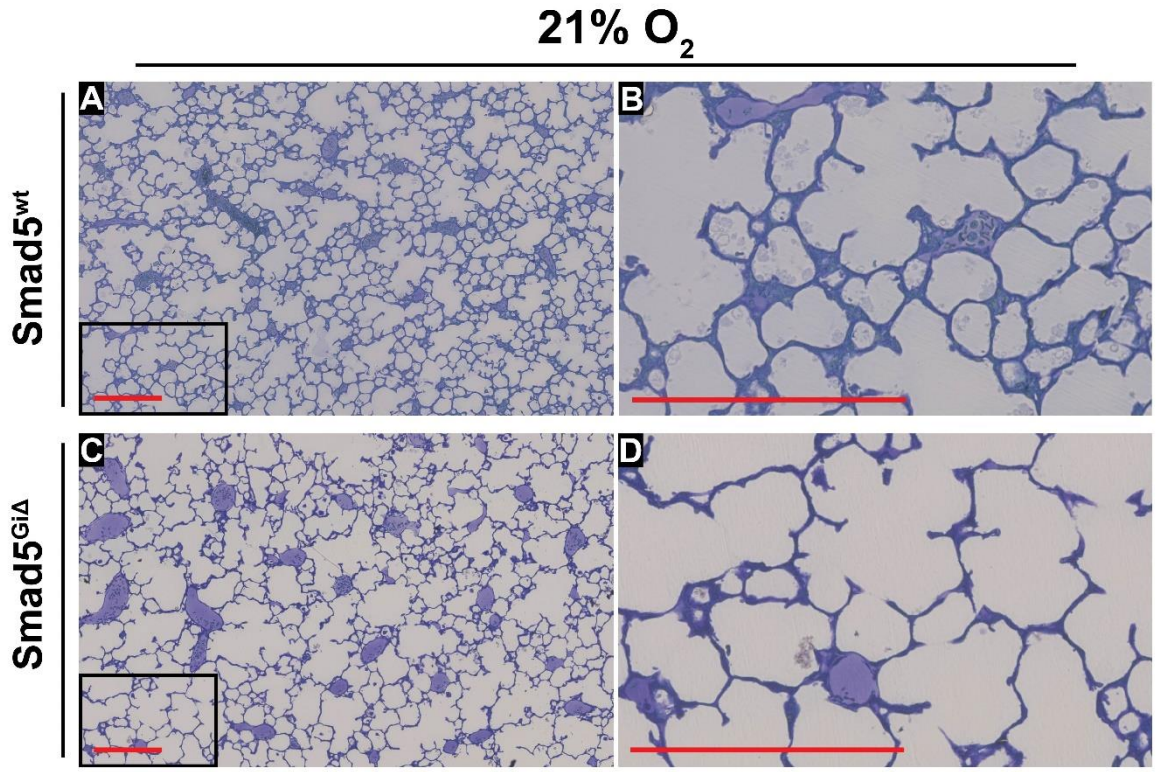

Figure 37. Stereology analysis of lung structure in Cre-ER^{T2}-Smad5^{wt} mice and Smad5^{GiΔ} mice at P14.

Newborn Cre-ER^{T2}-Smad5^{wt} (Smad5^{wt}) and Smad5^{GiΔ} mice were IP injected on P1 and P2 and exposed to 21% O_2 from the day of birth until P14. Lungs were collected and processed for analysis of the lung structure by design-based stereology on P14. (A and C) Lower magnification images from lungs. (B and D) Higher magnification images derived from the black rectangle on the corresponding image on the bottom left, to highlight changes in septal thickness. Each image is representative of images of lung sections obtained from four other mice within each experimental group (*n*=5, per experimental group). Scale bars in photomicrographs represent 200 µm. Design-based stereology was employed to assess (E) alveoli number, (F) alveolar density, (G) surface area of gas-exchange, (H) septal thickness (I) lung volume and (J) mean linear intercept. Data represent mean ± S.D. Data comparisons were made by using unpaired Student's *t*-test. Sex: blue square denotes males and red circle denotes females.

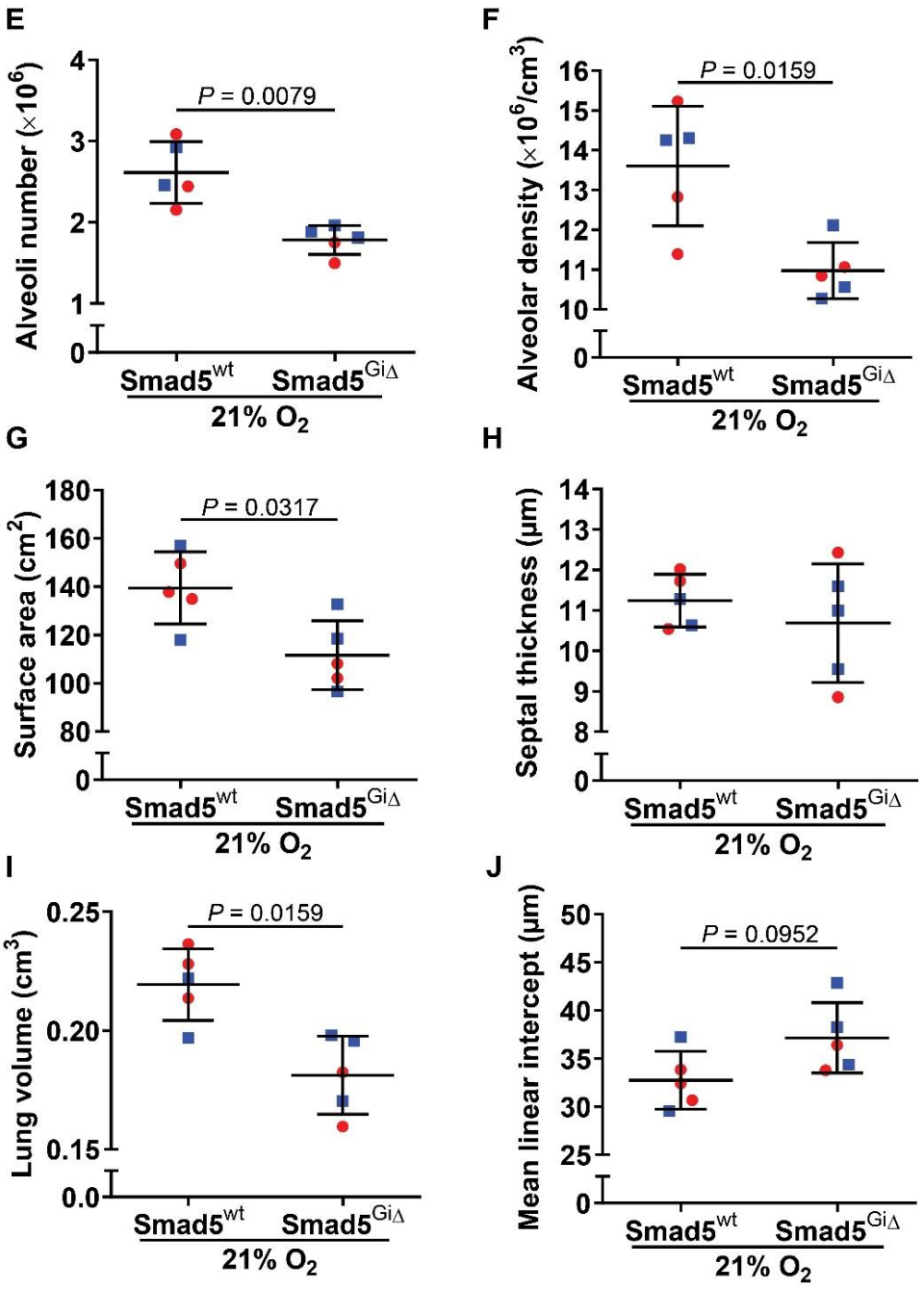

Figure 37-continued

Table 32. Stereological analysis of lungs from P14 Cre-ER^{T2}-Smad5^{wt} and Smad5^{GiΔ} mice exposed to normoxia.

Parameter	21% O_2		
	Cre-ER^{T2}-Smad5^{wt}	Smad5^{GiΔ}	
	mean ± SD	mean ± SD	*P* value *vs.* Cre-ER^{T2}-Smad5^{wt}
V (lung) [cm^3]	0.22 ± 0.01	0.18 ± 0.02	0.0050
CV [*V* (lung)]	0.07	0.09	
V_V (par/lung) [%]	87.50 ± 3.21	89.78 ± 0.05	0.3612
N (alv, lung) 10^6	2.61 ± 0.38	1.78 ± 0.18	0.0022
N_V (alv/par) 10^6 [cm^{-3}]	13.60 ± 1.50	10.97 ± 0.70	0.0077
CV [N (alv/lung)]	0.11	0.06	
S_V [cm^{-1}]	725.40 ± 31.61	685.00 ± 35.54	0.0944
S (alv epi, lung) [cm^2]	139.40 ± 14.97	116.60 ± 14.32	0.0169
CV [S (alv epi, lung)]	0.11	0.13	
τ (sep) [µm]	11.24 ± 0.65	10.69. ± 1.47	0.4612
CV [τ (sep)]	0.06	0.14	
MLI [µm]	32.74 ± 3.00	37.14 ± 3.66	0.0711
CV [MLI]	0.09	0.09	

Abbreviations: *alv*, alveoli; *alv air*, alveolar airspaces; *alv epi*, alveolar epithelium; *CV*, coefficient of variation; MLI, mean linear intercept; *N*, number; N_V, numerical density; *par*, parenchyma; *S*, surface area; S_V, surface density; *τ* (sep), arithmetic mean septal thickness; *V*, volume; V_V, volume density; wt, wild type.

The interaction between miR-135b-5p and Smad5 mRNA is a crucial point in normal and aberrant lung development. TSB-Smad5 was employed to bind between the miR-135b-5p binding site and the Smad5 3′-UTR mRNA. C57BL/6J mouse pups were injected IP on P1 and P3 with 10 mg/kg of TSB-Control (Scrambled) and 10 mg/kg TSB-Smad5 respectively and exposed to 21% O_2 and 85% O_2. R-Smad protein expression was analysed on P14 animals exposed to 21% O_2 and 85% O_2 by western blot. The Smad1 and Smad9 protein expressions were not impacted by the TSB-Smad5 but Smad5 protein expression was downregulated (**Figure 38A**). To investigate further the effect of TSB-Smad5 treatment in the 85% O_2 exposed group, a higher number of animals was employed. Six newborn mice for the scrambled control group and six newborn mice for the TSB-Smad5 group exposed to 85% O_2 were used. The Smad5 protein expression was decreased but not significantly in the TSB-Smad5 group (**Figure 38B**). The Smad5 protein expression was estimated by densitometry (**Figure 38C**).

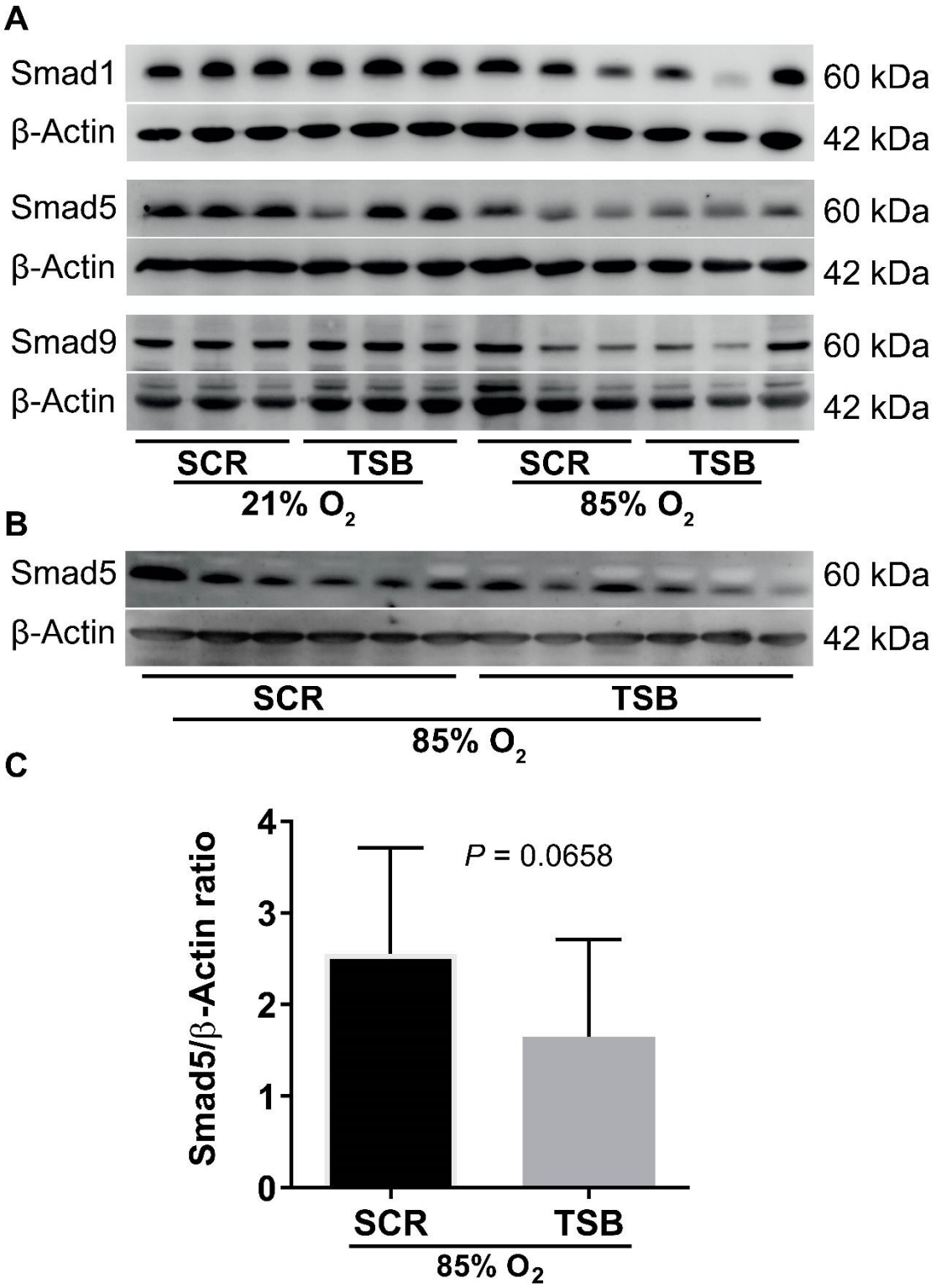

Figure 38. R-Smad protein expression in lung homogenates after TSB-Smad5 treatment at P14. (A) Smad1, Smad5 and Smad9 levels were assessed by western blot in lung homogenates in 21% O_2 scrambled control (SCR) and TSB-Smad5 (TSB) treated and in 85% O_2 scrambled control (SCR) and TSB-Smad5 (TSB) treated (*n*=3, per group). (B) Smad5 protein levels assessed by western blot in lung homogenates in 85% O_2 scrambled control and TSB-Smad5 treated animals (*n*=6, per group). (C) Smad5 protein expression was quantified by the ratio of Smad5 to total β-Actin (*n*=6, per group). Data represent mean ± SD. *P* values were determined by unpaired Student's *t*-test.

The TSB-Smad5 treatment worsened dramatically the lung structure in the first fourteen days of life in 85% O_2 treated animals (*n*=5, per group) compared to 85% O_2 control mice (**Figure 39G, H** *versus* **39E, F**), and in room air treated animals (*n*=5, per group) compared to room air exposed control animals (**Figure 39C, D** *versus* **39A, B**; complete data set in table 33). In detail, comparing TSB-Smad5 treated animals exposed to 85% O_2 *versus* scrambled control treated animals exposed to 85% O_2, total number of alveoli was reduced from 1.78×10^6 alveoli to 1.24×10^6 alveoli (**Figure 39I**), alveolar density was reduced from 7.12×10^6 alveoli/cm^3 to 5.5×10^6 alveoli/cm^3 (**Figure 39J**) and surface area of gas exchange was decreased from 126 cm^2 to 108 cm^2 (**Figure 39H**). The septal thickness was increased from 12.34 µm to 14.6 µm. Lung volume and MLI were not changed (**Figure 39M, O**). The harsh effect of the TSB-Smad5 treatment was observed also in the 21% O_2, where the total number of alveoli was reduced from 4.20×10^6 alveoli to 2.79×10^6 alveoli (**Figure 39I**), alveolar density was reduced from 17.20×10^6 alveoli/cm^3 to 13.60×10^6 alveoli/cm^3 (**Figure 39J**) and surface area of gas exchange was decreased from 241 cm^2 to 156 cm^2 (**Figure 39H**). Septal thickness was increased from 9.7 µm to 12.0 µm. Lung volume and MLI were not changed between the groups (**Figure 39M, O**).

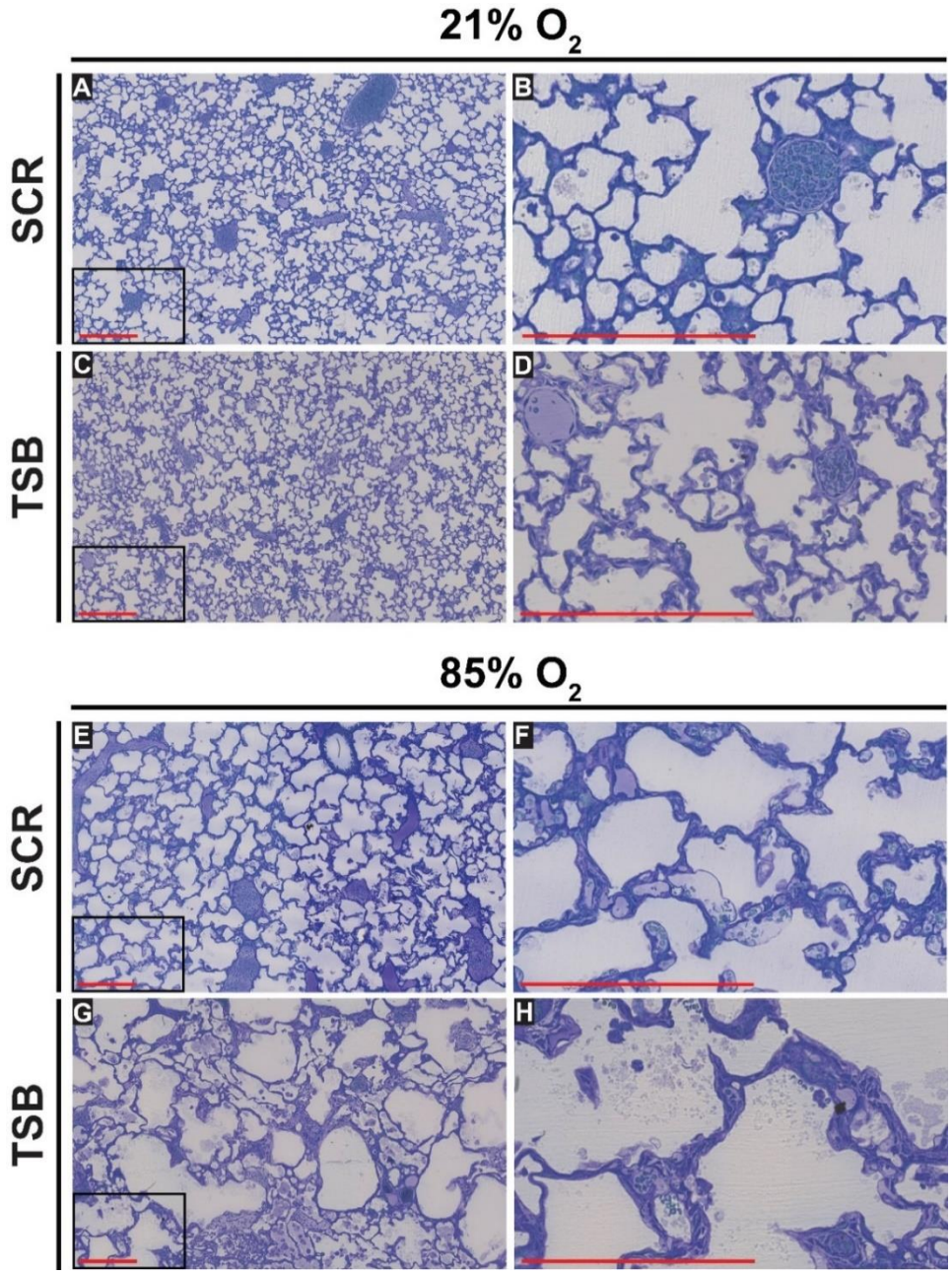

Figure 39. Stereological analysis of lung structure in newborn pups after TSB-Smad5 treatment. Newborn mice were IP injected on P1 and P3 with scrambled (SCR) and TSB-Smad5 (TSB) and exposed to 21% O_2 and 85% O_2 from the day of birth until P14. Lungs were harvested and processed for analysis of the lung structure by design-based stereology on P14. (A, C, E, G) Lower magnification images from lungs. (B, D, F, H) Higher magnification images derived from the black rectangle on the corresponding image on the bottom left, to highlight changes in the septum. Each image is a representative of images of lung sections obtained from four other mice within each experimental group (*n*=4,5, per group). Scale bars in photomicrographs represent 200 μm. Design-based stereology was employed to assess (I) alveoli number, (J) alveolar density, (K) surface area of gas-exchange, (L) lung volume, (M) septal thickness and (N) mean linear intercept. Data represent mean ± S.D. Data comparisons were made by one-way ANOVA with Tukey's *post hoc* test. Sex: blue square denotes males and red dot denotes females.

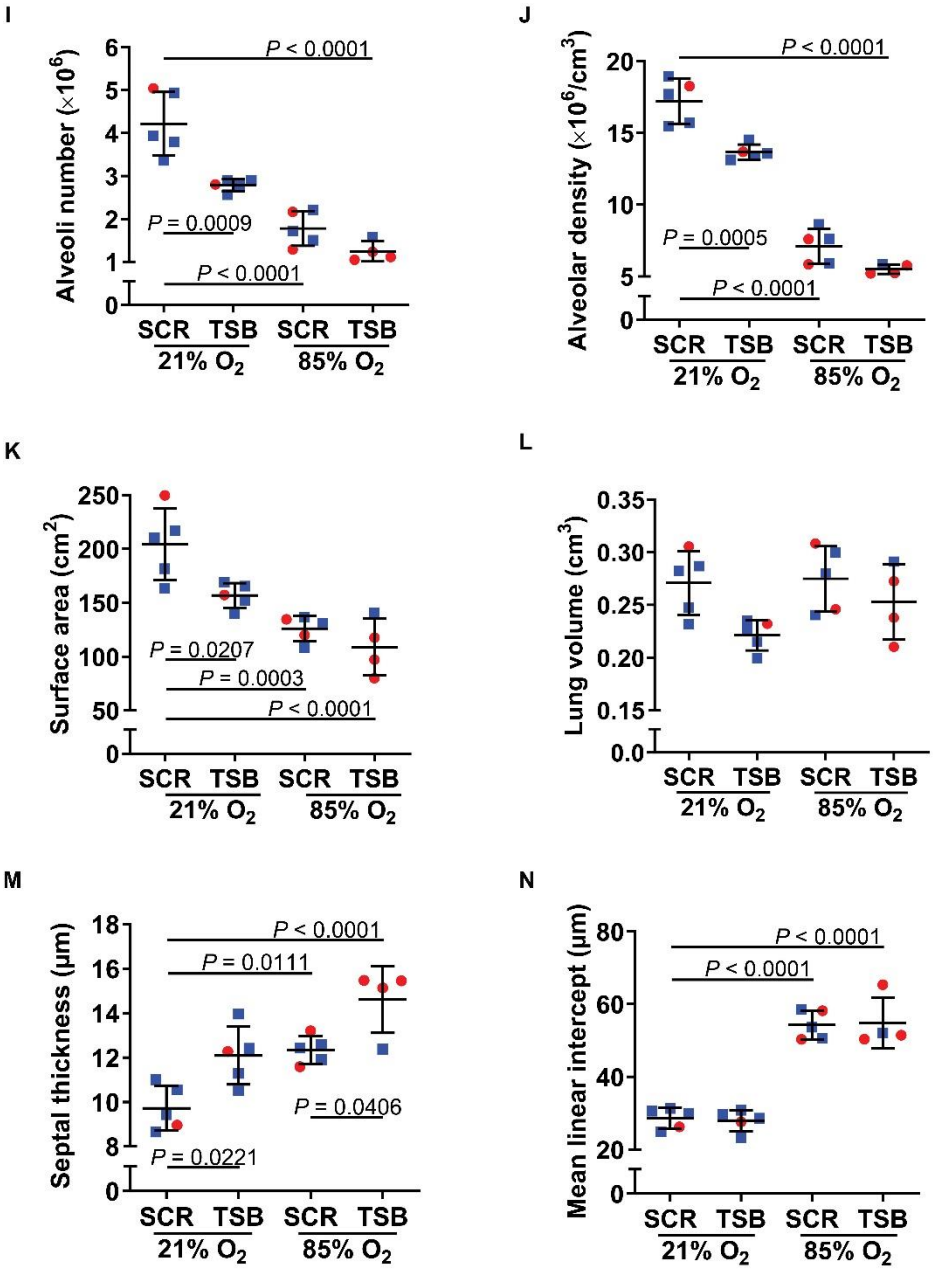

Figure 39-continued

Table 33. Stereological analysis of lungs from P14 TSB-Smad5 treated mice exposed either to normoxia or to hyperoxia compared to scrambled controls.

Parameter	21% O_2		85% O_2			
	scrambled	TSB-Smad5	scrambled		TSB-Smad5	
	mean ± SD	mean ± SD	mean ± SD	*P* value *vs.* scrambled/21% O_2	mean ± SD	*P* value *vs.* scrambled/85% O_2
V (lung) [cm^3]	0.27 ± 0.03	0.22 ± 0.01	0.27 ± 0.03	0.9959	0.25 ± 0.03	0.6661
CV [*V* (lung)]	0.11	0.06	0.11		0.14	
V_V (par/lung) [%]	87.37 ± 2.73	91.53 ± 3.82	90.50 ± 3.14	0.4988	88.85 ± 4.13	0.8907
N (alv, lung) 10^6	4.21 ± 0.74	2.79 ± 0.14	1.78 ± 0.41	< 0.0001	1.24 ± 0.24	0.3297
N_V (alv/par) 10^6 [cm^{-3}]	17.21 ± 1.56	13.66 ± 0.53	7.12 ± 1.20	< 0.0001	5.51 ± 0.33	0.1555
CV [N (alv/lung)]	0.09	0.04	0.17		0.06	
S_V [cm^{-1}]	834.90 ± 53.19	767.50 ± 27.97	508.50 ± 32.70	< 0.0001	479.40 ± 45.00	0.7150
S (alv epi, lung) [cm^2]	241.70 ± 33.44	156.80 ± 11.48	126.00 ± 11.81	0.0003	108.80 ± 26.28	0.6727
CV [S (alv epi, lung)]	0.16	0.07	0.09		0.24	
τ (sep) [µm]	9.72 ± 1.02	12.09 ± 1.30	12.34 ± 0.62	0.0111	14.61 ± 1.49	0.0406
CV [τ (sep)]	0.10	0.10	0.05		0.10	
MLI [µm]	28.62 ± 2.85	28.00 ± 2.91	54.25 ± 3.93	< 0.0001	54.81 ± 7.04	0.9972
CV [MLI]	0.10	0.10	0.07		0.13	

Abbreviations: *alv*, alveoli; *alv air*, alveolar airspaces; *alv epi*, alveolar epithelium; *CV*, coefficient of variation; MLI, mean linear intercept; *N*, number; N_V, numerical density; *par*, parenchyma; *S*, surface area; S_V, surface density; *τ* (sep), arithmetic mean septal thickness; TSB, Target Site Blocker; *V*, volume; V_V, volume density. Values are presented as mean ± SD, *n* = 4-5 lungs for each group. A one-way ANOVA with Tukey's *post-hoc* analysis was used to determine *P* values.

The TSB-Smad5 treatment worsened lung structure in the severe hyperoxia-based model of BPD with a significant reduction of the Smad5 protein expression in lung homogenates. To support these data, A549 cells were transfected with 50 nM, 100 nM and 200 nM of TSB-Smad5. The protein expression of Smad5 was decreased on higher concentrations of TSB-Smad5, demonstrating that the TSB-Smad5 was able to bind the Smad5 mRNA 3′-UTR and to reduce the protein expression of Smad5. The protein expression of Smad9 was not changed and the protein expression of Smad1 was changed only at 200 nM of TSB-Smad5 (**Figure 40**).

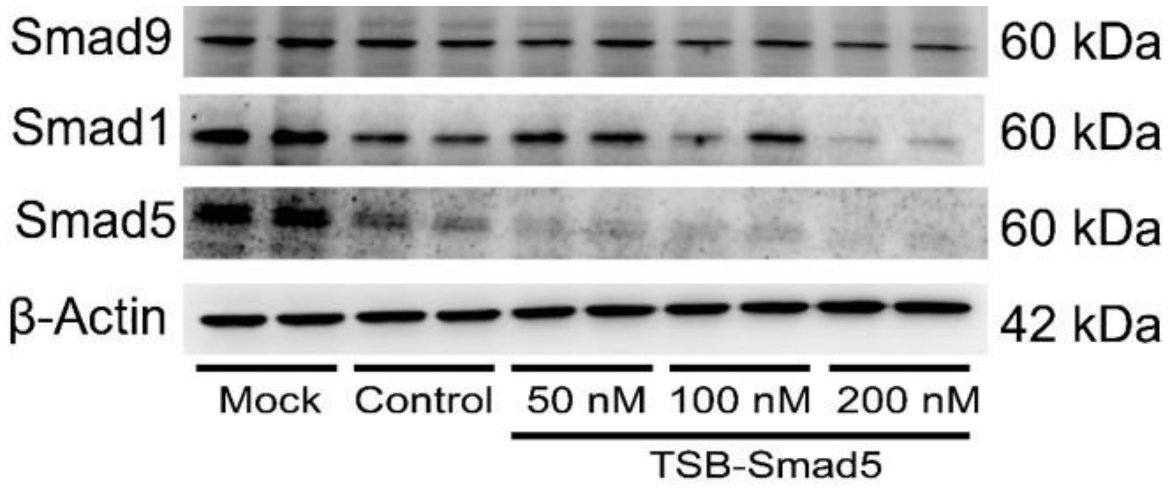

Figure 40. R-Smad protein expression in A549 cells treated with TSB-Smad5.
A549 cells were treated for 48 h with 50 nM, 100 nM and 200 nM of TSB-Smad5 and scrambled control. Protein expression of Smad1, Smad5 and Smad9 levels were assessed by western blot (*n*=2, per group).

4 Discussion

Bronchopulmonary dysplasia causes significant mortality and long-term morbidity in premature infants (38). Since the first description of this pathology by Dr. Northway, oxygen supplementation and/or mechanical ventilation remain the first response to treat premature infants. Treatments mitigate the oxygen toxicity and the barotrauma caused to the lung, but still induce an aberrant lung development. The lung architecture in BPD patients is mainly characterized by fewer and larger alveoli associated with increased septal thickness (122). So far, no treatment was successful to prevent BPD which remains a not fully understood disease. However, the use of a standardized animal model of BPD helps to recreate the phenotypical hallmarks of the disease and to study potential treatments (103).

In the hyperoxia-based mouse model of BPD was possible to identify a new class of modulators, the miRs, that have important role in the regulation of gene and protein expression during normal and aberrant lung development (124, 142).

4.1 MiR-135b-5p expression in human and experimental BPD

MiR-135b-5p was found to play a key role in aberrant lung development. MiR-135b-5p gene expression was upregulated in hyperoxic exposed newborn mice at P3, P5, P7, P10, and P14. This upregulation during the first 14 days of postnatal life revealed miR-135b-5p as an important regulator in the saccular and alveolar phase of lung development. Interestingly, these data correlate in human BPD material, where the miR-135b-5p was significantly upregulated in BPD patients compared to human control lungs. These results were crucial to link clinical and experimental BPD, indicating miR-135b-5p as a fundamental modulator in the postnatal lung development.

Likewise, other studies report the miRs as key regulators in human and experimental animal models of BPD. For example, miR-199a-5p was significantly overexpressed in tracheal aspirates of BPD infants and experimental BPD causing inflammation. Treatment against the overexpressed miR-199a-5p improved aberrant lung development (5). In other reports, miR-489 was significantly downregulated in BPD infants and experimental BPD. Blocking miR-489 significantly improved alveolarization in experimental BPD (109). These reports highlight the need and the importance to correlate experimental and human BPD to develop new therapeutic strategies to prevent BPD.

4.2 Global induced deletion and inhibition of miR-135b-5p improves lung architecture

The use of temporally induced conditional gene deletion in mice is an important genetic tool to investigate the role of gene expression in physiological and pathophysiological conditions. The tamoxifen injections on P1 and P2 to generate a null allele is challenging when combined with Cre expressing strains. The ability and the efficiency of the Cre driver is fundamental to “knock out” the gene of interest from the target tissue or cell type. For this reason, the use of Cre-ER^{T2}-mTmG mouse line was crucial to assess the efficiency of the Cre driver line. The driver efficiency was tested 12 days after injections to avoid driver leakage and/or tamoxifen inefficiency. Cre-ER^{T2}-mTmG mouse lungs presented a high percent of GFP positive cells after tamoxifen injection when compared to tomato positive cells, demonstrating the global induced deletion of miR-135b gene.

The induced global loss of miR-135b-5p was assessed by qPCR where P14 knockout mice had significantly reduced miR-135b-5p expression compared to miR135b^{wt} mice. Moreover, the efficiency of the Cre-ER^{T2} driver to delete miR-135b was confirmed by endpoint PCR. The genomic DNA extracted from tail biopsies was screened for miR-135b-5p gene and no amplicon was possible to observe on an agarose gel.

The global induced deletion of miR-135b-5p slightly improved lung architecture in the hyperoxic exposed mouse lungs. The miR135b$^{Gi\Delta}$ mice exposed to severe hyperoxia presented a tendency to an increased alveolar density, a total number of alveoli, and surface area of gas exchange compared to miR135b^{wt} mice. No impact was noticed in the arithmetic mean septal thickness and lung volume. Interestingly, the same trends were observed when LNA-Stabilized antimiR was employed against miR-135b-5p. This result is explained by the dosage of 10 mg/kg of antimiR-135b-5p employed, which was enough to knockdown significantly the miR-135b-5p expression by over 10-fold change. The drastic effect of LNA-stabilized antimiR on miR gene expression impacted lung architecture only during hyperoxia, as seen already in other studies (124).

The 85% O_2 exposure is a severe oxygen injury to the developing lungs. For this reason, beneficial treatments might not be observed due to the harsh insult. Moderate hyperoxic insult (60% O_2) does not impact the arithmetic mean septal thickness but only the alveolarization (103). During severe hyperoxia, the arithmetic

mean septal thickness was not impacted in the miR135b$^{Gi\Delta}$ mice either in antimiR-135b-5p treated wild type mice. All other parameters, such as alveolar density, the total number of alveoli, and surface area of gas exchange were slightly improved, respectively. As expected, the antimiR-135b-5p treatment completely restored the total number of alveoli, alveolar density, and surface area of gas exchange in newborn pups exposed to moderate hyperoxia. The moderate oxygen insult helped to observe the beneficial action of the antimiR-135b-5p on lung structure that might have been shadow during severe hyperoxia. These data confirm the importance to inhibit miR-135b-5p during hyperoxia and might be considered as a therapeutic candidate in human BPD.

4.3 MiR-135b-5p modulates the Smad5 expression

MiR-135b-5p expression was significantly upregulated in human and experimental BPD. To decipher which pathway could be modulated by the deregulation of miR-135b-5p, bioinformatics tools were used. TargetScan revealed that miR-135b-5p targeted *in silico* the Smad5 3′-UTR. This result was confirmed by Bhinge *et al.* (110). In detail, Bhinge and coworkers predicted targets of the miR-135b-5p using the DIANA-mirPath software (111). Smad5 along with other members of the TGF-β/BMP signaling were identified as potential targets for the miR-135b-5p. The authors observed a significant decrease of the luciferase activity when they cloned the 3′-UTR of the Smad5 gene, downstream of the firefly luciferase enzyme. Moreover, the investigators observed less luciferase activity when mutations were inserted in the cloned 3′-UTR of Smad5 gene. This excellent work confirmed that miR-135b-5p directly targets Smad5 and other TGF-β/BMP signaling molecules. The Smad5 is a member of the R-Smads of the TGF-β/BMP signaling superfamily. When Smad5 is phosphorylated together with Smad1 and Smad9 to form a heteromeric complex that binds Smad4. The phosphorylated R-Smads enter the nucleus acting as transcription factors. For this reason, Smad5 was studied along with the other two R-Smads. Smad5 gene and protein expression were significantly decreased in the hyperoxic exposed lungs related to an increase of miR-135b-5p expression. Blocking the miR-135b-5p activity using antimiR-135b-5p, restored Smad5 gene, and protein expression. Smad5 is the only R-Smad targeted by miR-135b-5p since Smad1 and Smad9 gene and protein expression were not affected after antimiR-135b-5p treatment.

4.4 MiR-135b-5p is mainly expressed in alveolar epithelial type II cells

MiR-135b-5p was found to target Smad5 of the TGF-β/BMP signaling pathway and to modulate normal and aberrant lung development. An important point was to elucidate in which cell-type of the lung miR-135b-5p was expressed. To address this question, 14-day old miR-135b$^{lacZ,fl/lacZ,fl}$ reporter mice were used for β-galactosidase activity staining. MiR-135b-5p expression was highly expressed in the lung septa. However, this staining cannot discriminate between endogenous mammalian β-galactosidase activity and lacZ gene expression (152). Therefore, β-galactosidase activity staining cannot distinguish macrophages from AEII cells. For this reason, this result had to be confirmed with additional techniques to avoid false positives.

To address this concern, FISH was performed using an LNA miR-135b-5p detection probe. Like the previous result, miR-135b-5p was expressed only in the septa after hyperoxia exposure. In contrast, the normoxic control mice do not highly express miR-135b-5p in the septa. This data confirmed the previous result observed by qPCR analysis of lung homogenates. The alveolar septum is composed of different cell types (67) which under stress conditions, like hyperoxia, could lead to perturbated and abnormal responses (151). The staining of cell-specific markers for colocalization with FISH was challenging and could not reveal the specific cell type of the septum. For this reason, FACS technique was employed to screen different lung cell types in normoxic exposed P14 wild type mice. The data showed that the miR-135b-5p was mostly expressed in EpCAM^{+} cells. Moreover, to investigate which EpCAM^{+} cells mostly expressed miR-135b-5p, a new FACS experiment was performed. The data showed that miR-135b-5p is mainly expressed in mouse AEII cells compared to mouse AEI cells. Furthermore, mouse AEII cells isolated from severe hyperoxia exposed P14 mice expressed an upregulated miR-135b-5p. The alveolar epithelial type II cells are crucial cell types to maintain the correct function of the alveolus (34), to produce surfactant proteins (86), to act as the stem cells and progenitors of the alveolar epithelial type I cells (37, 145) and to repair lung injuries (108). AEII cells that are exposed to high oxygen concentrations (115) might lose or decrease these functions and lead to disrupted epithelium that is observed in BPD (9).

4.5 Severe hyperoxia modulates Smad5 expression in primary mouse alveolar epithelial type II cells

The miR-135b-5p was significantly overexpressed in mouse AEII cells isolated from mice exposed to severe hyperoxia for the first fourteen days of postnatal life. To assess

if hyperoxia and overexpressed miR-135-5p could decrease protein expression of Smad5 like observed in lung homogenates, mouse AEII cells isolated from P14 mice exposed to severe hyperoxia were used and showed a significant decrease of Smad5 protein expression. This data was fundamental to confirm the importance of the miR-135b-5p/Smad5 axis in the *in vivo* experiment. To avoid transdifferentiation from mouse AEII cells to mouse AEI cells, mouse AEII cells were isolated and the proteins were extracted directly after isolation. The data here provided, demonstrated by western blot the high purity of the isolated mouse AEII cells, where only the Sftpc protein was expressed and Aqp5 protein, a marker of mouse AEI cells, was not present.

The mouse AEII cells isolated from adult mice and used for *in vitro* experiments present important limitations such as the lack of cell interactions (44). However, to assess the relationship between the TGF-β/BMP signaling and miR-135b-5p, the *in vitro* model is fundamental. The microarray analysis revealed few miRs that were deregulated in mouse AEII cells exposed to hyperoxia and one of them was the miR-135b-5p. The miR-135b-5p was not only overexpressed in mouse AEII cells *in vivo* but this overexpression could be mimicked in mouse AEII cells *in vitro* when exposed to 85% O_2. This upregulation of miR-135-5p also impacted Smad5 protein expression that was significantly downregulated, reinforcing the important relation between the TGF-β/BMP signaling and miR-135b-5p.

4.6 Severe hyperoxia modulates miR-135b-5p and Smad5 expression in human alveolar epithelial cells

The miR-135b-5p was significantly expressed in mouse AEII cells *in vitro* and *in vivo* and modulated the protein expression of Smad5. To prove if this pattern could be observed in human BPD, human alveolar epithelial cells were exposed to severe hyperoxia for 48 h. Interestingly, the miR-135b-5p expression was again upregulated after severe hyperoxia exposure. This important observation confirmed the importance of deregulated miR-135b-5p in human material. Moreover, the severe hyperoxia also modulated the protein expression of all the R-Smads, in particular Smad5 was significantly downregulated. This might influence negatively the TGF-β/BMP signaling and might be a cause of the epithelium disruption that is a key feature in the development of human and experimental BPD (9).

4.7 MiR-135b-5p modulates the Smad5 expression and cell functionality in A549 cell line

The mouse AEII cells were clearly showing *in vitro* overexpression of miR-135b-5p when exposed to severe hyperoxia and consequent downregulation of Smad5 protein expression. Transfection reagents, based on lipidic nanoparticle, offer an excellent tool to transfect cells with nucleic acids to study *in vitro* gene knockdowns and gene overexpression. However, the transfection of mouse AEII cells is not possible using lipidic reagents due to the cell morphology. The mouse AEII cells are enriched with lamellar bodies that contain phospholipids (64). The lamellar bodies capture the nucleic acids and releases into the cytoplasm, avoiding that nucleic acids can reach the nucleus (50). To study the effect of miR-135b-5p overexpression, adenocarcinoma human alveolar basal epithelial cells or A549 were used to observe the effects on the TGF-β/BMP signaling. Interestingly, also in hyperoxia exposed A549 cells, Smad5 protein expression was significantly reduced. To confirm this important aspect, A549 cells were transfected with different concentrations of synthetic scrambled miR mimic and a miR-135b-5p mimic for 48 hours. The 80 nM concentration was found to be the optimal amount to target Smad5. In a simple system like the A549 cells, synthetic miR-135b-5p mimic modulated the protein expression of Smad5, confirming furthermore the interaction and the importance of the miR-135b-5p/Smad5 axis concerning the TGF-β/BMP pathway. To test if the synthetic miR-135b-5p mimic could modulate cell functionality, apoptosis and viability assays were performed and no changes were observed. However, overexpression of miR-135b-5p significantly reduced cell proliferation. This data suggested that overexpressed miR-135b-5p influenced cell proliferation and probably this effected is attributed to reduced Smad5 protein levels. These data find support in different reports, for example, where Smad5 was highly expressed in proliferating chondrocytes (126). Inhibition or perturbations of Smad5 expression decreased erythroid differentiation (41) and blockage of Smad5 expression through TGF-β/BMP signaling caused arrested cell proliferation in endothelial cells (47). Overexpression of Smad5 instead is capable to induce cell differentiation and proliferation in granule neurons (118). In lung reports, increased Smad1 and Smad5 in A549 caused increased cell proliferation, according to the data observed in this study (73). In other reports, miR-322 reduced Smad5 expression, and as consequence, the pulmonary artery smooth muscle cells were less proliferative, suggesting also in this *in vitro* model the role of Smad5 in cell proliferation (159). Taken together this data, the

miR-135b-5p/Smad5 axis influences the TGF-β/BMP pathway and might have an impact on cell proliferation. However, to study the role of miR-135b-5p in A549 cells on apoptosis, proliferation, and viability is not a perfect approach. The A549 cells are immortalized cells and programmed not to die. The study should be conducted in primary mouse AEII cells by a viral infection that was already proven to be a successful method to knockdown and overexpress genes (36). Surely, the study conducted in A549 cells gave a hint to investigate the role of miR-135b-5p in cell proliferation.

4.8 The induced global deletion of Smad5 contributes to arrested alveolarization

MiR-135b-5p significantly impacted the expression of target gene Smad5. This impact was observed *in vitro* where synthetic miR-135b-5p mimic significantly reduced Smad5 protein expression. *In vivo,* the impact of LNA-stabilized antimiR directed against miR-135b-5p significantly restored Smad5 expression after blocking miR-135b-5p in hyperoxia exposed pups. To assess the role of Smad5 in normal lung development, the $Smad5^{Gi\Delta}$ mice were used to study lung structure. The loss of Smad5 decreased the total number of alveoli and alveolar density with a consequent reduction of surface area of gas exchange. This data clearly demonstrated that Smad5 is an important player in normal lung development. Overexpression of miR-135b-5p in the severe hyperoxia mouse model of BPD dramatically reduced Smad5 expression. However, the inhibition of miR-135b-5p restored Smad5 levels improving slightly lung structure. The loss of Smad5 expression in the knockout mice did not affect Smad1 and Smad9. This important result demonstrated the importance of Smad5 as a key player of the TGF-β/BMP signaling during normal lung development.

The overexpressed miR-135b-5p reduced Smad5 expression with consequentially worsening of lung architecture. To assess if the miR-135b-5p/Smad5 interaction could be blocked, TSB was employed. The use of this technology is new in the scientific field and few reports demonstrated the efficiency and potential therapeutic application of TSBs to block the interaction between miRs and target genes (31, 124, 137). However, the TSB employed in the present study had a different effect. *In vivo*, TSB treatment in newborn pups, dramatically reduced the Smad5 protein expression in the 85% O_2 treated lungs *versus* the 85% O_2 control lungs without modulating Smad1 and Smad9. Surprisingly, the TSB treatment worsened the lung structure in normoxia and hyperoxia. The total number of alveoli, alveolar density, and the surface area of gas exchange were significantly reduced. Furthermore, an increase of septal

thickness was observed in normoxia exposed mice. This result was surprising and at the same time interesting. The TSB is a new technique and few reports have successfully employed this technology. The manufacturer of TSBs, Exiqon, describes TSBs as customized sequence that interacts between the miR and the binding sites in 3′-UTR of target genes, unfortunately without revealing the sequence and the mechanism.

In the present study, the TSB-Smad5 treatment was deleterious, due, most probably, to the TSB sequence that was not removed from the Smad5 3′-UTR and acting as an inhibitor of Smad5. This theory is supported by significantly reduced Smad5 protein expression after TSB-Smad5 treatment in normoxic and hyperoxic mice. Likewise, TSB treated lungs pheno-copied lung structure of Smad5$^{Gi\Delta}$ mice. Moreover, when A549 cells were transfected with different concentrations of TSB-Smad5, the Smad5 protein expression decreased in a dose-dependent manner, meanwhile the other R-Smads were unchanged. This important observation might be a crucial starting point to investigate how the TSB technology is working and interacts with targets. In the present study, the TSB-Smad5 was intended to act as beneficial and therapeutic intervention to block the interaction between miR-135b-5p and Smad5, however, the intervention ended up damaging the lung structure and as a negative modulator of the TGF-β/BMP pathway.

4.9 Outlook and limitation of the study

Mir-135b-5p was found as a key regulator during normal and aberrant lung development. The hyperoxia-based mouse model of BPD revealed an upregulated expression of miR-135b-5p which downregulated Smad5 gene and protein expression. Also, inhibition of miR-135b-5p improved lung architecture and normalized Smad5 gene and protein expression. The global induced deletion of Smad5 gene and protein expression by using Smad5$^{Gi\Delta}$ mice revealed the importance of Smad5 during alveolarization. The present study described in detail the effects of upregulated miR-135b-5p on Smad5 gene and protein expression, and on lung architecture but does not reveal the mechanistic that is influenced by the miR-135b-5p/Smad5 axis. Hints indicate a role in proliferation or in transdifferentiation from AEII cells to AEI cells. These hints need further investigation and techniques such as single-cell RNA sequencing and RNA sequencing, could answer the question and elucidate the mechanism that is influenced by the miR-135b-5p/Smad5 axis. Moreover, the use of adenovirus to infect primary mouse AEII cells i) to overexpress miR-135b-5p gene

expression; and ii) to inhibit Smad1, Smad5 and Smad9 gene and protein expression; might help to elucidate the functionality and mechanistic behind the miR-135b-5p/Smad5 axis. Furthermore, the induced deletion of miR-135b-5p in AEII cells might explain the role of miR-135b-5p in AEII cells during postnatal lung development.

5 Conclusions

Bronchopulmonary dysplasia (BPD) is a chronic lung disease that occurs in premature infants. The oxygen toxicity and the physical forces applied to ventilate premature infants cause inflammation and deregulated gene expression that leads to arrested alveolarization, the formation of dysmorphic pulmonary microvasculature, and severely impaired extracellular matrix structures. Deregulated miRs have been reported in clinical and experimental BPD and might play a crucial role in the pathogenesis of the disease. However, therapeutic interventions to inhibit or enhance miRs expression are not found yet in literature.

In the present study, the miR-135b-5p was found as a key regulator during alveolarization in clinical and experimental BPD. This study demonstrated that the miR-135b-5p was mainly expressed in alveolar epithelial type II cells and targeted Smad5 of the TGF-β/BMP signaling. Moreover, the inhibition and the knockout of miR-135b-5p revealed an improvement in alveolarization. This improvement was even more pronounced when animals were exposed to moderate hyperoxia, where inhibition of miR-135b-5p completely restored alveolarization. Furthermore, Smad5 was found to be fundamental for normal and aberrant lung development. The use of target site blocker revealed the inefficiency of this compound to block the binding of miR-135b-5p to Smad5. Instead, the target site blocker acted as a mimic of miR-135b-5p and reduced dramatically Smad5 expression accompanied by a worsening of lung architecture. The study of Smad5 knockout animals showed a worsening of lung structure, like the target site blocker treatment, revealing the importance of Smad5 during alveolarization. This study gives strong evidence that the miR-135b-5p targets Smad5 and this interaction plays an important role in normal and aberrant lung development.

In summary, this data demonstrated the importance of miR-135b-5p/Smad5 axis in BPD for the first time, and miR-135b-5p inhibition could be proposed as a potential candidate for the treatment of BPD patients.

6 Bibliography

1. Abman SH, Collaco JM, Shepherd EG, Keszler M, Cuevas-Guaman M, Welty SE, et al. **Interdisciplinary Care of Children with Severe Bronchopulmonary Dysplasia**. *J Pediatr*. 2017;181:12-28.e1.
2. Addante A, Roncero C, Lazcanoiturburu N, Mendez R, Almale L, Garcia-Alvaro M, et al. **A Signaling Crosstalk between BMP9 and HGF/c-Met Regulates Mouse Adult Liver Progenitor Cell Survival**. *Cells*. 2020;9(3).
3. Agarwal V, Bell GW, Nam JW, Bartel DP. **Predicting effective microRNA target sites in mammalian mRNAs**. *eLife*. 2015;4.
4. Ahlfeld SK, Wang J, Gao Y, Snider P, Conway SJ. **Initial Suppression of Transforming Growth Factor-beta Signaling and Loss of TGFBI Causes Early Alveolar Structural Defects Resulting in Bronchopulmonary Dysplasia**. *Am J Pathol*. 2016;186(4):777-93.
5. Alam MA, Betal SGN, Aghai ZH, Bhandari V. **Hyperoxia causes miR199a-5p-mediated injury in the developing lung**. *Pediatr Res*. 2019;86(5):579-88.
6. Alejandre-Alcazar MA, Kwapiszewska G, Reiss I, Amarie OV, Marsh LM, Sevilla-Perez J, et al. **Hyperoxia modulates TGF-beta/BMP signaling in a mouse model of bronchopulmonary dysplasia**. *Am J Physiol Lung Cell Mol Physiol*. 2007;292(2):L537-49.
7. Alejandre-Alcazar MA, Michiels-Corsten M, Vicencio AG, Reiss I, Ryu J, de Krijger RR, et al. **TGF-beta signaling is dynamically regulated during the alveolarization of rodent and human lungs**. *Dev Dyn*. 2008;237(1):259-69.
8. Alejandre-Alcazar MA, Shalamanov PD, Amarie OV, Sevilla-Perez J, Seeger W, Eickelberg O, et al. **Temporal and spatial regulation of bone morphogenetic protein signaling in late lung development**. *Dev Dyn*. 2007;236(10):2825-35.
9. Baker CD, Alvira CM. **Disrupted lung development and bronchopulmonary dysplasia: opportunities for lung repair and regeneration**. *Curr Opin Pediatr*. 2014;26(3):306-14.
10. Balany J, Bhandari V. **Understanding the Impact of Infection, Inflammation, and Their Persistence in the Pathogenesis of Bronchopulmonary Dysplasia**. *Front Med (Lausanne)*. 2015;2:90.

11. Bao L, Lv L, Feng J, Chen Y, Wang X, Han S, et al. **MiR-876-5p suppresses epithelial-mesenchymal transition of lung cancer by directly down-regulating bone morphogenetic protein 4**. *J Biosci*. 2017;42(4):671-81.
12. Baraldi E, Filippone M. **Chronic lung disease after premature birth**. *N Engl J Med*. 2007;357(19):1946-55.
13. Bernstein E, Caudy AA, Hammond SM, Hannon GJ. **Role for a bidentate ribonuclease in the initiation step of RNA interference**. *Nature*. 2001;409(6818):363-6.
14. Bhinge A, Poschmann J, Namboori SC, Tian X, Jia Hui Loh S, Traczyk A, et al. **MiR-135b is a direct PAX6 target and specifies human neuroectoderm by inhibiting TGF-beta/BMP signaling**. *EMBO J*. 2014;33(11):1271-83.
15. Bik-Multanowski M, Revhaug C, Grabowska A, Dobosz A, Madetko-Talowska A, Zasada M, et al. **Hyperoxia induces epigenetic changes in newborn mice lungs**. *Free Radic Biol Med*. 2018;121:51-6.
16. Bohnsack MT, Czaplinski K, Gorlich D. **Exportin 5 is a RanGTP-dependent dsRNA-binding protein that mediates nuclear export of pre-miRNAs**. *RNA*. 2004;10(2):185-91.
17. Buckley S, Shi W, Barsky L, Warburton D. **TGF-beta signaling promotes survival and repair in rat alveolar epithelial type 2 cells during recovery after hyperoxic injury**. *Am J Physiol Lung Cell Mol Physiol*. 2008;294(4):L739-48.
18. Burri PH. **Postnatal growth and maturation of the lung**. *Chest*. 1975;67(2 Suppl):2s-3s.
19. Burri PH. **Structural aspects of postnatal lung development - alveolar formation and growth**. *Biol Neonate*. 2006;89(4):313-22.
20. Caduff JH, Fischer LC, Burri PH. **Scanning electron microscope study of the developing microvasculature in the postnatal rat lung**. *Anat Rec*. 1986;216(2):154-64.
21. Cardoso WV, Lu J. **Regulation of early lung morphogenesis: questions, facts and controversies**. *Development*. 2006;133(9):1611-24.
22. Cech TR, Steitz JA. **The noncoding RNA revolution-trashing old rules to forge new ones**. *Cell*. 2014;157(1):77-94.

23. Chang H, Huylebroeck D, Verschueren K, Guo Q, Matzuk MM, Zwijsen A. **Smad5 knockout mice die at mid-gestation due to multiple embryonic and extraembryonic defects**. *Development*. 1999;126(8):1631-42.
24. Chao CM, Carraro G, Rako ZA, Kolck J, Sedighi J, Zimmermann V, et al. **Failure to Down-Regulate miR-154 Expression in Early Postnatal Mouse Lung Epithelium Suppresses Alveologenesis, with Changes in Tgf-beta Signaling Similar to those Induced by Exposure to Hyperoxia**. *Cells*. 2020;9(4).
25. Chen X, Orriols M, Walther FJ, Laghmani EH, Hoogeboom AM, Hogen-Esch ACB, et al. **Bone Morphogenetic Protein 9 Protects against Neonatal Hyperoxia-Induced Impairment of Alveolarization and Pulmonary Inflammation**. *Front Physiol.* 2017;8:486.
26. Chen XQ, Wu SH, Luo YY, Li BJ, Li SJ, Lu HY, et al. **Lipoxin A4 Attenuates Bronchopulmonary Dysplasia via Upregulation of Let-7c and Downregulation of TGF-beta1 Signaling Pathway**. *Inflammation*. 2017;40(6):2094-108.
27. Corti M, Brody AR, Harrison JH. **Isolation and primary culture of murine alveolar type II cells**. *Am J Respir Cell Mol Biol*. 1996;14(4):309-15.
28. Daly AC, Randall RA, Hill CS. **Transforming growth factor beta-induced Smad1/5 phosphorylation in epithelial cells is mediated by novel receptor complexes and is essential for anchorage-independent growth**. *Mol Cell Biol*. 2008;28(22):6889-902.
29. Dasgupta C, Sakurai R, Wang Y, Guo P, Ambalavanan N, Torday JS, et al. **Hyperoxia-induced neonatal rat lung injury involves activation of TGF-{beta} and Wnt signaling and is protected by rosiglitazone**. *Am J Physiol Lung Cell Mol Physiol*. 2009;296(6):L1031-41.
30. de Larco JE, Todaro GJ. **Growth factors from murine sarcoma virus-transformed cells**. *Proc Natl Acad Sci U S A*. 1978;75(8):4001-5.
31. De Santi C, Fernández Fernández E, Gaul R, Vencken S, Glasgow A, Oglesby IK, et al. **Precise Targeting of miRNA Sites Restores CFTR Activity in CF Bronchial Epithelial Cells**. *Mol Ther*. 2020;28(4):1190-9.
32. Desai TJ, Cardoso WV. **Growth factors in lung development and disease: friends or foe?** *Respir Res*. 2002;3:2.

33. Dick A, Risau W, Drexler H. **Expression of Smad1 and Smad2 during embryogenesis suggests a role in organ development**. *Dev Dyn*. 1998;211(4):293-305.
34. Driscoll KE, Carter JM, Iype PT, Kumari HL, Crosby LL, Aardema MJ, et al. **Establishment of immortalized alveolar type II epithelial cell lines from adult rats**. *In Vitro Cell Dev Biol Anim.* 1995;31(7):516-27.
35. Durrani-Kolarik S, Pool CA, Gray A, Heyob KM, Cismowski MJ, Pryhuber G, et al. **miR-29b supplementation decreases expression of matrix proteins and improves alveolarization in mice exposed to maternal inflammation and neonatal hyperoxia**. *Am J Physiol Lung Cell Mol Physiol*. 2017;313(2):L339-l49.
36. Factor P, Saldias F, Ridge K, Dumasius V, Zabner J, Jaffe HA, et al. **Augmentation of lung liquid clearance via adenovirus-mediated transfer of a Na,K-ATPase beta1 subunit gene**. *J Clin Invest*. 1998;102(7):1421-30.
37. Fehrenbach H. **Alveolar epithelial type II cell: defender of the alveolus revisited**. *Respir Res*. 2001;2(1):33-46.
38. Filippone M, Nardo D, Bonadies L, Salvadori S, Baraldi E. **Update on Postnatal Corticosteroids to Prevent or Treat Bronchopulmonary Dysplasia**. *Am J Perinatol*. 2019;36(S 02):S58-s62.
39. Frank L, Bucher JR, Roberts RJ. **Oxygen toxicity in neonatal and adult animals of various species**. *J Appl Physiol Respir Environ Exerc Physiol.* 1978;45(5):699-704.
40. Friedman RC, Farh KK, Burge CB, Bartel DP. **Most mammalian mRNAs are conserved targets of microRNAs**. *Genome Res.* 2009;19(1):92-105.
41. Fuchs O, Simakova O, Klener P, Cmejlova J, Zivny J, Zavadil J, et al. **Inhibition of Smad5 in human hematopoietic progenitors blocks erythroid differentiation induced by BMP4**. *Blood Cells Mol Dis*. 2002;28(2):221-33.
42. Fukunaga R, Han BW, Hung JH, Xu J, Weng Z, Zamore PD. **Dicer partner proteins tune the length of mature miRNAs in flies and mammals**. *Cell*. 2012;151(3):533-46.

43. Garcia DM, Baek D, Shin C, Bell GW, Grimson A, Bartel DP. **Weak seed-pairing stability and high target-site abundance decrease the proficiency of lsy-6 and other microRNAs**. *Nat Struct Mol Biol.* 2011;18(10):1139-46.
44. Ghallab A. **In vitro test systems and their limitations**. *EXCLI journal*. 2013;12:1024-6.
45. Goto K, Kamiya Y, Imamura T, Miyazono K, Miyazawa K. **Selective inhibitory effects of Smad6 on bone morphogenetic protein type I receptors**. *J Biol Chem*. 2007;282(28):20603-11.
46. Goumans M-J, Liu Z, ten Dijke P. **TGF-β signaling in vascular biology and dysfunction**. *Cell Res*. 2009;19(1):116-27.
47. Goumans MJ, Valdimarsdottir G, Itoh S, Rosendahl A, Sideras P, ten Dijke P. **Balancing the activation state of the endothelium via two distinct TGF-beta type I receptors**. *EMBO J.* 2002;21(7):1743-53.
48. Greenough A. **Long-term pulmonary outcome in the preterm infant**. *Neonatology*. 2008;93(4):324-7.
49. Greenough A, Premkumar M, Patel D. **Ventilatory strategies for the extremely premature infant**. *Paediatr Anaesth.* 2008;18(5):371-7.
50. Grzesik BA, Vohwinkel CU, Morty RE, Mayer K, Herold S, Seeger W, et al. **Efficient gene delivery to primary alveolar epithelial cells by nucleofection**. *Am J Physiol Lung Cell Mol Physiol*. 2013;305(11):L786-94.
51. Ha M, Kim VN. **Regulation of microRNA biogenesis**. *Nat Rev Mol Cell Biol.* 2014;15(8):509-24.
52. Hammond SM, Boettcher S, Caudy AA, Kobayashi R, Hannon GJ. **Argonaute2, a link between genetic and biochemical analyses of RNAi**. *Science*. 2001;293(5532):1146-50.
53. Hata A, Lagna G, Massague J, Hemmati-Brivanlou A. **Smad6 inhibits BMP/Smad1 signaling by specifically competing with the Smad4 tumor suppressor**. *Genes Dev*. 1998;12(2):186-97.
54. Heldin CH, Miyazono K, ten Dijke P. **TGF-beta signalling from cell membrane to nucleus through SMAD proteins**. *Nature*. 1997;390(6659):465-71.
55. Herriges M, Morrisey EE. **Lung development: orchestrating the generation and regeneration of a complex organ**. *Development*. 2014;141(3):502-13.

56. Hsia CC, Hyde DM, Ochs M, Weibel ER. **An official research policy statement of the American Thoracic Society/European Respiratory Society: standards for quantitative assessment of lung structure**. *Am J Respir Crit Care Med*. 2010;181(4):394-418.

57. Hu Y, Xie L, Yu J, Fu H, Zhou D, Liu H. **Inhibition of microRNA-29a alleviates hyperoxia-induced bronchopulmonary dysplasia in neonatal mice via upregulation of GAB1**. *Mol Med.* 2019;26(1):3.

58. Hyde DM, Tyler NK, Putney LF, Singh P, Gundersen HJ. **Total number and mean size of alveoli in mammalian lung estimated using fractionator sampling and unbiased estimates of the Euler characteristic of alveolar openings**. *Anat Rec A Discov Mol Cell Evol Biol.* 2004;277(1):216-26.

59. Iliodromiti Z, Zygouris D, Sifakis S, Pappa KI, Tsikouras P, Salakos N, et al. **Acute lung injury in preterm fetuses and neonates: mechanisms and molecular pathways**. *J Matern Fetal Neonatal Med.* 2013;26(17):1696-704.

60. Jin M, Lee J, Lee KY, Jin Z, Pak JH, Kim HS. **Alteration of TGF-beta-ALK-Smad signaling in hyperoxia-induced bronchopulmonary dysplasia model of newborn rats**. *Exp Lung Res*. 2016;42(7):354-64.

61. Jobe AH, Bancalari E. **Bronchopulmonary dysplasia**. *Am J Respir Crit Care Med*. 2001;163(7):1723-9.

62. Kamiya Y, Miyazono K, Miyazawa K. **Smad7 inhibits transforming growth factor-beta family type i receptors through two distinct modes of interaction**. *J Biol Chem*. 2010;285(40):30804-13.

63. Khvorova A, Reynolds A, Jayasena SD. **Functional siRNAs and miRNAs exhibit strand bias**. *Cell*. 2003;115(2):209-16.

64. Kikkawa Y, Yoneda K, Smith F, Packard B, Suzuki K. **The type II epithelial cells of the lung. II. Chemical composition and phospholipid synthesis**. *Lab Invest.* 1975;32(3):295-302.

65. Kinsella JP, Greenough A, Abman SH. **Bronchopulmonary dysplasia**. *Lancet*. 2006;367(9520):1421-31.

66. Knight SW, Bass BL. **A role for the RNase III enzyme DCR-1 in RNA interference and germ line development in Caenorhabditis elegans**. *Science.* 2001;293(5538):2269-71.

67. Knudsen L, Ochs M. **The micromechanics of lung alveoli: structure and function of surfactant and tissue components**. *Histochem Cell Biol.* 2018;150(6):661-76.
68. Kretzschmar M, Doody J, Massague J. **Opposing BMP and EGF signalling pathways converge on the TGF-beta family mediator Smad1**. *Nature*. 1997;389(6651):618-22.
69. Kuo YC, Li YS, Zhou J, Shih YR, Miller M, Broide D, et al. **Human mesenchymal stem cells suppress the stretch-induced inflammatory miR-155 and cytokines in bronchial epithelial cells**. *PLoS One*. 2013;8(8):e71342.
70. Lagos-Quintana M, Rauhut R, Lendeckel W, Tuschl T. **Identification of novel genes coding for small expressed RNAs**. *Science*. 2001;294(5543):853-8.
71. Lagos-Quintana M, Rauhut R, Yalcin A, Meyer J, Lendeckel W, Tuschl T. **Identification of tissue-specific microRNAs from mouse**. *Curr Biol.* 2002;12(9):735-9.
72. Lambert JF, Benoit BO, Colvin GA, Carlson J, Delville Y, Quesenberry PJ. **Quick sex determination of mouse fetuses**. *J Neurosci Methods*. 2000;95(2):127-32.
73. Langenfeld EM, Kong Y, Langenfeld J. **Bone morphogenetic protein 2 stimulation of tumor growth involves the activation of Smad-1/5**. *Oncogene*. 2006;25(5):685-92.
74. Lau NC, Lim LP, Weinstein EG, Bartel DP. **An abundant class of tiny RNAs with probable regulatory roles in Caenorhabditis elegans**. *Science.* 2001;294(5543):858-62.
75. Lee RC, Ambros V. **An extensive class of small RNAs in Caenorhabditis elegans**. *Science.* 2001;294(5543):862-4.
76. Lee RC, Feinbaum RL, Ambros V. **The C. elegans heterochronic gene lin-4 encodes small RNAs with antisense complementarity to lin-14**. *Cell*. 1993;75(5):843-54.
77. Lee Y, Ahn C, Han J, Choi H, Kim J, Yim J, et al. **The nuclear RNase III Drosha initiates microRNA processing**. *Nature*. 2003;425(6956):415-9.

78. Li J, Liang H, Bai M, Ning T, Wang C, Fan Q, et al. **miR-135b Promotes Cancer Progression by Targeting Transforming Growth Factor Beta Receptor II (TGFBR2) in Colorectal Cancer**. *PLoS One*. 2015;10(6):e0130194.

79. Li S, Sun Z, Chen T, Pan J, Shen Y, Chen X, et al. **The role of miR-431-5p in regulating pulmonary surfactant expression in vitro**. *Cell Mol Biol Lett*. 2019;24:25.

80. Li Z, Choo-Wing R, Sun H, Sureshbabu A, Sakurai R, Rehan VK, et al. **A potential role of the JNK pathway in hyperoxia-induced cell death, myofibroblast transdifferentiation and TGF-beta1-mediated injury in the developing murine lung**. *BMC Cell Biol*. 2011;12:54.

81. Lignelli E, Palumbo F, Myti D, Morty RE. **Recent advances in our understanding of the mechanisms of lung alveolarization and bronchopulmonary dysplasia**. *Am J Physiol Lung Cell Mol Physiol*. 2019;317(6):L832-L87.

82. Llave C, Kasschau KD, Rector MA, Carrington JC. **Endogenous and silencing-associated small RNAs in plants**. *Plant Cell*. 2002;14(7):1605-19.

83. Lund E, Guttinger S, Calado A, Dahlberg JE, Kutay U. **Nuclear export of microRNA precursors**. *Science*. 2004;303(5654):95-8.

84. Madurga A, Golec A, Pozarska A, Ishii I, Mizikova I, Nardiello C, et al. **The H2S-generating enzymes cystathionine beta-synthase and cystathionine gamma-lyase play a role in vascular development during normal lung alveolarization**. *Am J Physiol Lung Cell Mol Physiol*. 2015;309(7):L710-24.

85. Madurga A, Mizikova I, Ruiz-Camp J, Vadasz I, Herold S, Mayer K, et al. **Systemic hydrogen sulfide administration partially restores normal alveolarization in an experimental animal model of bronchopulmonary dysplasia**. *Am J Physiol Lung Cell Mol Physiol*. 2014;306(7):L684-97.

86. Mason RJ, Williams MC. **Type II alveolar cell. Defender of the alveolus**. *Am Rev Respir Dis*. 1977;115(6 Pt 2):81-91.

87. Massague J, Blain SW, Lo RS. **TGFbeta signaling in growth control, cancer, and heritable disorders**. *Cell*. 2000;103(2):295-309.

88. Michel RP, Cruz-Orive LM. **Application of the Cavalieri principle and vertical sections method to lung: estimation of volume and pleural surface area**. *J Microsc*. 1988;150(Pt 2):117-36.

89. Miyazono K, Kamiya Y, Morikawa M. **Bone morphogenetic protein receptors and signal transduction**. *J Biochem*. 2010;147(1):35-51.

90. Mizikova I, Pfeffer T, Nardiello C, Surate Solaligue DE, Steenbock H, Tatsukawa H, et al. **Targeting transglutaminase 2 partially restores extracellular matrix structure but not alveolar architecture in experimental bronchopulmonary dysplasia**. *FEBS J*. 2018;285(16):3056-76.

91. Mizikova I, Ruiz-Camp J, Steenbock H, Madurga A, Vadasz I, Herold S, et al. **Collagen and elastin cross-linking is altered during aberrant late lung development associated with hyperoxia**. *Am J Physiol Lung Cell Mol Physiol*. 2015;308(11):L1145-58.

92. Morrisey EE, Hogan BL. **Preparing for the first breath: genetic and cellular mechanisms in lung development**. *Dev Cell*. 2010;18(1):8-23.

93. Morty RE, Konigshoff M, Eickelberg O. **Transforming growth factor-beta signaling across ages: from distorted lung development to chronic obstructive pulmonary disease**. *Proc Am Thorac Soc*. 2009;6(7):607-13.

94. Moses HL, Branum EL, Proper JA, Robinson RA. **Transforming growth factor production by chemically transformed cells**. *Cancer Res*. 1981;41(7):2842-8.

95. Mourelatos Z, Dostie J, Paushkin S, Sharma A, Charroux B, Abel L, et al. **miRNPs: a novel class of ribonucleoproteins containing numerous microRNAs**. *Genes Dev*. 2002;16(6):720-8.

96. Moustakas A, Pardali K, Gaal A, Heldin CH. **Mechanisms of TGF-beta signaling in regulation of cell growth and differentiation**. *Immunol Lett*. 2002;82(1-2):85-91.

97. Muhlfeld C, Hegermann J, Wrede C, Ochs M. **A review of recent developments and applications of morphometry/stereology in lung research**. *Am J Physiol Lung Cell Mol Physiol*. 2015;309(6):L526-36.

98. Muhlfeld C, Knudsen L, Ochs M. **Stereology and morphometry of lung tissue**. *Methods Mol Biol*. 2013;931:367-90.

99. Muhlfeld C, Ochs M. **Measuring structure - What's the point in counting?** *Ann Anat*. 2014;196(1):1-2.

100. Muzumdar MD, Tasic B, Miyamichi K, Li L, Luo L. **A global double-fluorescent Cre reporter mouse**. *Genesis*. 2007;45(9):593-605.

101. Nakanishi H, Sugiura T, Streisand JB, Lonning SM, Roberts JD, Jr. **TGF-beta-neutralizing antibodies improve pulmonary alveologenesis and vasculogenesis in the injured newborn lung**. *Am J Physiol Lung Cell Mol Physiol*. 2007;293(1):L151-61.

102. Nardiello C, Mizikova I, Morty RE. **Looking ahead: where to next for animal models of bronchopulmonary dysplasia?** *Cell Tissue Res*. 2017;367(3):457-68.

103. Nardiello C, Mizikova I, Silva DM, Ruiz-Camp J, Mayer K, Vadasz I, et al. **Standardisation of oxygen exposure in the development of mouse models for bronchopulmonary dysplasia**. *Dis Model Mech*. 2017;10(2):185-96.

104. Nardiello C, Morty RE. **MicroRNA in late lung development and bronchopulmonary dysplasia: the need to demonstrate causality**. *Mol Cell Pediatr*. 2016;3(1):19.

105. Northway WH, Jr., Rosan RC, Porter DY. **Pulmonary disease following respirator therapy of hyaline-membrane disease. Bronchopulmonary dysplasia**. *N Engl J Med*. 1967;276(7):357-68.

106. Noskovicova N, Petrek M, Eickelberg O, Heinzelmann K. **Platelet-derived growth factor signaling in the lung. From lung development and disease to clinical studies**. *Am J Respir Cell Mol Biol*. 2015;52(3):263-84.

107. Ochs M, Muhlfeld C. **Quantitative microscopy of the lung: a problem-based approach. Part 1: basic principles of lung stereology**. *Am J Physiol Lung Cell Mol Physiol*. 2013;305(1):L15-22.

108. Olajuyin AM, Zhang X, Ji HL. **Alveolar type 2 progenitor cells for lung injury repair**. *Cell Death Discov*. 2019;5:63.

109. Olave N, Lal CV, Halloran B, Pandit K, Cuna AC, Faye-Petersen OM, et al. **Regulation of alveolar septation by microRNA-489**. *Am J Physiol Lung Cell Mol Physiol*. 2016;310(5):L476-87.

110. Orvis GD, Jamin SP, Kwan KM, Mishina Y, Kaartinen VM, Huang S, et al. **Functional redundancy of TGF-beta family type I receptors and receptor-Smads in mediating anti-Mullerian hormone-induced Mullerian duct regression in the mouse**. *Biol Reprod*. 2008;78(6):994-1001.

111. Papadopoulos GL, Alexiou P, Maragkakis M, Reczko M, Hatzigeorgiou AG. **DIANA-mirPath: Integrating human and mouse microRNAs in pathways**. *Bioinformatics*. 2009;25(15):1991-3.

112. Park CY, Jeker LT, Carver-Moore K, Oh A, Liu HJ, Cameron R, et al. **A resource for the conditional ablation of microRNAs in the mouse**. *Cell Rep*. 2012;1(4):385-91.

113. Pozarska A, Rodriguez-Castillo JA, Surate Solaligue DE, Ntokou A, Rath P, Mizikova I, et al. **Stereological monitoring of mouse lung alveolarization from the early postnatal period to adulthood**. *Am J Physiol Lung Cell Mol Physiol*. 2017;312(6):L882-L95.

114. Rackley CR, Stripp BR. **Building and maintaining the epithelium of the lung**. *J Clin Invest*. 2012;122(8):2724-30.

115. Rath P, Nardiello C, Surate Solaligue DE, Agius R, Mizikova I, Huhn S, et al. **Caffeine administration modulates TGF-beta signaling but does not attenuate blunted alveolarization in a hyperoxia-based mouse model of bronchopulmonary dysplasia**. *Pediatr Res*. 2017;81(5):795-805.

116. Reinhart BJ, Weinstein EG, Rhoades MW, Bartel B, Bartel DP. **MicroRNAs in plants**. *Genes Develop*. 2002;16(13):1616-26.

117. Richardson KC, Jarett L, Finke EH. **Embedding in epoxy resins for ultrathin sectioning in electron microscopy**. *Stain Technol*. 1960;35:313-23.

118. Rios I, Alvarez-Rodríguez R, Martí E, Pons S. **Bmp2 antagonizes sonic hedgehog-mediated proliferation of cerebellar granule neurones through Smad5 signalling**. *Development.* 2004;131(13):3159-68.

119. Robbins ME, Dakhlallah D, Marsh CB, Rogers LK, Tipple TE. **Of mice and men: correlations between microRNA-17 approximately 92 cluster expression and promoter methylation in severe bronchopulmonary dysplasia**. *Am J Physiol Lung Cell Mol Physiol*. 2016;311(5):L981-l4.

120. Roberts AB, Anzano MA, Lamb LC, Smith JM, Sporn MB. **New class of transforming growth factors potentiated by epidermal growth factor: isolation from non-neoplastic tissues**. *Proc Natl Acad Sci U S A*. 1981;78(9):5339-43.

121. Rodriguez CI, Buchholz F, Galloway J, Sequerra R, Kasper J, Ayala R, et al. **High-efficiency deleter mice show that FLPe is an alternative to Cre-loxP**. *Nature Genet*. 2000;25(2):139-40.

122. Roth-Kleiner M, Post M. **Similarities and dissimilarities of branching and septation during lung development**. *Pediatr Pulmonol*. 2005;40(2):113-34.
123. Ruiz-Camp J, Morty RE. **Divergent fibroblast growth factor signaling pathways in lung fibroblast subsets: where do we go from here?** *Am J Physiol Lung Cell Mol Physiol*. 2015;309(8):L751-5.
124. Ruiz-Camp J, Quantius J, Lignelli E, Arndt PF, Palumbo F, Nardiello C, et al. **Targeting miR-34a/Pdgfra interactions partially corrects alveologenesis in experimental bronchopulmonary dysplasia**. *EMBO Mol Med*. 2019;11(3).
125. Ruiz-Camp J, Rodriguez-Castillo JA, Herold S, Mayer K, Vadasz I, Tallquist MD, et al. **Tamoxifen dosing for Cre-mediated recombination in experimental bronchopulmonary dysplasia**. *Transgenic Res*. 2017;26(1):165-70.
126. Sakou T, Onishi T, Yamamoto T, Nagamine T, Sampath T, Ten Dijke P. **Localization of Smads, the TGF-beta family intracellular signaling components during endochondral ossification**. *J Bone Miner Res*. 1999;14(7):1145-52.
127. Sakurai R, Li Y, Torday JS, Rehan VK. **Curcumin augments lung maturation, preventing neonatal lung injury by inhibiting TGF-beta signaling**. *Am J Physiol Lung Cell Mol Physiol*. 2011;301(5):L721-30.
128. Scherle W. **A simple method for volumetry of organs in quantitative stereology**. *Mikroskopie*. 1970;26(1):57-60.
129. Schittny JC. **Development of the lung**. *Cell Tissue Res*. 2017;367(3):427-44.
130. Schneider JP, Ochs M. **Alterations of mouse lung tissue dimensions during processing for morphometry: a comparison of methods**. *Am J Physiol Lung Cell Mol Physiol*. 2014;306(4):L341-50.
131. Schwarz DS, Hutvagner G, Du T, Xu Z, Aronin N, Zamore PD. **Asymmetry in the assembly of the RNAi enzyme complex**. *Cell*. 2003;115(2):199-208.
132. Shi W, Chen F, Cardoso WV. **Mechanisms of lung development: contribution to adult lung disease and relevance to chronic obstructive pulmonary disease**. *Proc Am Thorac Soc*. 2009;6(7):558-63.
133. Shi Y, Massague J. **Mechanisms of TGF-beta signaling from cell membrane to the nucleus**. *Cell*. 2003;113(6):685-700.

134. Silahtaroglu AN, Nolting D, Dyrskjot L, Berezikov E, Moller M, Tommerup N, et al. **Detection of microRNAs in frozen tissue sections by fluorescence in situ hybridization using locked nucleic acid probes and tyramide signal amplification**. *Nat Protoc*. 2007;2(10):2520-8.

135. Silva DM, Nardiello C, Pozarska A, Morty RE. **Recent advances in the mechanisms of lung alveolarization and the pathogenesis of bronchopulmonary dysplasia**. *Am J Physiol Lung Cell Mol Physiol*. 2015;309(11):L1239-72.

136. Somashekar ST, Sammour I, Huang J, Dominguez-Bendala J, Pastori R, Alvarez-Cubela S, et al. **Intra-Amniotic Soluble Endoglin Impairs Lung Development in Neonatal Rats**. *Am J Respir Cell Mol Biol*. 2017;57(4):468-76.

137. Sonneville F, Ruffin M, Coraux C, Rousselet N, Le Rouzic P, Blouquit-Laye S, et al. **MicroRNA-9 downregulates the ANO1 chloride channel and contributes to cystic fibrosis lung pathology**. *Nat Commun*. 2017;8(1):710.

138. Sterio DC. **The unbiased estimation of number and sizes of arbitrary particles using the disector**. *J Microsc*. 1984;134(Pt 2):127-36.

139. Stoll BJ, Hansen NI, Bell EF, Walsh MC, Carlo WA, Shankaran S, et al. **Trends in Care Practices, Morbidity, and Mortality of Extremely Preterm Neonates, 1993-2012**. *JAMA*. 2015;314(10):1039-51.

140. Su J, Morgani SM, David CJ, Wang Q, Er EE, Huang YH, et al. **TGF-beta orchestrates fibrogenic and developmental EMTs via the RAS effector RREB1**. *Nature*. 2020;577(7791):566-71.

141. Sureshbabu A, Syed MA, Boddupalli CS, Dhodapkar MV, Homer RJ, Minoo P, et al. **Conditional overexpression of TGFbeta1 promotes pulmonary inflammation, apoptosis and mortality via TGFbetaR2 in the developing mouse lung**. *Respir Res*. 2015;16:4.

142. Syed M, Das P, Pawar A, Aghai ZH, Kaskinen A, Zhuang ZW, et al. **Hyperoxia causes miR-34a-mediated injury via angiopoietin-1 in neonatal lungs**. *Nat Commun*. 2017;8(1):1173.

143. Tremblay KD, Dunn NR, Robertson EJ. **Mouse embryos lacking Smad1 signals display defects in extra-embryonic tissues and germ cell formation**. *Development*. 2001;128(18):3609-21.

144. Tschanz SA, Salm LA, Roth-Kleiner M, Barre SF, Burri PH, Schittny JC. **Rat lungs show a biphasic formation of new alveoli during postnatal development**. *J Appl Physiol (1985)*. 2014;117(1):89-95.

145. Uhal BD. **Cell cycle kinetics in the alveolar epithelium**. *Am J Physiol*. 1997;272(6 Pt 1):L1031-45.

146. Umans L, Vermeire L, Francis A, Chang H, Huylebroeck D, Zwijsen A. **Generation of a floxed allele of Smad5 for cre-mediated conditional knockout in the mouse**. *Genesis*. 2003;37(1):5-11.

147. Ventura A, Kirsch DG, McLaughlin ME, Tuveson DA, Grimm J, Lintault L, et al. **Restoration of p53 function leads to tumour regression in vivo**. *Nature*. 2007;445(7128):661-5.

148. Warburton D, Bellusci S, De Langhe S, Del Moral PM, Fleury V, Mailleux A, et al. **Molecular mechanisms of early lung specification and branching morphogenesis**. *Pediatr Res*. 2005;57(5 Pt 2):26r-37r.

149. Warburton D, Olver BE. **Coordination of genetic, epigenetic, and environmental factors in lung development, injury, and repair**. *Chest*. 1997;111(6 Suppl):119s-22s.

150. Ward HE, Nicholas TE. **Alveolar type I and type II cells**. *Aust N Z J Med*. 1984;14(5 Suppl 3):731-4.

151. Waters CM, Roan E, Navajas D. **Mechanobiology in lung epithelial cells: measurements, perturbations, and responses**. *Compr Physiol*. 2012;2(1):1-29.

152. Weiss DJ, Liggitt D, Clark JG. **Histochemical discrimination of endogenous mammalian beta-galactosidase activity from that resulting from lac-Z gene expression**. *Histochem J*. 1999;31(4):231-6.

153. Winter J, Jung S, Keller S, Gregory RI, Diederichs S. **Many roads to maturity: microRNA biogenesis pathways and their regulation**. *Nat Cell biol*. 2009;11(3):228-34.

154. Witsch TJ, Niess G, Sakkas E, Likhoshvay T, Becker S, Herold S, et al. **Transglutaminase 2: a new player in bronchopulmonary dysplasia?** *Eur Respir J*. 2014;44(1):109-21.

155. Wozney JM, Rosen V, Celeste AJ, Mitsock LM, Whitters MJ, Kriz RW, et al. **Novel regulators of bone formation: molecular clones and activities**. *Science*. 1988;242(4885):1528-34.

156. Wu YT, Chen WJ, Hsieh WS, Tsao PN, Yu SL, Lai CY, et al. **MicroRNA expression aberration associated with bronchopulmonary dysplasia in preterm infants: a preliminary study**. *Respir Care*. 2013;58(9):1527-35.

157. Yi R, Qin Y, Macara IG, Cullen BR. **Exportin-5 mediates the nuclear export of pre-microRNAs and short hairpin RNAs**. *Genes Develop.* 2003;17(24):3011-6.

158. Yin Q, Wang X, Fewell C, Cameron J, Zhu H, Baddoo M, et al. **MicroRNA miR-155 inhibits bone morphogenetic protein (BMP) signaling and BMP-mediated Epstein-Barr virus reactivation**. *J Virol*. 2010;84(13):6318-27.

159. Zeng Y, Liu H, Kang K, Wang Z, Hui G, Zhang X, et al. **Hypoxia inducible factor-1 mediates expression of miR-322: potential role in proliferation and migration of pulmonary arterial smooth muscle cells**. *Sci Rep*. 2015;5:12098.

160. Zhang H, Du L, Zhong Y, Flanders KC, Roberts JD, Jr. **Transforming growth factor-beta stimulates Smad1/5 signaling in pulmonary artery smooth muscle cells and fibroblasts of the newborn mouse through ALK1**. *Am J Physiol Lung Cell Mol Physiol*. 2017;313(3):L615-l27.

161. Zhang X, Xu J, Wang J, Gortner L, Zhang S, Wei X, et al. **Reduction of microRNA-206 contributes to the development of bronchopulmonary dysplasia through up-regulation of fibronectin 1**. *PLoS One*. 2013;8(9):e74750.

162. Zhang XQ, Zhang P, Yang Y, Qiu J, Kan Q, Liang HL, et al. **Regulation of pulmonary surfactant synthesis in fetal rat type II alveolar epithelial cells by microRNA-26a**. *Pediatr Pulmonol*. 2014;49(9):863-72.

163. Zhang Y, Coarfa C, Dong X, Jiang W, Hayward-Piatkovskyi B, Gleghorn JP, et al. **MicroRNA-30a as a candidate underlying sex-specific differences in neonatal hyperoxic lung injury: implications for BPD**. *Am J Physiol Lung Cell Mol Physiol*. 2019;316(1):L144-l56.

7 Declaration

I declare that I have completed this dissertation single-handedly without the unauthorized help of a second party and only with the assistance acknowledged therein. I have appropriately acknowledged and referenced all text passages that are derived literally from or are based on the content of published or unpublished work of others, and all information that relates to verbal communications. I have abided by the principles of good scientific conduct laid down in the charter of the Justus Liebig University of Giessen in carrying out the investigations described in the dissertation.

Claudio Nardiello

8 Acknowledgements

At the end of this educational path, firstly, I would like to thank my supervisor, Dr. Rory E. Morty for the opportunity to join the PhD program in his laboratory. For his great advices and encouragement during these years. For providing me a critical point of view and guidance in science. These years were fantastic and if I have become a scientist the merit is also his.
I thank Prof. Dr. Werner Seeger for giving me the opportunity to join the Max Planck Institute and for the suggestions during the lab meetings.

A big thanks to all the present and past lab mates and friends, for the support, the troubleshooting and especially all the funny moments in these years. A special thanks to Jordi, Alberto, Lina, Diogo, Despina, Misa, David Bravo, Jan, Solmaz, and Francisco. Thanks to Ettore and Francesco to have a little Italy in the lab. A special thanks also to my students Phil, Tuong-Van, and Sophie, it was a pleasure to have you as students.
Thank you to the technicians: Nili, Diana and Uta for the help in these years. Thank you to Monika for the support.
A big thank you to the MBML friends, for the good moments in classes, during study and the time outside.

Thanks to my friends Antonello, Nicola and Fabio, for being there when needed.

Thanks to the entire German family, in particular to aunts Birgit and Barbara, and uncle Wolf.
Un ringraziamento speciale va alla mia famiglia in Italia, al fratellonzolo Gerardo e Angela per il costante supporto, e ai miei genitori, mia madre per tutte quelle volte che non è mai mancata per ascoltarmi e darmi consigli sui miei problemi e mio padre per i suoi consigli.

At the end, I would like to thank the most important person, my girlfriend Claudia. Thank you so much for the tremendous support in these years. Without you would this achievement not be possible. Thank you so much in believing in me and being always on my side. Te quiero un montonasso!

9 Appendix

Publications authored:

Elevated FiO_2 increases SARS-CoV-2 co-receptor expression in respiratory tract epithelium.
Am J Physiol Lung Cell Mol Physiol 2020 Sep
Myti D, Gunjak M, Casado F, Khaghani Raziabad S, **Nardiello C**, Vadász I, Herold S, Pryhuber G, Seeger W, Morty RE

World health observances in September 2020: sepsis, the lung and heart, and pulmonary fibrosis in focus.
Am J Physiol Lung Cell Mol Physiol 2020 Sep
Nardiello C, Morty RE

Commercially available transfection reagents and negative control siRNA are not inert.
Anal Biochem. 2020 Oct
Kleefeldt JM, Pozarska A, **Nardiello C**, Pfeffer T, Vadász I, Herold S, Seeger W, Morty RE.

Impact of litter size on survival, growth and lung alveolarization of newborn mouse pups.
Ann Anat. 2020 Nov
Feddersen S, **Nardiello C**, Selvakumar B, Vadász I, Herold S, Seeger W, Morty RE.

Mouse genetic background impacts susceptibility to hyperoxia-driven perturbations to lung maturation.
Pediatr Pulmonol. 2019 Mar
Tiono J, Surate Solaligue DE, Mižíková I, **Nardiello C**, Vadász I, Böttcher-Friebertshäuser E, Ehrhardt H, Herold S, Seeger W, Morty RE

Targeting miR-34a/Pdgfra interactions partially corrects alveologenesis in experimental bronchopulmonary dysplasia.
EMBO Mol Med. 2019 Mar
Ruiz-Camp J, Quantius J, Lignelli E, Arndt PF, Palumbo F, **Nardiello C**, Surate Solaligue DE, Sakkas E, Mižíková I, Rodríguez-Castillo JA, Vadász I, Richardson WD, Ahlbrecht K, Herold S, Seeger W, Morty RE

Control Interventions Can Impact Alveolarization and the Transcriptome in Developing Mouse Lungs.
Anat Rec (Hoboken). 2019 Feb
Fehl J, Pozarska A, **Nardiello C**, Rath P, Surate Solaligue DE, Vadász I, Mayer K, Herold S, Seeger W, Morty RE

Targeting transglutaminase 2 partially restores extracellular matrix structure but not alveolar architecture in experimental bronchopulmonary dysplasia.
FEBS J. 2018 Jun
Mižíková I, Pfeffer T, **Nardiello C**, Surate Solaligue DE, Steenbock H, Tatsukawa H, Silva DM, Vadász I, Herold S, Pease RJ, Iismaa SE, Hitomi K, Seeger W, Brinckmann J, Morty RE

Transmission of microRNA antimiRs to mouse offspring via the maternal-placental-fetal unit.
RNA. 2018 Jun
Hönig J, Mižíková I, **Nardiello C**, Surate Solaligue DE, Daume MJ, Vadász I, Mayer K, Herold S, Günther S, Seeger W, Morty RE

Stereological analysis of individual lung lobes during normal and aberrant mouse lung alveolarisation.
J Anat. 2018 Mar
Hoang TV, **Nardiello C**, Surate Solaligue DE, Rodríguez-Castillo JA, Rath P, Mayer K, Vadász I, Herold S, Ahlbrecht K, Seeger W, Morty RE

A new target for caffeine in the developing lung: endoplasmic reticulum stress?
Am J Physiol Lung Cell Mol Physiol. 2017 Oct
Rath P, **Nardiello C**, Morty RE

Caffeine administration modulates TGF-β signaling but does not attenuate blunted alveolarization in a hyperoxia-based mouse model of bronchopulmonary dysplasia.
Pediatr Res. 2017 May
Rath P, **Nardiello C**, Surate Solaligue DE, Agius R, Mižíková I, Hühn S, Mayer K, Vadász I, Herold S, Runkel F, Seeger W, Morty RE

Standardisation of oxygen exposure in the development of mouse models for bronchopulmonary dysplasia.
Dis Model Mech. 2017 Feb
Nardiello C, Mižíková I, Silva DM, Ruiz-Camp J, Mayer K, Vadász I, Herold S, Seeger W, Morty RE

Looking ahead: where to next for animal models of bronchopulmonary dysplasia?
Cell Tissue Res. 2017 Mar
Nardiello C, Mižíková I, Morty RE

MicroRNA in late lung development and bronchopulmonary dysplasia: the need to demonstrate causality.
Mol Cell Pediatr. 2016 Dec
Nardiello C, Morty RE

Recent advances in the mechanisms of lung alveolarization and the pathogenesis of bronchopulmonary dysplasia.
Am J Physiol Lung Cell Mol Physiol. 2015 Dec
Silva DM, **Nardiello C**, Pozarska A, Morty RE

The H2S-generating enzymes cystathionine β-synthase and cystathionine γ-lyase play a role in vascular development during normal lung alveolarization.
Am J Physiol Lung Cell Mol Physiol. 2015 Oct
Madurga A, Golec A, Pozarska A, Ishii I, Mižíková I, **Nardiello C**, Vadász I, Herold S, Mayer K, Reichenberger F, Fehrenbach H, Seeger W, Morty RE